UNIVERSITÀ DEGLI STUDI DI PADOVA

DIPARTIMENTO DI INGEGNERIA DELL'INFORMAZIONE

# UNIVERSITÀ DEGLI STUDI DI PADOVA

*Dipartimento di Ingegneria dell'Informazione*

*Dipartimento di Ingegneria Industriale*

CORSO DI LAUREA MAGISTRALE IN BIOINGEGNERIA INDUSTRIALE

# PEEK FOR BONE TISSUE ENGINEERING: COVALENT FUNCTIONALIZATION IMPROVES BIOACTIVITY


***Relatore: Prof.ssa Monica Dettin***

***Correlatore: Dott. Leonardo Cassari***

***Laureanda: Martina Ravanello***


Anno Accademico 2022/2023

# ABSTRACT

Bone tissue has the capability to renew itself; however, defects of a critical size prevent bone from regeneration. The development of bone tissue engineering has been used to create functional alternatives to regenerate bone. A range of different biomaterials have been used for this purpose, including synthetic polymers as Poly (Ether-Ether-Ketone) (PEEK).

PEEK has been gaining increasing attention as candidate for orthopaedic and dental implants, due to its biocompatibility, chemical stability, and elastic modulus similar to that of natural bone. However, PEEK has a bioinert surface that inhibits the adhesion and proliferation of osteoblasts and, consequently, osseointegration process. Several improvements have been made to the osseointegration potential of PEEK, including modifications of surface roughness through sandblasting and covalent functionalization of the surface with bioactive molecule.

To investigate the best surface roughness for osteoblasts adhesion, two different types of PEEK surface were analysed and compared to the smooth samples (PEEK): (i) 60 μm grit-blasted (R60-PEEK) and (ii) 110 μm grit-blasted (R110-PEEK) surface. An osteoblast proliferation test was performed on the different surfaces and revealed that R110-PEEK significantly improve osteoblasts proliferation.

To make PEEK bioactive, R110-PEEK disks were covalently functionalized via oxime formation with two peptides: (i) EAK, an ionic-complementary self-assembling peptide and (ii) GBMP1α, the sequence (48–69) mapped on the Bone Morphogenetic Protein 2. The peptides were synthetized with an aminooxy group at the N-terminus of the sequence; in the functionalization process the aminooxy group will bound the ketones on PEEK surface. A spacer was introduced between the aminooxy group and the other amino-acids, in order to separate the anchoring group and the bioactive sequence.

X-ray spectroscopy analysis confirmed the presence of the peptides covalently bind on PEEK samples. Furthermore, Water Contact Angle and Force Spectroscopy measurements were carried out and showed that the peptides modified the surface and properties of PEEK.

Gene expression assays were performed on the functionalized samples and confirmed that the bioactive sequences-enriched surface led to overexpression of all analysed genes.

# ABSTRACT

Il tessuto osseo possiede la capacità di auto-rimodellamento; tuttavia, difetti di dimensioni superiori ad una soglia critica impediscono all'osso di rigenerarsi. L'ingegneria tissutale ossea è stata introdotta allo scopo di proporre alternative che riuscissero a supportare il tessuto osseo nella rigenerazione. Recentemente, i materiali utilizzati in questo ambito sono stati molti, inclusi i polimeri sintetici, tra cui il Poli (Eter-Eter-Chetone) (PEEK).

Il PEEK è considerato un ottimo materiale per impianti in ambito ortopedico e dentale, grazie alla sua biocompatibilità, stabilità chimica e modulo elastico simile a quello del tessuto osseo nativo. Tuttavia, il PEEK presenta una superficie bioinerte che inibisce l'adesione e la proliferazione e, conseguentemente, l'osteointegrazione. Per migliorare l'osteointegrazione del PEEK sono stati testati diversi metodi, tra cui la modifica della rugosità superficiale attraverso sabbiatura e la funzionalizzazione covalente della superficie con molecole bioattive.

Per identificare la rugosità superficiale ottimale per l'adesione degli osteoblasti, due tipi di superficie di PEEK sono state analizzate e comparate con i campioni lisci: (i) una superficie sabbiata con particelle di 60 μm (R60-PEEK) e (ii) una superficie sabbiata con particelle di 110 μm (R110-PEEK). È stato poi effettuato un test di proliferazione degli osteoblasti sulle diverse superfici, il quale ha dimostrato che il R110-PEEK migliora significativamente la proliferazione degli osteoblasti.

Per rendere il PEEK bioattivo, i campioni R110-PEEK sono stati funzionalizzati covalentemente, tramite formazione di ossime, con i peptidi (i) EAK, un peptide auto-assemblante ionico-complementare e (ii) GBMP1α, un peptide contenente la sequenza (48-69) mappata sulla proteina morfogenetica dell'osso 2 (BMP-2). I peptidi sono stati sintetizzati con un gruppo ossiamminico all'N-terminale della sequenza; durante la funzionalizzazione il gruppo ossiamminico si legherà ai chetoni sulla superficie del PEEK. È stato introdotto anche uno spaziatore tra il gruppo ossiamminico e gli altri amminoacidi, in modo da separare il gruppo per l'ancoraggio dalla sequenza bioattiva.

L'analisi di spettroscopia a raggi X (XPS) ha confermato la presenza dei peptidi sul PEEK. Inoltre, le analisi di angolo di contatto (WCA) e Spettroscopia a Forza Atomica (FS) hanno mostrato che i peptidi ancorati alla superficie modificano la superficie e le proprietà del PEEK.

Sono stati effettuati anche dei saggi di espressione genica sulle superfici funzionalizzate; questi hanno confermato che l'ancoraggio di sequenze bioattive alla superficie permette di avere una sovra-espressione di tutti i geni analizzati.

# CONTENTS

# CHAPTER 1
# INTRODUCTION

## 1.1 BONE TISSUE

Bone is a metabolically active and dynamic connective tissue that works as structural support and facilitate movement providing levers for muscles, protection of organs, reserve for minerals and growth factors, maintenance of homeostasis and a site for haematopoiesis. [1,2,3]

### 1.1.1 Bone composition

Bone tissue is made of two main elements: cells, approximatively 10% of the total volume, and extracellular matrix (ECM), approximatively 90% of the total volume. [1]

#### *1.1.1.1 Bone Cells*

Bone cells (Fig. 1.1) derive from two cell lines: osteoprogenitor cells, able to differentiate in osteoblasts and osteocytes, come from mesenchymal stem cells, while osteoclasts have hematopoietic origin. [1,2,4]

Osteoprogenitor cells are bone stem cells and reside in endosteum, periosteum, bone canals and marrow; they remain undifferentiated until they receive a signal allowing them to migrate to a site, and consequentially to proliferate and differentiate into osteoblasts. [1]

Osteoblasts line the surfaces and are tightly packed; they are considered bone forming cells, in fact osteoblasts produce bone matrix. Once activated they can differentiate into osteocytes, remain quiescent osteoblasts or return to the osteoprogenitor cell line [1,2,3]. They also secrete growth factors and proteins that are very important in differentiation, activation and proliferation of osteoblasts

themselves: among these, very important are the Bone Morphogenetic Proteins (BMPs) and Transforming Growth Factors-β (TGF-βs). [1,4]

Osteocytes account for 90% of all bone cells. [2] Osteocytes are osteoblasts that, once completed their function, surround themselves with bone matrix formed and reside in the lacunae (lacunar-shaped spaces). Once the matrix surrounds them, they develop cytoplasmic extensions that cross the bone and come into contact with other osteocytes allowing direct communications, exchanges of nutrients, oxygen and signal molecules. The main function of osteocytes is to provide for the maintenance of the bone matrix formed. After injury, osteocytes can transform back into osteoblasts for bone remodelling. [1,2,4]

Osteoclasts are large multinucleated cells whose job is to resorb mineralized bone. They are cells that reside in depressions of the bone surface, called Howship lacunae, but during bone remodelling, they can reside in much deeper areas. Once the cells come in contact with bone, they attach to the matrix and solubilize it by acidification, enabling its phagocytosis: they are therefore crucial in the process of bone remodelling. [1,2,3,4]

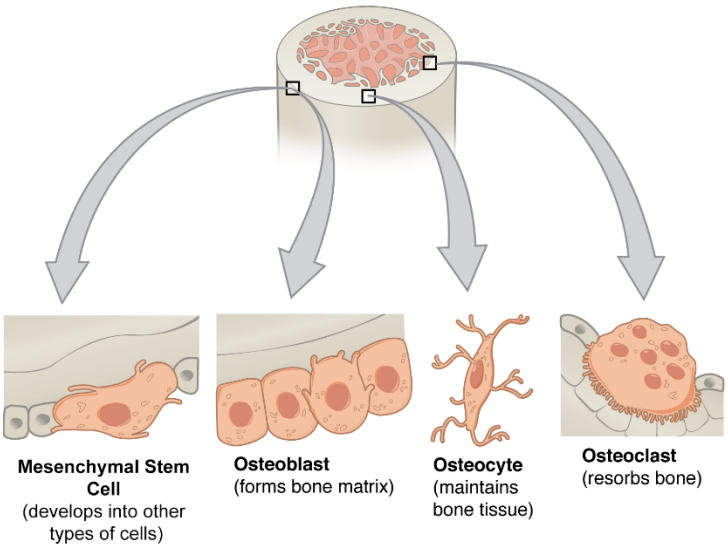


*Fig 1.1: bone cells*

### *1.1.1.2 Bone extracellular matrix*

Bone extracellular matrix occupies about 90% of the tissue total volume. It is a complex structure consisting mainly of an inorganic or mineral matrix (about 65%) and an organic matrix (about 35%). [1]

The inorganic matrix is a very large source of calcium and phosphorus but also magnesium and sodium. It consists mainly of needle-like crystals of hydroxyapatite and provides excellent mechanical properties, including bone strength and excellent stiffness in tests of compression. [1,2]

The organic matrix is produced by osteoblasts and consists in two parts: the fibrous part, that consists mainly of type I collagen (about 90%), and the interfibrillar part, consisting of proteoglycans, glycoproteins and growth factors in smaller amounts that are fundamental in osteogenesis, remodeling and mineralization of bone. The organic matrix gives bone its shape, but also good mechanical properties, especially tensile strength. [1,2,4]

### 1.1.2 Bone structure

There are two types of bone tissue: cortical and cancellous bone (Fig. 1.2); both have same matrix composition but differ for density or porosity, 3D structures, and metabolic activity.
Cortical bone has a porosity of 5%-10% and makes up 80% of adult human skeleton. It is characterized by high torsion resistance and gives bone its compressive strength.
Cancellous bone is characterized by a porosity of 50%-90%, makes up approximately 20% of adult human skeleton, and has surface area per unit volume significatively greater than cortical bone. Cancellous bone has a higher rate of remodeling and metabolic activity, and this tissue is characterized by rapid response to mechanical stimuli, considering that primary bone cells are on the surface in proximity to circulating growth factor and cytokines. [1,2]

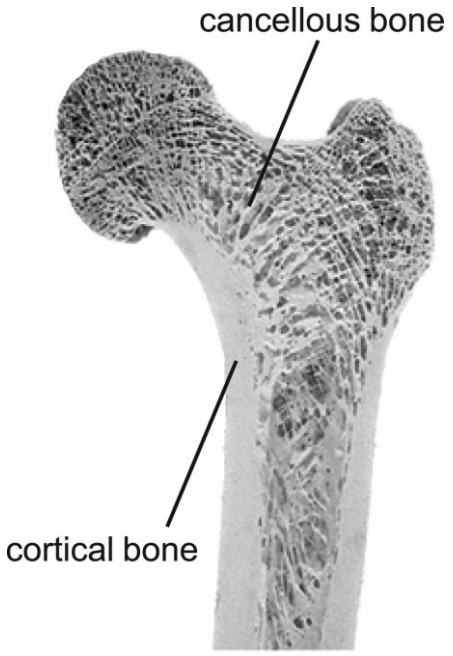


*Fig 1.2: Types of bone tissue.*

The size and distribution of collagen fibres identify two varieties of bone tissue: woven and lamellar.

Woven bone is characterized by non-uniform mineralization and irregular pattern of collagen fibrils that make the tissue flexible but weak.

Lamellar bone has an organized architecture that consist of fibrils of collagen packed in sheets with uniform-distributed bone matrix and osteocytes. This tissue replaces woven bone during growth and in the later stage of fracture healing and is rigid and strong due to highly organized concentric sheet orientation. There are four possible shapes of lamellar bone: osteons trabecular, circumferential, and interstitial. [2]

Lamellar bone is contained both in cortical and cancellous bone in form of osteons and trabecular structure, respectively. (Fig. 1.3).

Osteons are longitudinal cylinders consisting of 4-20 concentric lamellar sheets that run parallelly to the axis of the bone and are made of concentric lamellae surrounding central Haversian canals, lined by endosteal cells and containing mostly blood and lymphatics vessels. A large number of canaliculi connect the central canal to osteocytes allowing the diffusion of nutritive substances through the matrix. Osteons are separated by cement lines, that are layers of organic matrix dividing the resorption of bone area and new formation of bone area. [1,2,4]

On the other hand, trabecular structure provides wider surface area to cancellous bone and is characterized by a greater vascularity and a higher metabolic activity than cortical osteons. Cancellous trabeculae do not contain Haversian canals but the contact between bone structures and marrow is allowed by sinusoids. [1,2]

Bone is formed by bone lacunae, small depressions in the matrix where osteocytes are deposited; from the lacunae, bone canaliculi branch off in all directions, which allow for communication between the various nearby lacunae. [1,4]

Periosteum is a two-layer structure made by hypocellular outer layer that continues into joint capsules connecting adjacent bones; and an inner layer containing osteoprogenitor cells and a vascular plexus. Periosteum covers the external surface of bones providing an attachment site for ligaments and tendons and contributing to the bone blood supply. [2,4]

Endosteum is a membranous structure covering the inner surfaces of bone; it contains vasculature and osteoprogenitors cells. [2,4]

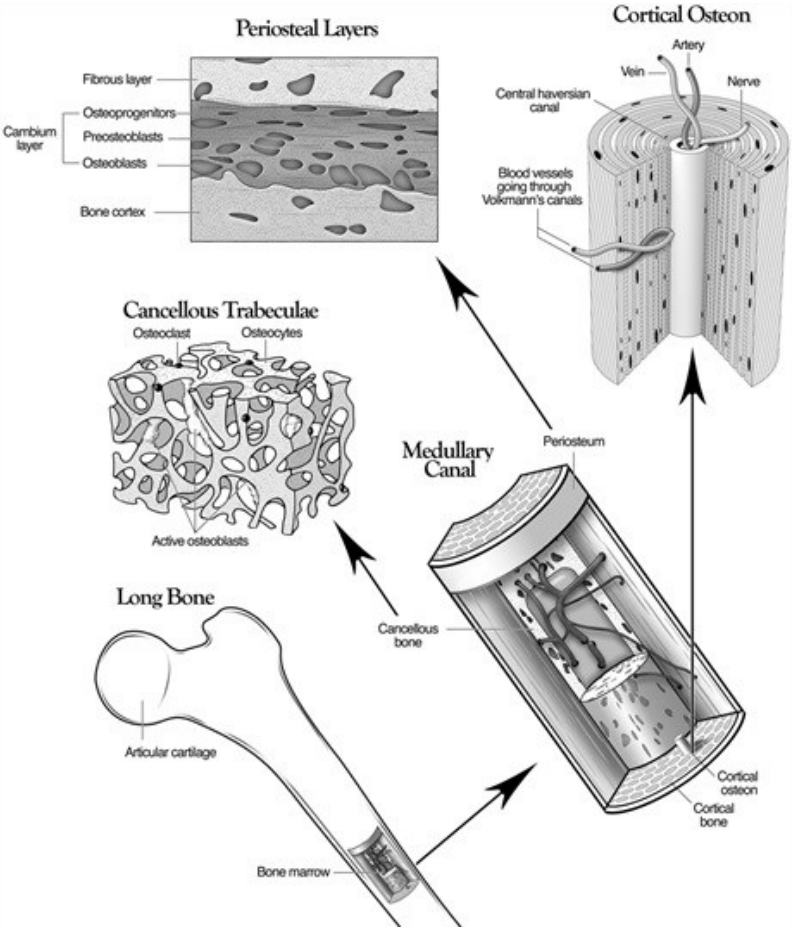


*Fig 1.3: Osteons and trabecular structure.*

On the base of shape, bones can be classified into three groups: short, flat, and long or tubular.

Short bones, for example tarsals or carpals, measure roughly the same in all dimensions, can be trapezoidal, cuboidal, cuneiform, or irregular shaped and have relatively thin cortices.

Flat and tubular bones have one dimension that is significatively shorter or longer than the other two. Examples of flat bones are scapula and the wing of the ileum; examples of long or tubular bones are femur, tibia, and humerus that are characterized by an expanded metaphysis and an epiphysis at either end of a thick-walled tubular diaphysis. [2]

## 1.2 BONE GRAFTS

Bone grafts are one of the surgical techniques capable to improve and increase the regeneration of bone. Bone substitutes must provide both mechanical support and bone regeneration, in terms of osteoconduction, osteoinduction, and osteogenesis.

Osteoconduction is the ability of allowing migration and growth of osteoblasts and osteoprogenitor cells within the graft, while osteoinduction allows primitive, undifferentiated, and pluripotent cells to differentiate into cells suitable for bone formation. Osteogenesis refers to the production of new bone tissue by cells derived from grafts.

The main grafts used are autograft, allograft, and xenograft. [5,6]

### 1.2.1 Autograft

Autograft, or autologous graft, is a graft harvested from an anatomical site and transplanted to another body site but always within the same individual. It possesses osteoconductive, osteoinductive and osteogenic potential, so it is capable of bone regeneration. Autografts are considered the gold standard in the treatment of bone defects, since they are biocompatible, lacking immunogenic reactions, and capable of osteogenesis, osteoconduction, and osteointegration. However, the surgical procedure may cause inflammation, infection, and chronic pain; autografts are also limited in availability. [5,6,7]

### 1.2.2 Allograft

Allogenic bone grafting involves the use of bone tissue harvested from an individual and transplanted into a genetically different member of the same species. It is considered the best alternative to autografts for patients with poor healing, extensive osteoarthritis, and plural fractures.
However, allografts are characterized by higher immunogenicity, high failure rate and possible viral transmission of diseases such as hepatitis B or C. [5,6]

### 1.2.3 Xenograft

Xenogeneic grafts involve the use of tissue from non-human species. A typical problem for these grafts is antigenicity, greater than allografts; for this reason, they require a careful sterilization, resulting in a loss of osteoinductive properties.

These grafts have abundance of donors; therefore, they are much less expansive and have a longer shelf life, due to the sterilization process. [8]

## 1.3 TISSUE ENGINEERING

Autografts are the gold standard but shows limitations described above; for these reasons tissue engineering is a better choice for bone reconstruction.

Tissue engineering is a multidisciplinary field involving a combination of cells, engineering techniques, material methods, and biochemical and physiochemical factors to restore, maintain, improve, or replace different types of biological tissues. [9]

Tissue engineering approach involves the use of scaffolds, which should provide the ideal environment for tissue and organ regeneration; in fact, they are seeded with cells, which will be specific for the new tissue to be formed. Furthermore, by means of growth factors or bioreactors, the appropriate chemical and/or mechanical stimuli are given to make them grow (Fig. 1.4). [4,10]

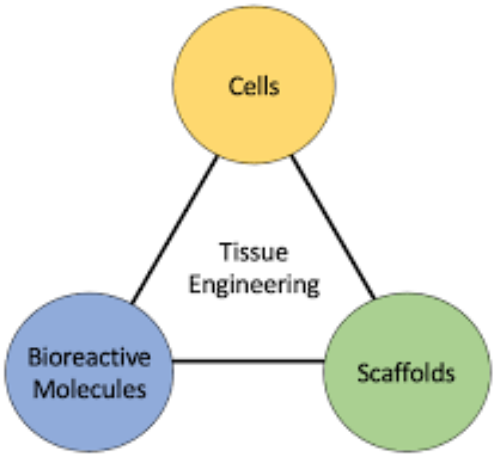


*Fig 1.4 Elements of tissue engineering approach*

### 1.3.1 Scaffolds

Many scaffolds are used for tissue and organ regeneration, but they must have specific characteristics to be suitable for tissue engineering [11]. Some of them are:

- Biocompatibility: scaffold must not cause inflammatory reactions or rejection because cells need to adhere, differentiate, and proliferate.

- Biodegradability: once the tissue has been regenerated, scaffold has to be replaced by extracellular matrix secreted by cells; therefore, biodegradation products must not be toxic.
- Mechanical properties: each scaffold must have mechanical properties suitable for the tissue to be regenerate or replaced.
- Architecture of the scaffold: scaffold must have a porous structure allowing cells to move and nutrients to reach cells. Porosity must be large enough to allow the interactions of cells, but small enough to increase the surface area promoting the anchoring of proteins able to enhance cells binding, especially for synthetic scaffolds.
- Manufacturing technologies: the development of scalable manufacturing processes according to the standard of Good Manufacturing Practice (GMP) is fundamental to ensure the success of strategies for tissue engineering. [11]

#### *1.3.1.1 Scaffolds for bone tissue engineering*

A proper scaffold for bone tissue engineering must have a 3D structure capable of supporting adhesion, proliferation, and differentiation of cells into bone [12]. A bone scaffold must be also: biocompatible, non-toxic and non-tumorigenic, radiotransparent, stable over time, resistant, and able to induce osteoconductivity. [12,13]

From the structural point of view, bone scaffolds must be porous with pores size suitable for cell seeding, cells migration, matrix deposition, vascularization and transport of nutrients. The optimal pore size to promote bone tissue growth is in the range of 100-500 μm. [14]

From a mechanical point of view, the materials for bone scaffolds must provide mechanical support to preserve and regenerate bone tissue, structure stiffness, resistance, and fatigue strength. [13,14]
Stiffness is a critical parameter for bone scaffolds: if it exceeds the natural bone one, the concentration of stress in the surrounding bone may cause bone failure; on the other side, if the scaffold stiffness is lower than the natural bone one, there can be the failure of the implant. This diskrepancy in stiffness values can lead to the sharing of irregular loads between bone and implant, causing stress-shielding, that affects both bone remodelling and healing process. In particular, when bone is underloaded, it adapts to the low-stress environment, becoming less dense and weaker. [15]
The scaffold must be able to withstand the physiological forces within the implant site and must have enough strength and stiffness to perform well until the tissue has grown.
For a non-resorbable scaffold, strength to fatigue must also be considered, as the scaffold will be subjected to cyclic loads for all patient's life.

The design of the scaffold will have to take into account both the mechanical properties and the biological requirements to achieve an optimized overall structure that can ensure regeneration of the tissue. [14,15]

Surface scaffold properties must be considered, including topography, surface energy, chemical composition, wettability, and surface bioactivity. For example, using bioactive molecules is one of the techniques to improve bioactivity of scaffolds and surface roughness affects cell morphology and growth. [16]

### 1.3.2 Cells for bone tissue engineering

Cells are a key element in the regeneration of bone; they must be able to maintain the appropriate phenotype and perform the biological functions required. [17,18]
Cells mainly used in tissue engineering are primary cells and undifferentiated stem cells.

#### *1.3.2.1 Primary cells*

Primary cells are mature cells of the specific tissue. These cells do not cause immunologic reaction, but they are differentiated and do not renew themselves; therefore, these cells perform their biological function until they die. Other disadvantages of primary cells are that they tend to de-differentiate during ex vivo cultivation, expressing an inappropriate phenotype, and they are also lacking in availability. [17]

#### *1.3.2.2 Stem cells*

Stem cells are undifferentiated cells that are capable of self-renewal and differentiation into one or more specialized cell types [4,17]. There are different types of stem cells but those widely used in tissue engineering are multipotent stem cells and pluripotent stem cells. [17,18]

Multipotent stem cells can differentiate into different types of cells, for example adult stem cells. Adult stem cells are undifferentiated cells located among differentiated cells in tissues or organs capable of renewing themselves. They have a good degree of plasticity and, if autologous, they have no ethical or immunological problems. Adult stem cells of particular interest are umbilical cord stem cells, hematopoietic stem cells, and mesenchymal stem cells. [19]

Pluripotent stem cells are cells that can differentiate and give origin to most of the biological tissues; they can be divided into embryonic stem cells (ESCs) and induced pluripotent stem cells (iPSCs). [17,18]

- ESCs can be derived from the inner cell mass of the blastocyst. They have unlimited self-renewal activity and originate any cell lineage, but they may cause immunologic rejection, since they are harvested during embryonic development [18,19].
- iPSCs are similar to ESCs, but they are obtained reprogramming adult cells. The original cells are taking from the patient itself so iPSCs are not immunogenic and not exposed to ethical problems. iPSCs have limitation in pluripotency and may cause cancer. [4,17]

## 1.4 BIOMATERIALS FOR BONE TISSUE ENGINEERING

Bone is a highly regenerative tissue, in which only small defects can spontaneously begin the healing process; large-scale defects, instead, require surgery and implant materials to initiate and accelerate the healing process.

To work properly, a biomaterial must show specific properties, such as biocompatibility and biodegradability, referring to the chemical or enzymatic degradation of the material once implanted into living organisms. The degradation rate must match the new bone formation and no production of toxic particles must be guaranteed during the degradation process. A possible bio-incompatibility, in fact, would cause the activation of the immune system and a chronic immune response. [20]

### 1.4.1 Types of bone tissue engineering biomaterials

There are five main categories of biomaterials used in bone tissue engineering, that are polymeric biomaterials, metals, bioceramics, composite materials, and biologically derived materials [4].

Metallic materials are characterized by metallic bond, have crystalline structure and are good conductors of electricity and heat. Biocompatibility of these materials depends on the ability to resist the aggression of biological fluids and corrosion; coating the material surface with an oxide layer prevent the release of toxic ions. In the biomedical field the most used metallic materials are stainless steel, titanium, titanium-alloys, cobalt-alloys, aluminium, and silver due to their excellent mechanical strength and fatigue resistance. [4,13]

Ceramic materials consist of the combination of metallic and non-metallic elements linked together through covalent or ionic bonds. They are characterized by toughness and resistance to both high temperatures and wear, but they are also brittle [21]. Bioceramics are widely used is bone tissue engineering due to their biocompatibility, bioactivity, osteoconductivity potential, and mechanical

strength; the most common are calcium phosphates, such as hydroxyapatite, calcium sulphates, and bioactive glasses. [13]

Composite materials are usually composed of a matrix containing compounds in order to reinforce and increase the mechanical strength of the material. They are characterized by good mechanical propertied and good biocompatibility. [4]

Biologically derived materials include natural proteins and polysaccharides, such as collagen, gelatine, elastin, and chitosan. These materials are used in combination with synthetic materials. [4]

### 1.4.2 Polymeric materials

Polymeric materials consist of large molecules, called macromolecules, formed by the repetition of same or different units, called monomers. The structure of these materials is poorly crystalline; moreover, they are poor conductors and are characterized by low density values, low softening, and chemical decomposition temperatures. [4]

Polymers are biomaterials widely used in regeneration medicine and tissue engineering and can be divided into natural and synthetic polymers.

Bone tissue engineering employs natural polymers due to their capability of providing a suitable bioactive environment and mechanical support, able to promote the growth of bone tissue in defect sites. Due to their biocompatibility and minimal immunological reaction caused, natural polymers like collagen, elastin, actin, keratin, chitosan and cellulose are largely implied in bone tissue engineering. [4,22,23]

Synthetic polymers are used due to their availability, controllable degradation rate and easy adaptation for bone tissue engineering; the main synthetic polymers used in bone tissue engineering are poly(lactic acid) (PLA), poly(glycolic acid) (PGA), poly(lactide-co-glycolic acid) (PLGA), poly(polycaprolactone) (PCL), poly(polyurethanes) (PU), poly(ethylene glycol) (PEG), and poly(ether-ether-ketone) (PEEK). [4,13,23]

## 1.5 POLY(ETHER-ETHER-KETONE) (PEEK)

PEEK is a synthetic polymeric material obtained from polymerization of a monomer (figure 1.5) via step-growth dialkylation reaction of bis-phenolates. It is a polyaromatic semicrystalline thermoplastic polymer with chemical formula $(-C6H4-O-C6H4-O-C6H4-CO-)_n$. [24,25]

PEEK has been widely used in tissue engineering, especially in face and cranial reconstruction, tooth replacement, orthopaedic, and spine surgery, but also in cardiac surgery [25]. Nowadays research is focusing on functionalizing PEEK with bioactive molecules to improve physical, chemical, mechanical properties, and biocompatibility.

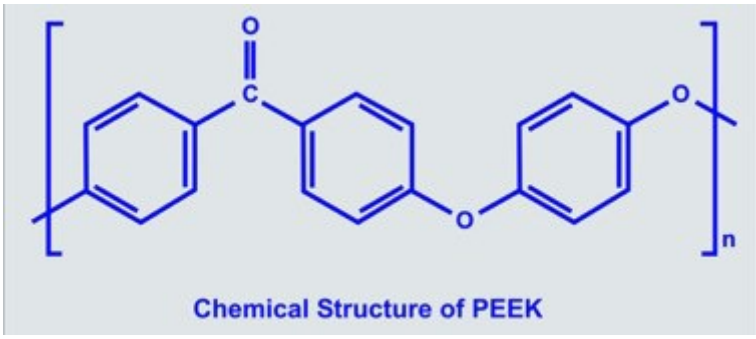


*Fig 1.5 Structure of PEEK*

### 1.5.1 Structure and properties

PEEK is a two-phase semi-crystalline polymer, characterized by an amorphous and a crystalline phase, that varies in content depending on the thermal processing history of the polymer. PEEK crystals consist of lamellae organized under certain conditions in larger spherulites (20-50 μm in diameter), visible with scanning electron microscopy or polarized light microscopy. [26,27]

PEEK is stable due to its structure, in fact the aryl rings are interconnected through ketone and ether groups located at the opposite ends of the ring (in 'para' position), making the polymer unreactive and resistant to chemical, thermal and post-irradiation degradation. [26,27]

### 1.5.2 Mechanical properties

Mechanical properties of PEEK are influenced by strain rate, temperature, molecular weight and size/orientation of the crystalline regions. [25,28]

PEEK is considered ductile; in fact, it is able to accommodate large deformation plastic flows in both uniaxial tension and compression. Its behaviour is plastic: at small deformations the material shows an elastic behaviour, with a linear relationship between tension and strain. Then by increasing the

deformation, the material will have plastic behaviour; once reached the tensile yield strength, will meet irreversible deformation. After yielding, PEEK exhibits hardening (or softening) characteristics that vary depending on the type of mechanical test performed, on temperature and strain rate.
The elastic modulus of pure PEEK is 4 GPa. [23]

### 1.5.3 Surface properties and modifications

Surface properties are defined by the interactions intercurrent at the interface of the material. Despite PEEK is biocompatible, since it did not show cytotoxic or mutagenic effects [28] and is characterized by good mechanical, chemical, and physical properties, the bioinertia and hydrophobicity of pure PEEK may induct difficulties in tissue ingrowth. [29] Thus, the need to modify the surface of PEEK, allowing better interactions between implant surface and surrounding tissues.

Commonly used techniques are physical treatments, chemical treatments, surface coatings, and use of bioactive molecules (Fig 1.6).

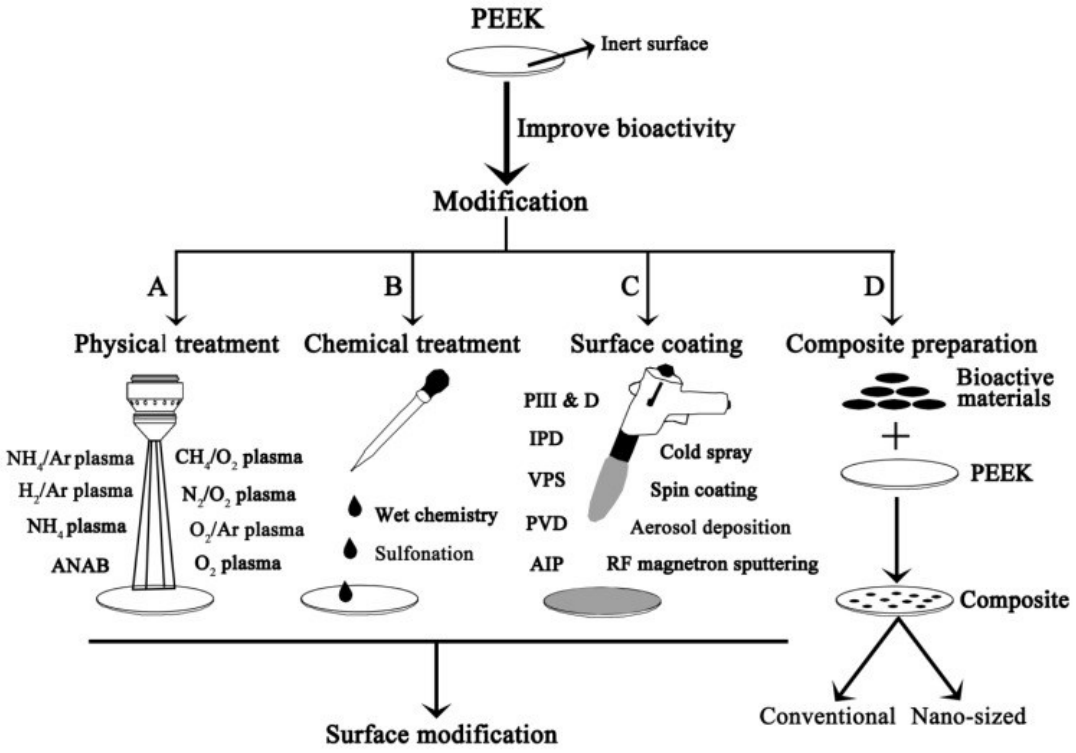


*Fig 1.6 Methods for PEEK surface modification*

Commonly used physical treatments are plasma modifications (oxygen plasma, ammonia plasma, nitrogen/oxygen plasma, methane/oxygen plasma, oxygen/argon plasma, ammonia/argon plasma, hydrogen/argon plasma) accelerated neutral atom beam. For plasma modifications, the biomaterial is

placed in a reactor where reactive particles interact with the surface, modifying mechanical, electrical and optical properties of interest. [30]

Chemical treatments used to modify PEEK surface are sulfonation and wet surface chemistry. Through wet surface chemistry can be obtained hydroxylated polymer (PEEK-OH) by reduction, carboxylated polymer (PEEK-NCO) by coupling a diisocyanate reagent to PEEK-OH, aminated polymer (PEEK-N$H_2$) by hydrolysis of PEEK-NCO and aminocarboxylated polymers (PEEK-GABA and PEEK-Lysine) by coupling of aminoacids to PEEK-NCO.
Using sulfonation, a 3D nano-structured network with bio-functional groups is produced on PEEK. [30]

PEEK can be coated with materials carrying bioactive affects, using techniques as cold spray, radio frequency (RF) magnetron sputtering, spin coating, aerosol deposition (AD), ionic plasma deposition (IPD), plasma immersion ion implantation and deposition (PIII&D), electron beam deposition, vacuum plasma spraying (VPS), physical vapor deposition (PVD), and arc ion plating (AIP) [30].
Various material can be deposited on PEEK surface, such as hydroxyapatite, titanium, gold, titanium dioxide, diamond-like carbon and tert-butoxides, able to enhance the bioactivity.

Coupling of PEEK with peptide sequences, bioactive molecules, and biochemical factors confer the material bioactivity. Mechanical and physical properties are given by PEEK, while bioactive molecules are able to promote adhesion of cells from different biological tissue. [30]

Bone is characterized by a complex topography, consequently, PEEK surface roughness plays and essential role in bone formation and implant fixation; a proper surface roughness is able to promote the adsorption of ECM proteins and the adhesion of osteoblasts. [24,28]
Biocompatibility of materials is directly influenced by the interactions between the surface of the biomaterial and the host tissue; controlling surface properties such as chemistry, charge, texture, and porosity can significatively improve tissue response *in vivo*. [29]

### 1.5.4 Surface topographical modification

Surface topographical modification is a crucial approach to improve the biological performance mimicking the hierarchical structure of bone. Moderating the surface roughness can enhance the biological properties of PEEK, but oversize or undersize in roughness could not promote biocompatibility. By literature evidence, a rough microtopography can also promote ingrowth of soft and hard tissue into the PEEK scaffold. [31]

Deng et al. studied the influence of four different degree of surface roughness in osteoblast adhesion and proliferation; they evaluated biofunctionalities of microroughened PEEK *in vitro* and *in vivo* [31].

Different roughness was obtained through sandblasting technique and then surfaces were characterized (Table 1.7).

| Sample names | Control | Group 1 | Group 2 | Group 3 |
|---|---|---|---|---|
| Surface treatment | Polished with 2,000-grit paper | 60–80 μm $Al_2O_3$ | 110–150 μm $Al_2O_3$ | 180–250 μm $Al_2O_3$ |
| Ca content* | 6.0%±1.5% | 11.5%±3.4% | 21.4%±2.2% | 30.9%±2.6% |
| P content* | 3.8%±0.9% | 8.7%±1.1% | 13.9%±1.2% | 19.5%±1.1% |
| Ra (μm) | 0.12±0.01 | 0.93±0.09 | 1.96±0.21 | 2.95±0.35 |
| Rq (μm) | 0.17±0.02 | 1.28±0.17 | 2.49±0.27 | 3.64±0.56 |

**Note:** *The concentrations of calcium and phosphorus were reported and estimated from XPS analysis.
**Abbreviations:** PEEK/n-HA/CF, carbon fiber-reinforced polyetheretherketone–nanohydroxyapatite; Ra, average roughness; Rq, root-mean-square average roughness; XPS, X-ray photoelectron spectroscopy.

*Table 1.7 Surface roughness characterization [31]*

Results revealed better cell adhesion on the microroughed surface, compared to the smooth counterpart; in fact, roughened surface had a greater surface area offering more binding sites for adhesive protein that is an essential prerequisite for cell adhesion. [31]

Significant improvements in osteoblasts adhesion were detected in Group 1 over control and in Group 2 compared to Group 1; no statistical increase or decrease was found between Group 2 and Group 3, indicating that surface roughness at a greater level may not be favourable to cell adhesion (figure 1.8).

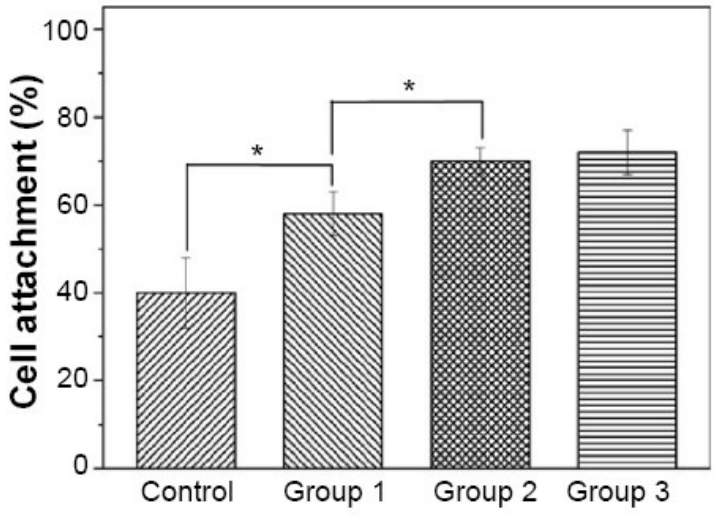


*Figure 1.8 - Cell adhesion at 4 hours. [31]*

In order to investigate the long-term cell responses, cell proliferation tests were carried out at 3, 7 and 14 days (figure 1.9). At 3 days no statistical differences among groups were detected. At 7 days results

showed that proliferation on the surface of Group 2 had the best viability; this indicates that cells prefer to proliferate on moderate microroughness, and that excessive surface roughness suppress cell proliferation. At 14 days cells on roughened surface showed lower proliferation, possibly because cells became differentiated. [31]

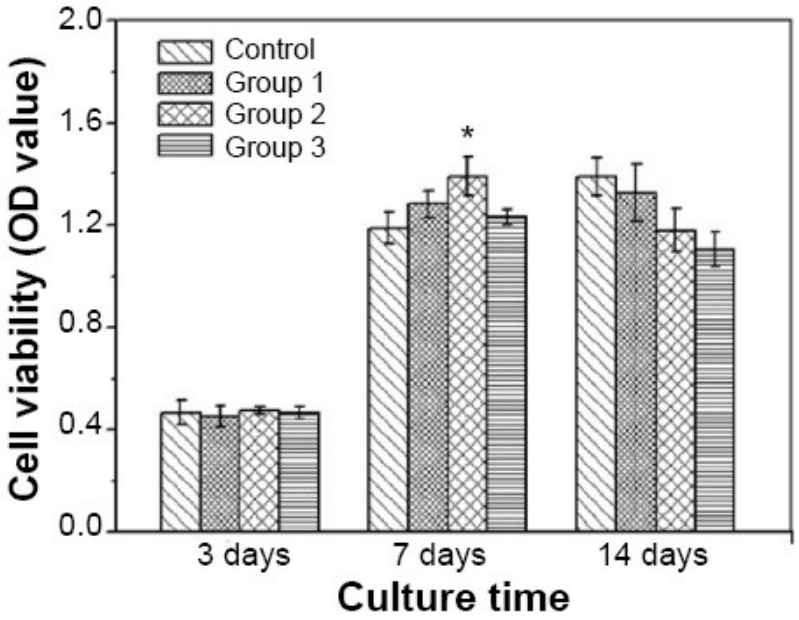


*Figure 1.9 - Cell proliferation rates at 3, 7 and 14 days. [31]*

## 1.6 BIOCHEMICAL FACTORS

Treatments with biologically active molecules, such as adhesion molecules and growth factors, are promising approaches to obtain bioactive surfaces able to induce specific cell/tissue responses [29]; however, these factors may have limitations such as instability, poor availability, and cost. [4]

### 1.6.1 Peptide Mimicry

Proteins play important roles in many biological processes, including enzymatic reactions, structural integrity of cells, organs and tissues, cell motility, immune responses signal transduction, and sensing [33].

Since the use of entire proteins is strongly limited by their costs, availability, and stability, a new technique has been developed, the peptide-mimicry. [29]

This strategy involves the individuation of peptides, protein fragments maintaining, totally or partially, the biological activity of the entire macromolecule. Peptides are more stable, since their bioactivity do not depend on tertiary structure, cheaper and simpler to synthetize and purify. [29]

Such molecules can be generated by means of chemical peptide synthesis; they can be generated as copies of protein fragments, as modified in order to increase their proteolytic stability. [33]

## 1.6.2 Self-assembling peptides (SAP)

Self-assembly is the ability of a molecule to spontaneously establish non-covalent interactions forming ordered 3D structures [34]. Self-assembly is commonly found in nature; examples of self-assembling in nature are phospholipid bilayer, which form cell membranes, vesicles, and organelle membranes in cells and bacteria, protein folding in enzymes and DNA double helix formation.

### *1.6.2.1 Conformation and 3D structure*

Self-assembling peptides (SAPs) are characterized by monomers of short amino acid sequences or repeated amino acid sequences assembling to form nanostructures. [35]

In aqueous environment, self-assembly is driven by non-covalent interactions, forming ordered nanometric or micrometric structures. Non-covalent interactions include Van Der Waals forces, electrostatic interactions, hydrophobic interactions, and hydrogen bonding; these forces are weak individually taken but strong enough to form robust structures.

Secondary structure of SAPs is β-sheet, obtained by the packing of monomers; this phenomenon is driven by the formation of hydrogen bond between the backbone of peptide chains. On the other side, lateral packing of β-sheet structure is regulated by inter β-sheet interactions between hydrophilic-hydrophobic side chains of the peptide (Fig 1.10) [34]. This way self-assembly creates aggregates that precipitates in form of hydrogels, extremely soft and water-enriched matrices.
β-sheet structures stack and form fibrils, giving origin to membranes.

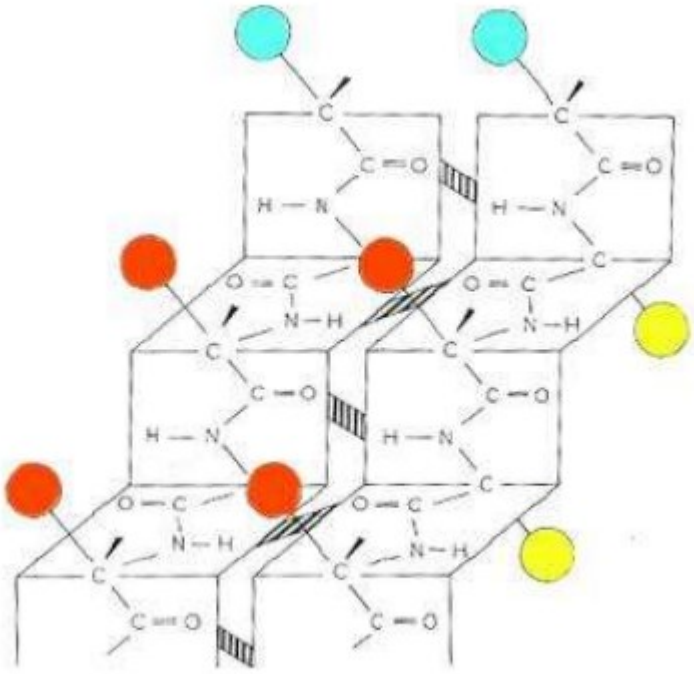

*Fig 1.10 β-sheet structure of SAP*

The peptide assemblies have different characteristics depending on their morphology, size, and accessibility of the reactive surface area.

Two main factor that influence peptides self-assembly are pH and temperature.

pH fluctuation affects the side chain charges through protonation and deprotonation; these changes disrupt the hydrogen bonds among residues and the ionic bonds between positively and negatively charged side chains of the amino acids. [35]

Peptides that self-assemble by temperature variations, once heated they form structures such as nanofibrils, micelles, and non-specific-aggregate-like network, depending on calcium concentration and pH of buffer. [35]

Some of the most common structures obtained are micelles, spherical, worm-like or disk shaped, vesicles, lamellar structures, and fibrillar structures such as fibrils or nanotubes (Fig 1.11).

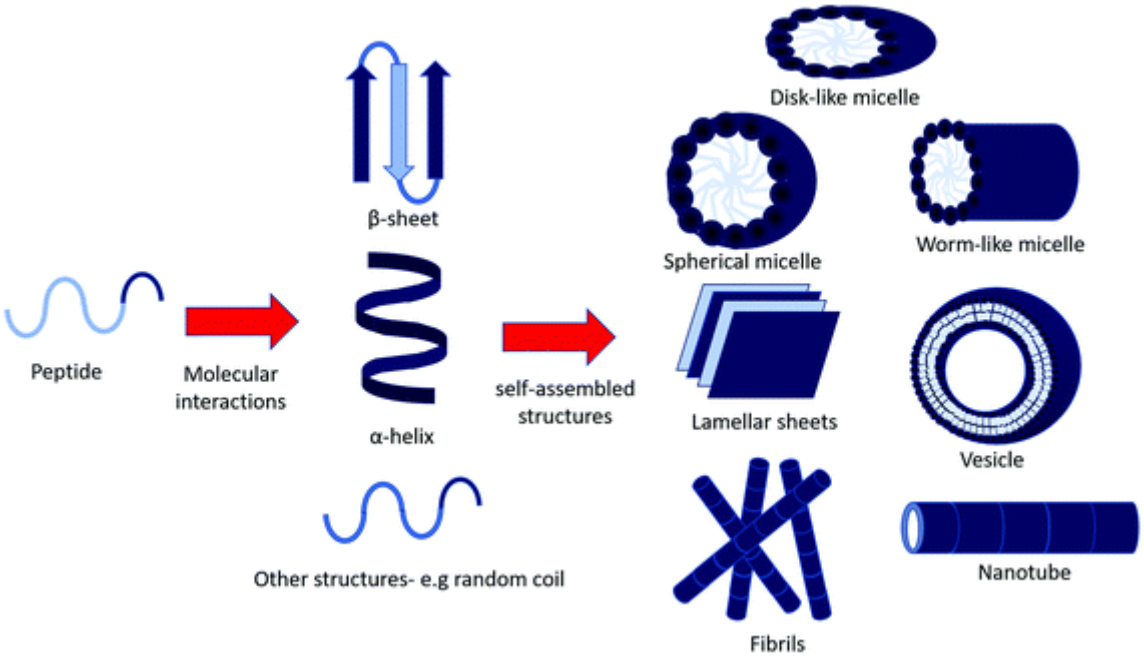


*Fig 1.11 Possible self-assembled structures*

### *1.6.2.2 Types*

Self-assembling peptides are categorized by the building blocks, which differ from the constituent amino acids and the various bound chains or motifs; on the basis of the type of building block, the main categories of self-assembling peptides surfactant-like peptides, amphiphiles peptides and ionic-complementary peptides. [34,35]

- Amphiphile peptide are characterized by a hydrophobic tail group usually given by an alkyl chain, a peptide sequence capable of intramolecular hydrogen bonding, a group of charged amino acids improving solubility and a bioactive peptide epitope (Fig 1.12). Self-assembling is driven by amphiphilicity above a critical aggregation concentration and forms monolayer or bilayer structures. [34]

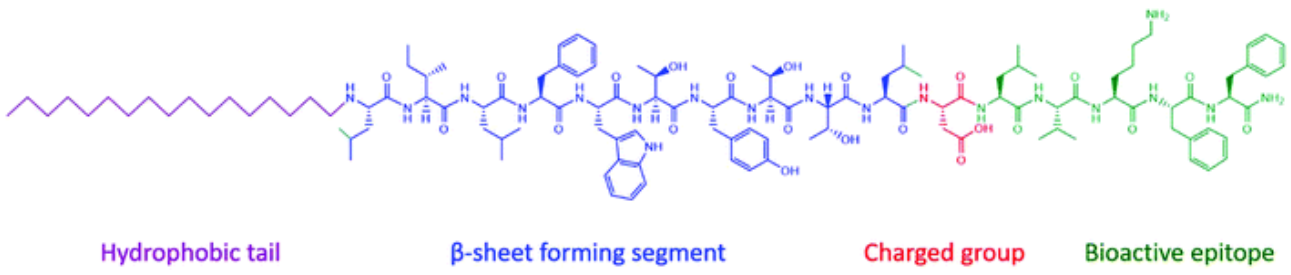


*Fig 1.12 Typical structure of a peptide amphiphile*

- Surfactant-like peptides contain sequence of hydrophobic and hydrophilic amino acids assembling in a similar way to peptide amphiphile. They can form layered structures like lipids and can be used to bind the hydrophobic part of membrane protein, preventing denaturation. [34]
- Ionic-complementary peptides are able to form membrane-like structures and show alternating arrangement of negatively and positively charged residues. Based on the charge distribution, ionic-complementary peptides can be distinguished in three types:
    - Type I: + − + −
    - Type II: + + − −
    - Type III: + + + − − −
    - Type IV: + + + + − − − −

EAK is an ionic-complementary SAP made by 16 amino acids; it is characterized by periodically repeating of positive and negative charges forming a β-sheet structure stabilized by ionic forces.

### 1.6.3 Adhesion factors

Cell adhesion occurs following two different mechanisms; the first is the interaction with RGD motif via cell membrane integrin receptors, the second is the interaction between cell membrane heparin sulphate proteoglycans and heparin binding sites on extracellular matrix proteins.

RGD sequence is an adhesive motif found in many proteins, including fibronectin, osteonectin and osteopontin, that are bone extracellular matrix proteins. Attachment of cells to RGD modified surfaces is nonspecific, since different types of cells have the same integrins and the affinity of integrins for the adhesion proteins are redundant.

Regarding the second mechanism of adhesion, heparin-binding sequences of amino acids, such as X-B-B-X-B-X and X-B-B-B-X-X-B-X (where X is a basic amino acid and X is a non-basic amino acid), have been searched in fibronectin, vitronectin and osteopontin, in order to identify adhesive proteins promoting proteoglycan-mediated mechanism of cell adhesion. [29]

### 1.6.4 Growth factors

Growth factors are proteins able to bind appropriate cell membrane receptors to induce, activate, and improve cell growth, proliferation and differentiation. [36]

There are different types of growth factors: fibroblasts growth factors (FGFs), insulin-like growth factors (IGFs) and TGF-βs, which includes BMPs. [36]

BMPs as secreted proteins are crucial for both many pathologies, such as obesity and diabetes, and physiological processes, such as bone metabolism. [37] In particular, BMP-2 demonstrated to be the protein with the best osteoconductivity among the BMPs.
Since BMP-2 is a complex protein made of 396 amino acids, it has been substituted with a peptide named GBMP1α, consisting of 22 amino acids. GBMP1α demonstrated to promote the differentiation of mesenchymal staminal cells to osteoblastic phenotype. [36]

## 1.7 BIOCHEMICAL FUNCTIONALIZATION

Biochemical functionalization is defined as a particular technique of surface modification involving the retention of biomolecules, such as peptides, proteins, bioactive drugs, or polysaccharides able to improve surface bioactivity. [29]

The retention of above molecules can be obtained using different methods, including adsorption, covalent bonding, and inclusion of bioactive molecules in a resorbable carrier. (Fig. 1.13)

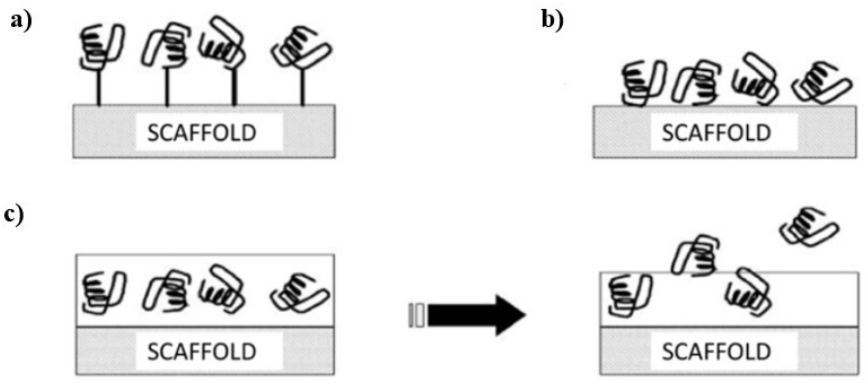


*Fig 1.13: a) adhesion through covalent bond in the presence of a spacer; b) superficial adsorption through weak interactions; c) biomolecule inclusion within a carrier*

### 1.7.1 Physio-adsorption

In adsorption, secondary bonds between surface and peptide are exploited; adsorption involves the immersion of the surface in a solution in which the molecules are dissolved; molecules will be spontaneously adsorbed on the surface. However, this method does not allow a proper control over the quantities of adsorbed biomolecules. Additionally, the secondary bond can be easily disrupted, causing the presence of biomolecules in solution and, consequently, inhibition of cell adhesion.

### 1.7.2 Inclusion of biomolecules in a resorbable carrier

Inclusion of biomolecules in a resorbable carrier is based on the inclusion of biomolecules within a carrier that allows the transport and release according to kinetics that depend on the characteristics of the biomolecules, the carrier, and the mode of inclusion: the molecules can be either encapsulated or bound chemically bound to the carrier. The characteristics of the carrier must be precise: it must be biocompatible, biodegradable, and bioresorbable. The most commonly used materials in the creation of carriers are polymeric materials, such as hyaluronic acid and copolymers of PLA and PGA.

### 1.7.3 Covalent bonding

Covalent bonding is the most stable among the functionalization techniques. A chemical bond is formed, allowing the anchoring of biomolecules on the material surface.

The bonding can be direct or achieved through the introduction of a spacer between the molecule and the material: this promotes exposure of the molecule to the cells and increase the degrees of freedom of the biomolecule.

Covalent functionalization allows for a better control over the molecule's orientation, binding stability, and surface density than other methods.

Usually, molecules tend to bound randomly to the surface of the material (nonspecific binding), so it is not possible to determine if a molecule will be recognized because the side chains that contact the receptor may be engaged in surface binding (Fig. 1.14)

*Fig 1.14 – Aspecific covalent functionalization (left) and specific covalent functionalization (right)*

This issue has been solved by specific covalent immobilization techniques (specific binding) by which all molecules are able to bind the surface using the same functional group with consequent ability to present the same active site to cells. To reach this issue the techniques used are photoactivation, reversable selective protection, and introduction of a functional group.

Photoactivation involves the introduction in the aminoacidic sequence of a group activable through UV light, guaranteeing selectivity of chemic reaction and specific binding.

Reversable selective protection involves the use of protector groups that inactivate functional groups potentially reactive, except for the group that will be used for binding. The bonding of these protector groups is reversible, so that they can be removed.

The introduction of a functional group, not present in the original structure of the molecule, will allow the bonding with the surface of the material.

In this thesis, the spacer 7-aminoheptanoic acid has been used to separate the functional group of the peptide and the bioactive sequence.

### 1.7.4 Chemoselective ligation via oxime

Chemoselective ligation involves a selective reaction between a group of the peptide and another specific group, located in a protein, in another peptide, or in a synthetic scaffold. This technique is often employed for the creation of peptide conjugates and the condensation of unprotected peptide fragments.

Such an approach can take place via oxime ligation, a highly efficient strategy not requiring pre-activation or stabilization steps. [39,40]

Oxime ligation is a typical example of the so-called “click chemistry”, an approach defined for the first time by Sharpless et al. that involves the building of complex substances starting from simple molecules, following nature’s examples. A reaction can be considered an example of click chemistry if it fulfills a few criteria: it must be “modular, wide in scope, give very high yields, generate only inoffensive byproducts that can be removed by nonchromatographic methods, and be stereospecific” [41].

Oxime ligation involves a conjugation between an aldehydic or ketonic group with an aminooxy group. To obtain such a ligation, it is first necessary to bound an aminooxy group at N-terminus of the bioactive sequence synthesized with Solid Phase Peptide Synthesis method (SPPS) [42].

Compared to primary ammines, the reactivity of aminooxy groups with carbonyl groups is significantly higher, and the formed oximes have the advantage of being highly stable to hydrolysis [43].

In this work, chemoselective legation via oxime was used to bind the N-terminus of Aoa-x-EAK and Aoa-x-GBMP1α to ketonic groups of PEEK.

### 1.7.5 Peptides and methods for PEEK functionalization

Previous studies investigated the effect of functionalizing PEEK with different peptides and different methods of functionalization.

In the paper of Cassari et al., PEEK disks were covalently functionalized via oxime with: (i) an adhesive peptide reproducing [351–359] h-Vitronectin sequence (HVP) and (ii) HVP retro-inverted dimer (D2HVP), that combines the bioactivity of the native sequence (HVP) with the stability toward proteolytic degradation. In this study PEEK functionalized with D2HVP showed the best cell viability and the best results in proliferation tests. However, calcium ion deposition of D2HVP-functionalized PEEK did not show a significant increase compared to non-functionalized PEEK [44].

In another study [45], the sequence (48–69) mapped on the BMP-2 growth factor (GBMP1α) was covalently grafted at PEEK surface employing two different strategies: (i) oxime chemistry and (ii) the photoactivation of azido groups present in the peptides’ N-terminal sites, which produces nitrene radicals able to react with PEEK surface. In this case, no major difference in the outcome of functionalization with the two strategies was detected; both increase proliferation at 1 day and both increase mineralisation at 21 days although photoactivation increases mineralization by 11% compared to oxime chemistry. However, oxime ligation is a highly efficient strategy not requiring

pre-activation or stabilization steps while (ii) is more versatile since the photoactivated azido group can react with different groups of the PEEK's surface but is more complex, since it requires photoactivation. [45]

Based on considerations above, in a previous thesis work [44, 45] PEEK was covalently functionalized via oxime formation with bioactive sequences HVP and GBMP1α and with EAK, a self-assembling peptide. Results showed that EAK-functionalized PEEK had the best results in calcium deposition assays and that both EAK and GBMP1α-functionalized PEEK significantly increase osteoblast proliferation at 7 days.

Consequently, in this thesis, a mixed functionalization of PEEK surface with both EAK and GBMP1α was chosen, using the oxime formation technique.

## 1.8 AIM OF THE THESIS

PEEK is a promising synthetic material for bone applications due to its biocompatibility, resistance to thermal radiation, and mechanical properties similar to those of bone tissue. However, PEEK is biologically inert, limiting osteointegration with bone tissue.

The aims of this thesis were (i) investigate the role of PEEK disks surface roughness in osteoblast proliferation and (ii) improve the bioactivity of PEEK, using more than one bioactive peptide.

Three different surfaces of increasing roughness were analysed: one smooth surface obtained with lapping technique and two sand-blasted surfaces with increasing grit dimensions were tested.

In order to increase the bioactivity of PEEK, the surface with the preferred roughness to the cells was identified and functionalized with both EAK and GBMP1α, using the oxime formation technique.

# CHAPTER 2
# MATERIALS AND METHODS

## 2.1 MATERIALS

Columns:

- Nova-Pak HR C18 (4 μm, 60 Å, 3.9 x 300 mm, Waters) for purification purposes
- Zorbax 300SB C18 (5 μm, 300 Å, 9.4 × 250 mm, Agilent) for purification purposes
- Vydac C18 218TP54 (5 μm, 300 Å, 4.6 x 250 mm, Grace) for analytic purposes
- Nova-Pak C18 (4 μm, 60 Å, 3.9 x 300 mm) for analytic purposes

Reagents purchased from *Merck Millipore* (Burlington, Massachusetts, United States):

- 7-amino heptanoic acid, Fmoc protected;
- Acetic Acid (AcOH);
- Acetone;
- Acetonitrile;
- Amino acids used;
- Bis-Boc-aminooxy acetic acid (Bis-Boc-Aoa);
- Dichloromethane (DCM);
- N,N-Diisopropylethylamine (DIPEA);
- N,N-dimethylformamide (DMF);
- Ethyl cyano(hydroxyimino)acetate (Oxyma Pure);
- Methanol;
- Rink-Amide MBHA resin;

- Triethylsilane (TES);
- 2-(1H-benzotriazol-1-yl)-1,1,3,3-tetramethyluronium hexafluoro phosphate (HBTU)

Reagents purchased from *Biosolve* (Valkenswaard, Holland):

- Diethyl ether;
- Trifluoroacetic acid (TFA).

Reagents purchased from *PanReac AppliChem* (Darmstadt, Germany):

- 2-Propanol (isopropanol) for HPLC

Reagents purchased from *Carlo Erba* (Milan, Italy):

- Ethanol.
- Sodium phosphate monobasic.

Reagents purchased from *Iris Biotech GmbH* (Marktredwitz, Germany):

- N-Methyl-2-pyrrolidone (NMP).

Kaiser Test reagents purchased from *Applied Biosystem* (Perkin-Elmer, Waltham, MA, USA):

- Monitor 1: Phenol solution, 76% (w/w) Phenol/Ethanol;
- Monitor 2: Potassium cyanide solution, 0.2 mM KCN/Pyridine;
- Monitor 3: Ninhydrin solution, 0.28 M Ninhydrin/Ethanol.

Material from *King's College* (London, United Kingdom):

- PEEK disks: diameter 1 cm, width 0.4 cm (Figure 2.1)

*Figure 2.1 - PEEK disk*

Material purchased from *Sigma-Aldrich:*

- Papain (from papaya latex EC 3.4.22.2)

## 2.2 LABORATORY INSTRUMENTATION

Synthesizer Syro I (MultiSynTech, GmbH, Witten, Germany) (Figure 2.2):

*Figure 2.2 – Synthesizer Syro I (MultiSynTech)*

Spectrophotometer UV/Vis model Lambda 2 (Perkin-Elmer) for piperidine and ninhydrin tests (Figure 2.3):

*Figure 2.3 – Spectrophotometer UV/Vis Lambda 2 (Perkin-Elmer)*

Mass analyses were performed at the Department of Chemical Science and at the Department of Pharmaceutical Science (University of Padua). MALDI-TOF (MALDI-TOF 4800 Plus, AB SCIEX) instruments was used.

For chromatographic analysis, two chromatographic systems were used:

- HPLC Waters 600 Controller (Figure 2.4), coupled with UV/Vis multichannel detector, model 2487, with programmable wavelength. Data acquisition is carried out with a recorder, model BD40/BD41, obtained from Carlo Erba Strumentazione and produced by Kipp&Zonen (Delft, Holland).
- HPLC Waters 1525 Binary Pump (Figure 2.5) coupled with Waters 2707 autosampler and UV/Vis multichannel detector, model 2498, with programmable wavelength. Empower Pro software (Waters, Milford, MA. U.S.A) has been used to obtain chromatograms and data integrations.


*Figure 2.4 – HPLC Waters 600 Controller (Waters)*

*Figure 2.5 – HPLC Waters 1525 Binary Pump with Waters 2707 autosampler and UV/Vis multichannel detector, model 2498*

FreeZone 2.5 Liter Benchtop freeze dryer (Labconco, Kansas City, Missouri, USA) for lyophilization (figure 2.6):


*Figure 2.6 – Freeze dryer (Labconco)*

Rotary evaporator (Laborota 4100-Efficient, Heidolph Instruments s.r.l., Milan, Italy) (Figure 2.7):

*Figure 2.7 – Rotary evaporator (Laborota 4100-Efficient, Heidolph Instruments s.r.l., Milan, Italy.*

## 2.3 METHODS

### 2.3.1 Solid Phase Peptide Synthesis

In order to synthesize the peptides for this thesis work, SPPS was employed. SPPS is a technique that involves the use of a solid support made of an insoluble resin, to which peptides are bound (*coupled*) in succession.

Introduced in 1963 by Bruce Merrifield [46], it consists in four different steps:

1. Coupling of the first amino acid of the chain with a solid polymeric resin through a covalent bond between the resin and the carboxyl end of the amino acid.
2. Removal of the protecting group, generally obtained with piperidine.
3. Anchoring of the N-end of the resin-bound peptide with the C-end of another amino acid through a condensation reaction. Steps 2 and 3 are repeated until the desired peptide sequence is obtained.
4. Removal of the peptide from the solid support.

A schematic representation of the aforementioned process is shown in Figure 2.8.

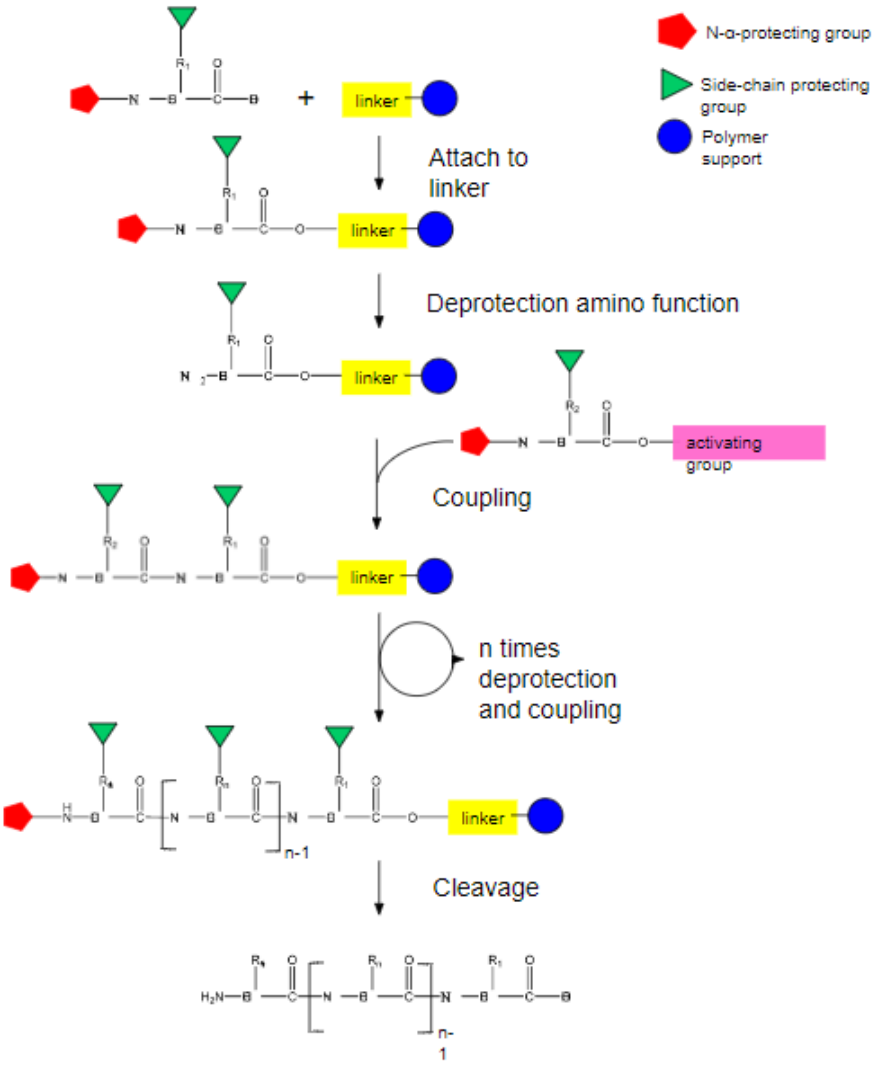


*Figure 2.8 – Schematic representation of a SPPS process*

SPPS, along with liquid phase peptide synthesis (LPPS), is one of the main techniques for the artificial production of peptides in scientific research and in pharmaceutical/commercial sector. However, unlike LPPS, SPPS has the advantage of an insoluble solid matrix; this solid support allows us to isolate the growing peptide at each reaction step, so the whole process can take place in a single reactor. This allows high automation of the process and less handling of the reagents.

There are two possible strategies for the protection of the amino functional group and the side chains:

- Boc chemistry
- Fmoc chemistry

In Boc chemistry, the amino functional group is protected with terz-butossicarbonyl group (Boc), that is removed with mildly strong organic and inorganic acids, for example with TFA. The side chains'

protection is obtained with ether, ester and urethan groups. These groups are stable in Boc removal conditions and are instead removed by hydrofluoric acid.

In the case of Fmoc chemistry, developed by Carpino *et al*. and used for this thesis project, the amino acids for SPPS are protected on the α-aminic group with the base-labile group 9-Fluorenylmethoxycarbonyl (Fmoc) [47] [48]. On the reactive functional groups of the side chains other more stable, acid-labile protecting groups are present: these are necessary to avoid undesired reactions that could create bonds different from the α-amidic ones in the backbone. Temporary α-aminic protecting groups are removed in every step of peptide growth. In fact, each SPPS cycle involves at first the deprotection of the amino functional group with 40% piperidine solution in DMF for 3 minutes, then a condensation between the free amino group on the resin and the carboxyl group of the new amino acid introduced. This last step is called coupling, and it can be repeated in order to maximize the reaction yield; for example, in this thesis work a double coupling was performed. The reaction yield can also be monitored through a ninhydrin test, that assesses a quantitative percentage of the yield. At the end of the synthesis all the side chain protecting groups are removed using TFA, and the peptide is cleaved from the resin support.

The selection of the resin depends on the type of chemistry used in the synthesis and on the type of peptide desired. Usually, polymer-based resins are used: these resins swell when in contact with aprotic polar solvents like DMF, NMP and DCM. Different types of resins are available commercially, with a wide variety of linkers or with the C-terminal amino acid already attached. During this thesis project we used the Rink-Amide MBHA resin, shown in Figure 2.9.

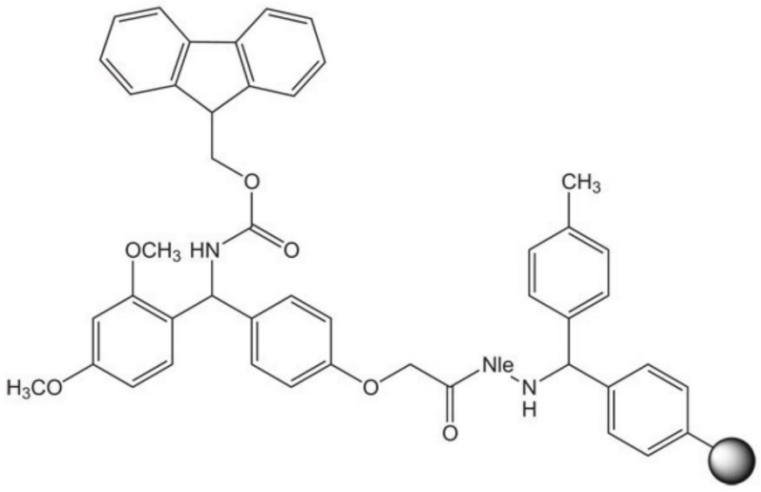


*Figure 2.9 – Structure of Fmoc-protected Rink-Amide MBHA resin*

### 2.3.2 Piperidine test

The piperidine test is an assay that is performed to quantify the anchoring yield of the first amino acid to the resin after the first coupling. It is an assay that uses spectrometric quantification of the N-(9-fluorenylmethyl) piperidine product at 301 nm. This product is obtained as a result of Fmoc deprotection.

The procedure performed is listed below:

- The resin, after the first coupling, is washed with 2/3 washes of DCM, to remove organic solvent residues, and is dried in a vacuum bell for at least 1h.
- Two solutions of 50 ml each are prepared. The first solution is called White and it is the control. It contains 0.5 ml of the solution 20% of Piperidine in DMF; it is then brought to volume using DMF. The second solution is the one containing the resin; 4 mg to 8 mg of dry resin are taken and placed in a test tube. 0.5 ml of the 20% Piperidine solution in DMF is then inserted and allowed to react for 15 min. At the end of the time, DMF is inserted, up to about half of the test tube, to stop the reaction. DMF is added until solution is brought to volume (50 mL).
- With the solutions ready, two cuvettes are taken and filled with the *White*. These cuvettes are used for analysis in the spectrophotometer. This must be set at a wavelength of 301 nm. The cuvettes are inserted, and the spectrophotometer is set to zero. One cuvette will remain inside and will be used as a reference for the next reading, the other needs to be washed and dried and will be filled with the second solution.
- Cuvette is filled with the second solution being careful not to pick up the resin. Spectrophotometer will return the absorbance value.
- The experimental substitution is calculated:

$$Experimental\ substitution = \frac{Abs(301\ nm) \cdot Vol}{\varepsilon \cdot W}$$

Where:

- $Abs(301\ nm)$ is the value of absorbance at 301 nm.
- $Vol$ [50 ml] is the volume of the solution.
- $\varepsilon = 7800\ [M^{-1}cm^{-1}]$ is the molar extinction coefficient.

- $W$ [g] is the weight of the resin.

Theoretical substitution is calculated:

$$Theoretical\ substitution = \frac{1}{MW_{resin} + MW_{amino\ acids}}$$

Where:

- $MW_{resin}$ is the molecular weight of the resin, obtained by $MW_{resin} = \frac{1000}{resin\ substitution}$
- $MW_{amino\ acids}$ is the molecular weight of the amino acid with protector groups.

Reaction yield can be calculated:

$$Yield\% = \frac{Experimental\ substitution}{Theoretical\ substitution} \cdot 100$$

A percentage above 97% is considered a good result.

### 2.3.3 Ninhydrin test

The ninhydrin test, or Kaiser test, is a qualitative and quantitative test that evaluates the coupling yield of a synthesis reaction by detecting free amino groups in the peptide chain.

The procedure used in this thesis project was the following:

- A certain amount of resin, in a range from 2 to 8 mg, was picked up and put in a test tube;
- The test tube with the resin was filled with the following solutions: 100 µl of monitor 1, 75 µl of monitor 2, and 100 µl of monitor 3. In another empty test tube the same solutions were poured in the same order: this sample is the reference (control) of the test;
- Both test tubes were placed in a laboratory block heater at 100°C for 5 minutes;
- Once the test tubes were removed from the heater, 4.8 ml of monitor 4 were rapidly added, to block the reaction. If the solution, after some time, changes colour into blue or purple, it is an index that there are a lot of free aminic groups, so probably the reaction yield will be low;
- Two cuvettes with only monitor 4 were placed in the spectrophotometer at 570 nm for the back correction; one of the two cuvettes was then removed and replaced with a cuvette containing the control solution. The absorbance was therefore registered;

- The test tube with the resin was centrifugated and the supernatant was moved in a cuvette that replaces the one with the control in the spectrophotometer. The absorbance was registered again.

A qualitative indication of the coupling yield is obtained by observing the colour intensity of the solution, as described before. The quantitative measurement is instead obtained by the below reported formula:

$$\frac{\mu mol}{g} = \frac{\Delta \mathrm{Abs} \cdot \mathrm{V} \cdot 10^6}{\varepsilon \cdot P}$$

Where:

- $\Delta \mathrm{Abs}$ is the difference of absorbance between the sample with the resin and the control;
- V is the volume of the mixture (in ml);
- ε is the coefficient of molar extinction equal to 15000 $M^{-1}cm^{-1}$;
- $P$ is the sample weight (in mg).

The coupling efficiency is given by:

$$Yield\% = \left\{ 1 - \left[ \frac{\frac{\mu mol}{g}_{\ amino\ groups}}{new\ substitution \left[\frac{\mu mol}{g}\right] \cdot 10^3} \right] \right\} \cdot 100$$

Where $new\ substitution$ is the new resin substitution, obtained by:

$$new\ substitution = \frac{1000}{MW_{growing\ peptide}}$$

And $MW_{growing\ peptide}$ is obtained by the sum of the resin's molecular weight with the molecular weight of all the amino acidic residues.

$$MW_{resin} = \frac{1000}{substitution}$$

A percentage above 97% is considered a good result.

### 2.3.4 Cleavage

When in SSPS an acid-labile resin is used, it is possible to cleave both the peptide and the side chain protecting groups from the resin at the same time. The cleavage procedure takes place in acidic environment with the help of some nucleophilic reagents called *scavengers*, that have similar properties as the species that we want to protect.

In this project, the cleavage was performed with the subsequent procedure:

- The resin is washed with DCM to remove DMF and dried under vacuum for 1 hour;
- The resin is treated with 0.125 ml of MilliQ water, 0.125 ml of TES and 4.75 ml of TFA, then left to react for 1.5 hours. At the end of the reaction, the mixture is washed with TFA;
- The liquid obtained is put in a rotary evaporator and reduced to a small volume;
- The peptide is precipitated with cold diethyl ether under magnetic stirring, then it is filtered with a Gooch 4 and dried under vacuum for 1 hour.

### 2.3.5 Mass spectroscopy

Mass spectroscopy (MS) is a destructive analysis method that allows to measure the molecular weight of unknown substances, thus recognizing their structural formula.

Before the mass analysis, a molecule must be ionized, then the gas ions can be separated, in time or space, on the basis of their mass/charge ratio (m/z). The sample is ionized in a special chamber, called ionization chamber, thanks to the impact with an electron, atom, ion, or photon beam. Some ionization techniques operate at high energy levels and cause a high fragmentation (hard techniques), while some others operate at low energy and produce a lesser number of ions (soft techniques).
The ionization techniques can be divided by the source used.

In this project, Matrix Assisted Laser Desorption Ionization (MALDI) technique was employed.

MALDI technique consists in hitting a sample soaked in a matrix with a laser beam. The laser beam hits the matrix molecules, that absorb the ultraviolet light, switch to an excited status, and heat the close area. The solvated analyte is separated from the matrix molecules, and then it is de-solvated, causing a proton transfer (acid-base reaction between the analyte and matrix molecules, Figure 2.10).

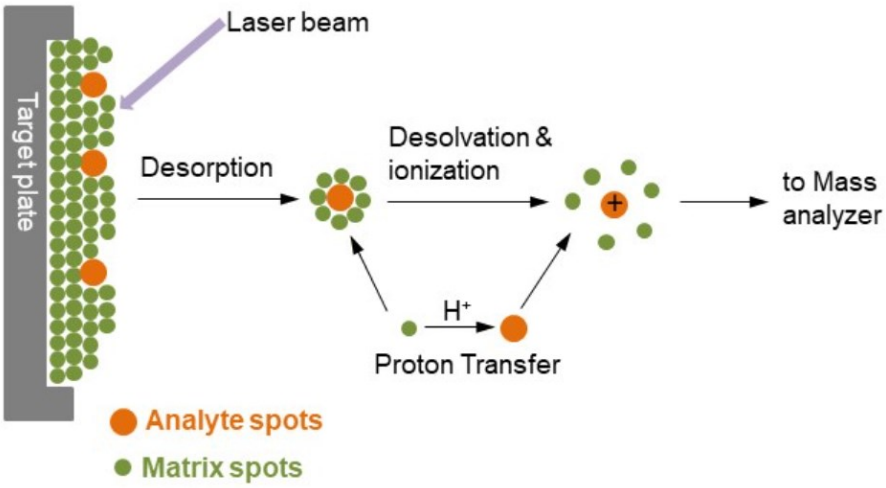


*Figure 2.10 – MALDI ionization process*

After the sample ionization, the signal measurement is performed using a Time of Flight (TOF) analyzer. The principle is that different m/z values have the same kinetic energy but different speed after ionization: this means that the time spent crossing the analyzer is different for every ion. So, the ions from the source are accelerated by a strong electric field and they cross with different speeds the analyzer, that works under vacuum without any electrical or magnetic fields. This analyzer measures mass values with a high sensitivity. [49]

### 2.3.6 Chromatographic purification and characterization

The purification and characterization of the different peptides synthetized in this thesis work was conducted with a Reverse Phase-High Performance Liquid Chromatography (RP-HPLC).

Chromatography is a chemical-physical approach that relies on the equilibrium between two different phases, one stationary, made of a gas or a liquid on a solid support, and one mobile, made of a gas, a liquid, or a supercritical fluid. The sample is dissolved in the mobile phase and flows continuously through the immiscible stationary phase. The components with the most affinity to the stationary phase are retained for a considerable amount of time, while the others with less affinity move faster. In this way, different components of the sample are separated and analysed or collected. In liquid chromatography, the mobile phase is a liquid, while the stationary phase can be a solid or another immiscible liquid. An evolution of classic liquid chromatography is HPLC, where columns filled with functionalized silica gel are employed.

The RP HPLC is a partition chromatography where the stationary phase is non-polar, and the mobile phase can be a mixing of different percentage of water and organic solvents (in this particular case, isopropanol). For the stationary phase, columns containing silica gel functionalized with linear, 18 C atoms hydrocarbon chains were used.

The interaction which allows the retention of peptides in the stationary phase is a hydrophobic one. The chromatography can be performed in "isocratic mode" or in "gradient mode". In the latter case, increasing the organic solvent concentration leads to an increase in the mobile phase hydrophobicity. This leads to a competition between the two phases, so the analyte is de-adsorbed at a specific percentage (concentration) of the organic solvent.

Generally, peptides are better separated in acidic environment, so most of the mobile phases includes low concentration of TFA (0.05% in our case).

In this thesis work, analyses were performed using 0.05% TFA in MilliQ water and 0.05% TFA in 40% isopropanol and 60% MilliQ water as eluents. Usually, 0.05% TFA in acetonitrile is used instead of isopropanol-based eluent, but aminooxy-acetylated peptides showed a high reactivity to ketones [50], that are commonly in HPLC-grade acetonitrile as contaminant: so, an eluent change was necessary.

A UV-spectrophotometer detector is placed at the column output, with a wavelength ($\lambda$) of 214 nm, which is the peptide bond's absorption peak.

Semipreparative HPLC analysis allows the isolation and purification of compounds starting from a mixture, while analytic HPLC is used to obtain information on a sample, for example the identification and characterization of a peptide. Once the chromatographic conditions (column, mobile phase, and gradient) are fixed, the retention time represents a fingerprint of the molecule. The area under the peak is directly proportional to the injected sample amount. So, by integrating all the chromatogram peaks, it is possible to evaluate the homogeneity grade of the purified product.

### 2.3.7 PEEK disks lapping

The term "lapping" is used to describe a number of various surface finishing operations where loose abrasive powders are used as the grinding agent at normally low speeds. It is a process reserved for products that demand very tight tolerances of flatness, parallelism, thickness, or finish.

Loose Abrasive Process (LAP) (figure 2.11) involves the use of abrasive particles to modify the workpiece. Abrasive particles are mixed with a water-based or oil-based liquid; the combined

abrasive and liquid are called slurry. Slurry is placed on a rotating motorized platform called lap plate; then the workpiece is placed against the slurry on the lap plate to modify its surface through rolling/sliding action of abrasive grains.

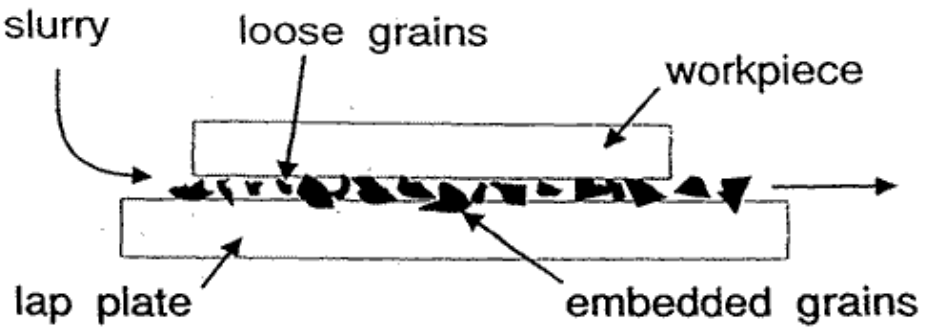


*Figure 2.11: lapping scheme*

In this work, lapping technique was used to smooth the originally patterned surface of PEEK disks.

### 2.3.8 PEEK disks sandblasting

In this project a dental sandblaster (Emmevi Apparecchi Dentali, Settimo Milanese, Italy) has been used to modify the surface roughness of PEEK disks.

Sandblasting is a mechanical process by which the superficial part of a material is eroded through abrasion, obtained through a high-speed stream of aluminium oxide particles propelled by compressed air.

The PEEK disks were kept at a distance of 2-3 cm from the compressed air outlet, which was kept constant by means of a manual controller. Each disk was held in the blasting machine for approximately 10 seconds.

### 2.3.9 Digestion with Papain

Disks that had been previously functionalized and/or seeded with osteoblasts for tests were subjected to digestion with papain, a proteolytic enzyme belonging to the class of hydrolases, which catalyses hydrolysis of proteins, in order to degrade the peptide and free any cellular residual.

Disks were suspended in final 0.1 M sodium acetate buffer (15 mg wet weight/mL) and 5 mM ethylenediamine tetra-acetic acid (EDTA) at pH 6.0; papain (from papaya latex (EC 3.4.22.2), Sigma-Aldrich) was added in concentration 2.8 mg/mL. Disks were maintained at 60°C for 48 h under periodical agitation. [51]

Disks were then washed 3 times with sodium acetate-EDTA buffer and 3 times with MilliQ water.

### 2.3.10 Scaffold functionalization

As described in paragraph 1.7.5, various peptides and methods for PEEK functionalization were tested. The simplest but also effective method proved to be functionalization via oxime formation. The peptide that achieved the best overall results in biological tests was GBMP1α, which, however, being a hydrophobic peptide, does not contribute to making the surface of PEEK more hydrophilic. On the other hand, the functionalization with peptide EAK was shown to make the surface of PEEK much more hydrophilic, also performing well in biological tests.

For these reasons in this thesis work, PEEK scaffolds were covalently functionalized with both the peptides obtained by SPPS, to investigate the synergetic effect of the contribution of both peptides.

The linkages between the aminooxy group at the end of the peptide chain and ketonic groups in PEEK surface are realized by means of chemoselective ligation via oxime.

PEEK is a highly hydrophobic polymer, insoluble in conventional solvents, thus the need to improve its solubility by the use of organic solvents for functionalization. Dimethylformamide (DMF), dimethylsulphoxide (DMSO) and acetonitrile (ACN) are widely used as solvents or co-solvents with water. Recently, many oxime ligation protocols have involved acetic acid (AcOH), both as a buffer component and as an acidic co-solvent. [52]

Following the indications of Liu et al. [53], the solution for functionalization employed was DMSO with one equivalent of AcOH. The advantages of the solvent AcOH/DMSO were assessed comparing the functionalization with the technique that employs MilliQ water.

All the details about scaffold functionalization for this project are provided in paragraph 3.2.

### 2.3.11 X-ray photoelectron spectroscopy

X-ray photoelectron spectroscopy (XPS) is a quantitative analysis that relies on the photoelectric effect to identify the elements that cover the surface of a sample and their properties.

XPS instrument uses metallic anodes as X-ray sources; these anodes are exposed to electrons characterized by an elevated energy. The ionization of the core level of the metal atom causes an X-ray release by the metal anodes. The sample is irradiated by the X-rays produced and emits photoelectrons. In fact, in the photoelectron effect when a material is hit by an electromagnetic radiation with an adequate energy content, the atom's electrons can be emitted.

Irradiation by photons with an energy $h\nu$ produces an electron that has a kinetic energy (KE) equal to the photon's energy minus the bond energy of the atom and minus the work function:

$$KE = h\nu - BE - \Phi$$

By measuring the KE of the expelled electron, it is possible to trace its energy of linkage, which is indicative of the chemical element involved, so, by analysing the photoemitted electrons' spectrum, it will be possible to determine which elements are present on the sample surface.

XPS spectrum is composed by a series of peaks:

- Core level emission peaks, distinctive of the energetic levels of an atom's inner shells. They have a bond energy which is higher than 20 eV.
- Valence level emission peaks, which have less intensity than core peaks. These peaks derive from external energy levels of electrons and have a bond energy lower than 0.3 KeV.
- Auger emission peaks, caused by electrons emitted from the material due to an internal relaxation process. These peaks are typical of the material considered and appear in the low KE region.

A representation of the XPS equipment is shown in Figure 2.12.

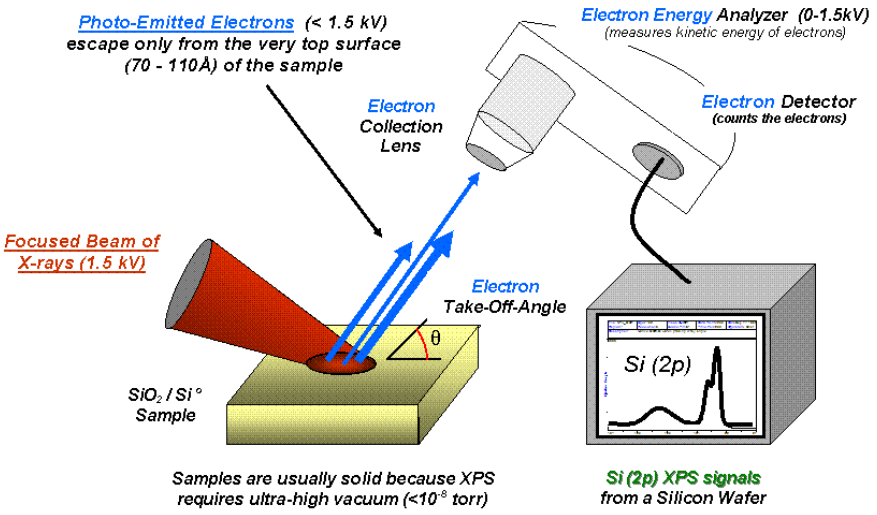


*Figure 2.12 – XPS equipment*

In this work, XPS analysis was conducted in collaboration with the University of Rome Tre (Professor Giovanna Iucci). As described by Professor Iucci's report, XPS analysis was performed with a homemade instrument, consisting of a preparation and an analysis UHV chambers, separated by a gate valve. The analysis chamber is equipped with a six-degree-of freedom manipulator and a 150 mm mean radius hemispherical electron analyser with a five-lens output system combined with a 16-channel detector giving a total instrument resolution of 1.0 eV as measured at the Ag $3d_{5/2}$ core level. Samples were introduced in the preparation chamber and left outgassing overnight at a base pressure of about $10^{-8}$ Torr, before introduction in the analysis chamber. Typical vacuum pressure in the analysis chamber during measurements was in the $10^{-9}$–$10^{-10}$ Torr range. The used X-ray radiation was a non-monochromatized Mg Kα (1253.6 eV).

## 2.3.12 Water contact angle

Water contact angle (WCA) is a thermodynamic quantity determined by the measure of a surface's wettability (Figure 2.13). The concept of wettability describes the ability of a liquid to wet completely or partially the surface in which it is settled. A surface characterized by a high wettability is called hydrophilic, and has a WCA that is less than 90°, while a surface with a low wettability is hydrophobic, and has a WCA higher than 90°. Hydrophilic scaffolds tend to react easily with water due to the presence of polar functional groups, while hydrophobic scaffolds tend not to react with water.

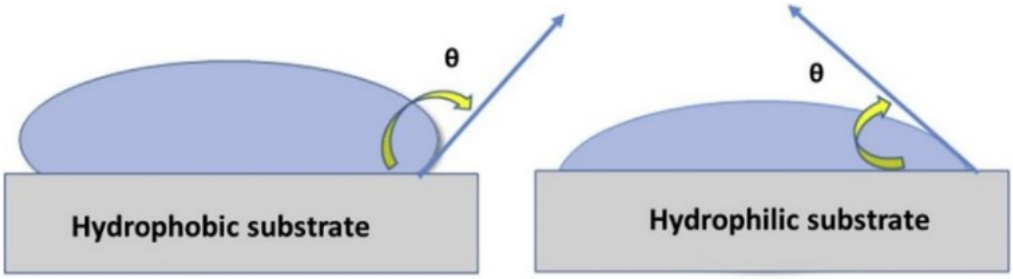


*Figure 2.13 – Contact angle for a hydrophobic surface (left) and a hydrophilic surface (right)*

The contact angle is the internal angle between liquid-vapor interface and solid-liquid interface (Figure 2.14).

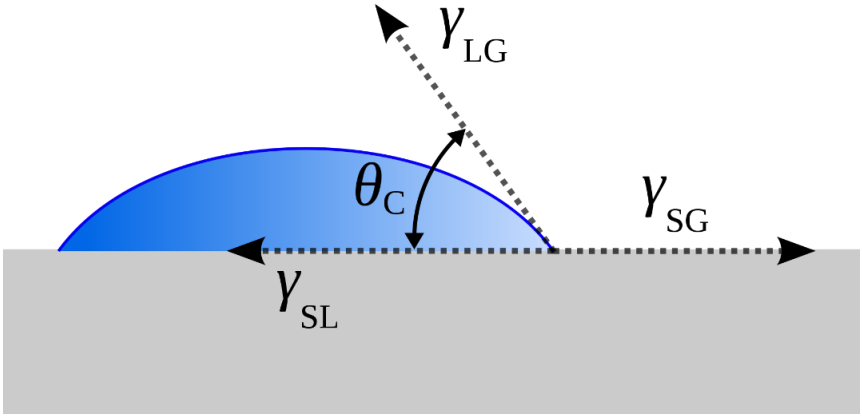


*Figure 2.14 – Contact angle ($\theta_c$) between a liquid droplet and a solid surface*

WCA is linked to surface tension γ, which is the quantity of free energy observed on the surface of a material, so it is possible to determine the wettability of a surface by using γ values. A less wettable material has a higher contact angle and surface tension. The contact angle is described by Young's equation:

$$cos\theta_c = \frac{\gamma_{SG} - \gamma_{SL}}{\gamma_{LG}}$$

This equation represents the thermodynamic equilibrium of a drop under the activity of three interfacial tensions, namely the tension between solid and vapor ($\gamma_{SG}$), the tension between solid and liquid ($\gamma_{SL}$) and the tension between liquid and vapor ($\gamma_{LG}$). Young's equation is valid on the hypothesis that the scaffold's surface is stiff, flat, non-reactive, inert, homogeneous, insoluble, smooth and non-porous (ideal surface).

WCA measurements in this thesis work were performed in the laboratory of the Department of Chemical Sciences of Catania, in collaboration with Professor Giovanni Marletta.

### 2.3.13 Force Spectroscopy (FS) Analysis

FS analysis was conducted on non-functionalized and functionalized PEEK at room temperature to investigate the impact of peptides on the mechanical properties of interfaces. The Young modulus was determined from the force–distance curves collected using an NTEGRA Atomic Force Microscope (NTE-AFM, NT-MDT, Moscow, Russia) and stiff single-crystal silicon cantilevers with a symmetric tip shape (model Tap300Al-G, BudgetSensors, Bulgaria: nominal frequency 300 kHz, nominal spring constant 40 $Nm^{-1}$, tip radius < 10 nm). The AFM measurements were carried out in triplicate, and the cantilever spring constant was measured using the Sader method. To calibrate each probe, a force curve was executed on a hard-cleaned substrate (<100> silicon wafer) where no indentation took place. This calibration was necessary to determine the probe's sensitivity and spring constant. The Derjaguin–Müller–Toporov (DMT) model was utilized to compute the Young modulus from the experimental force–distance curves:

$$F + F_{ad} = \frac{4E_s}{3(1-\nu_s^2)} R^{\frac{1}{2}} \delta^{\frac{3}{2}}$$

Where $F$ is the applied force, $F_{ad}$is the adhesion force, $E_s$ is the Young modulus, $\nu_s$is the Poisson's ratio, $R$ is the cantilever's radius and $\delta$ is the elastic indentation depth.

Each surface was indented in different areas and approximately three hundred curves were obtained, with a tip–sample approaching rate of 0.3 $\mu ms^{-1}$ for all force curves. The DMT model was used to fit the experimental curves in the elastic region and calculate the Young modulus. The distribution of the elastic modulus was analyzed using OriginPro 8.5 software. Au-coated silicon nitride tips with spring constants ranging from 0.003 to 0.13 N/m were employed to carry out adhesion force measurements. These tips were calibrated via the Sader method. The adhesion force was determined by measuring the pull-off force required to separate the AFM tip from the surface. The PEEK surfaces were probed in various regions, and approximately three hundred approach–retract cycles were recorded for each system. The tip–sample approaching velocity remained constant at 0.3 $\mu s^{-1}$ for all force curves. Hooke's law was used to calculate the adhesion force between the tip and surface, based on the cantilever deflection distance and cantilever spring constant:

$$F = k \cdot \Delta L$$

where F is the force (nN), k is the spring constant of the cantilever, and ΔL is the deflection distance (nm). [45,54,55]

## 2.3.14 Biological assays

All *in vitro* biological assays were performed in collaboration with Prof. Paola Brun of the Department of Molecular Medicine, University of Padua.

### *2.3.14.1 Human osteoblast cells' isolation and culture*

Human osteoblast cells were obtained from explants of cortical mandible bone collected during a surgical procedure. After collection, the bone fragments were cultured at 37 °C in 5% $CO_2$ and 95% humidity in a complete medium (DMEM supplemented with 10% *v*/*v* heat-inactivated fetal bovine serum, and penicillin-streptomycin solution, all provided by ThermoFischer) and incubated until the cells migrated from the bone fragments. At the cell confluence, the bone fragments were removed, and the cells were detached using trypsin EDTA (Gibco) and cultured in a complete medium supplemented with 50 mg/mL ascorbic acid, 10 nm dexamethasone, and 10 mM β-glycerophosphate (all purchased from Merck). The osteoblast phenotype was confirmed by the von Kossa staining. The study was approved by the Ethical Committee of the University Hospital of Padova. The patients were informed of the study's aims and protocol and gave their written informed consent. [56]

### *2.3.14.2 Proliferation assays on non-functionalized PEEK*

Proliferation tests were carried out on PEEK disks with different surface roughness, in order to identify the surface improving osteoblasts proliferation and differentiation. The cells were incubated at 37 °C for 10 min in a prewarmed PBS containing 0.1% *v*/*v* BSA and a 25 mM carboxyfluorescein diacetate succinimidyl ester (CFSE, Molecular Probe, Invitrogen). Staining was quenched by adding five volumes of ice-cold culture media. The cells were then washed, counted using Trypan blue, seeded at $8 \times 10^4$ cells/mL, and incubated in a fresh culture medium at 37 °C for 72 h. Cell proliferation was evaluated by the partitioning of a fluorescent dye between daughter cells using a BD FACS-Calibur flow cytometer. [56]

### *2.3.14.3 Quantitative Real-Time Polymerase Chain Reaction (qRT-PCR)*

H-osteoblast cells were cultured on different functionalized scaffolds for 3 days at 37 °C. Specific mRNA transcript levels coding human vitronectin (VTN), human Secreted Phosphoprotein 1 (*Spp1*) and Runt-related transcription factor 2 (*Runx2*) were quantified. At the end of incubation, the total RNA was extracted using the EZN.A lysis buffer (Total R.N.A. Kit I (Omega Bio-Tek, Milan, Italy). Contaminating DNA was removed by DNase I treatment (Omega Bio-Tek). cDNA synthesis and subsequent polymerization were performed in a one-step using the iTaq Universal SYBR Green One-Step Kit (Bio-Rad). The reaction mixture contained a 200 nM forward primer, 200 nM reverse primer, iTaq universal SyBR Green reaction mix, and iScript reverse transcriptase, and a 200 ng total RNA Real-time PCR was performed using the ABI PRISM 7700 Sequence Detection System (Applied Biosystems, Milan, Italy). Data were quantified by the $\Delta\Delta C_T$ method using human glyceraldehyde-3-phosphate dehydrogenase (GAPDH) as the reference gene. Target and reference genes were amplified with efficiencies near 100%. [56, 57] $2^{\Delta\Delta Ct}$

## 2.3.15 Statistical analysis

Data obtained by biological and surface assays were analyzed and processed with Prism (GraphPad Software 9). Different tests' results were compared using one-way analysis of variance (ANOVA) test, followed by Tukey's multiple comparisons to confront every condition or two-way ANOVA test, followed by Tukey's post-hoc test. The significance level applied was 5%.

# CHAPTER 3
# EXPERIMENTAL PART

## 3.1 PEPTIDE SYNTHESIS AND PURIFICATION

### 3.1.1 Aoa-x-EAK

The peptide was obtained through solid phase synthesis using Fmoc chemistry and automatic synthesizer Siro I. 202 mg of Rink Amide MBHA resin (with substitution of 0.62 mmol/g) were used, which is equal to 0.125 mmol.

Peptide sequence:

H-Aoa-(7-aminoheptanoicacid)-Ala-Glu-Ala-Glu-Ala-Lys-Ala-Lys-Ala-Glu-Ala-Glu-Ala-Lys-Ala-Lys-$NH_2$

Theoretical weight of peptide is 1813.986 Da.

Aoa group was attached separately since different conditions are needed; in fact, the aminooxy group tends to react with ketones.

#### *3.1.1.1 Peptide Synthesis*

A DMF solution 0.62 M was prepared for amino acids:

- Fmoc-Ala-OH
- Fmoc-Glu(OBut)-OH,
- Fmoc-Lys(Boc)-OH
- Fmoc-7-aminoheptanoic acid
- BisBoc-Aoa

5 equivalents of each amino acid were used with respect to resin reactive groups, to increase the efficiency of the coupling.

Three solutions needed for the reaction were prepared:

- 0.5 M solution of HBTU/Oxyma Pure in DMF
- 1.8 N solution of DIPEA in NMP
- 40% piperidine solution in DMF

The synthesis reaction is composed of 18 cycles, all set to double coupling, each one with a 45-minute span time.

Fmoc group removal was obtained by treating the growing peptide with 1 ml of 40% piperidine solution in DMF for 3 minutes, then again with 0.9 ml of 40% piperidine solution in DMF for 12 minutes.

The activation of the carboxyl group, during the condensation reaction, was obtained dissolving 1 ml of amino acid solution in 1.4 ml of HBTU/Oxyma Pure in DMF and 0.695 ml of DIPEA solution in NMP.

For the last cycle, the coupling of Aoa group, the 1.8 N solution for DIPEA in NMP was replaced with a 2 N solution of collidine in NMP, in order to maximize the yield.

At the end of the synthesis, some washings with DCM were performed, then the resin was dried under vacuum for about 1 hour.

At the end of the first cycle a piperidine test was performed, giving yield 99.23%.

Before the coupling with Aoa and at the end of the synthesis, ninhydrin tests were performed, giving yield, respectively, 99.7% and 99.86%.

### *3.1.1.2 Peptide cleavage from the resin*

Peptide cleavage from the resin was carried out on 2/3 of the resin obtained, to see if the aminooxy group had bound correctly. 508.45 mg of resin were weighed, and 339 mg were taken.

The cleavage solution was prepared with:

- 0.125 ml of MilliQ water

- 0.125 ml of TES
- 4.75 ml of TFA

The solution obtained was reacted for 1 hour and 30 minutes at room temperature, rotating the reactor occasionally. The solution was then filtered, washed with TFA and dried out with rotary evaporator. The peptide synthetized was precipitated adding cold ethyl ether (4°C) under magnetic stirring, then it was filtered in a Gooch 4 and dried under vacuum for 1 hour.

Dried crude peptide obtained was 91 mg.

### *3.1.1.3 Crude peptide characterization*

To characterize Aoa-x-EAK peptide, 1 mg of crude peptide was dissolved in 1 ml of eluent A, and then the solution was filtered using a PVDF filter. (Figure 3.1)

The analysis was performed under the following conditions:

- Column: Nova-Pak C18 (4 μm, 60 Å, 3.9 x 300 mm)
- Injected volume: 150 μl
- Flow rate: 0.5 mL/min
- Detector wavelength: 214 nm
- Eluent A: 0.05% TFA in MilliQ water
- Eluent B: 0.05% TFA in 40% isopropanol and 60% MilliQ water
- Gradient: from 25% to 35 %of B in 15 minutes
- Paper velocity: 0.5 cm/min

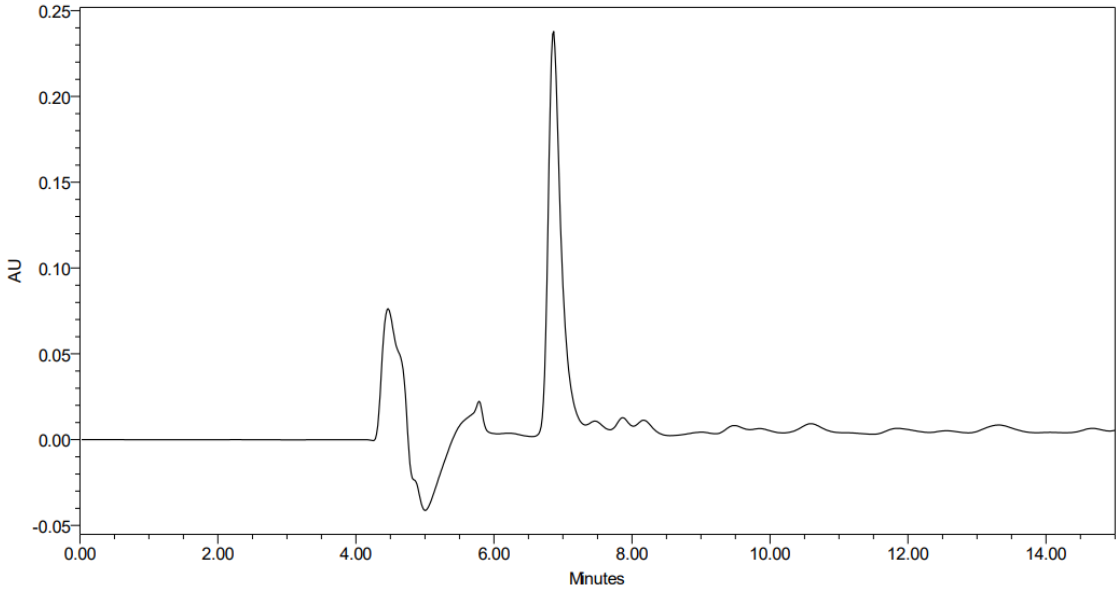


*Figure 3.1 - Crude Aoa-x-EAK RP-HPLC analytical chromatogram. Column: Nova-Pak C18, flow: 0.5 ml/min, eluent A: 0.05% TFA in MilliQ water, eluent B: 0.05% TFA in 40% isopropanol and 60% MilliQ water solution, gradient: from 15% to 35% of B in 20 minutes, injected volume: 50 µl, detector wavelength: 214 nm*

A mass spectroscopy analysis was performed on small amount of crude peptide to ensure the correct molecular weight of peptide. Results of MALDI-TOF are reported in Figure 3.2.

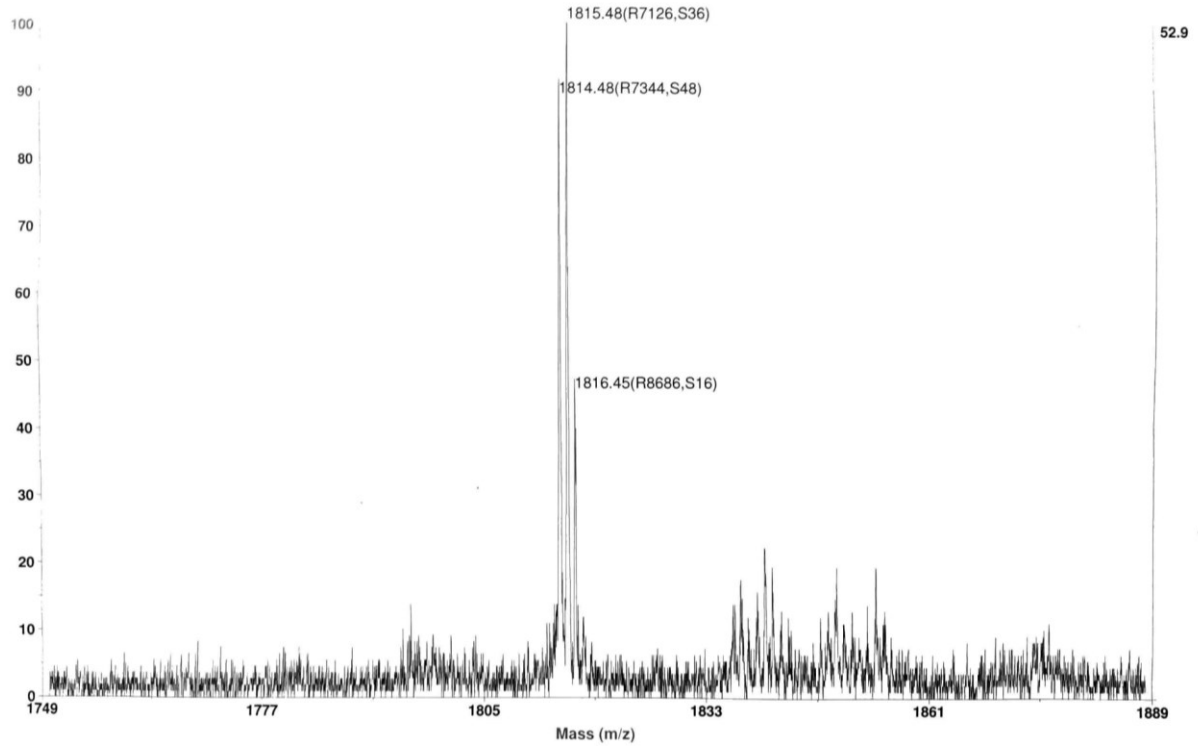


*Figure 3.2 - Mass analysis of crude Aoa-x-EAK peptide (theoretic weight: 1813.99 Da)*

### *3.1.1.4 Peptide purification*

Aoa-x-EAK crude peptide was purified through RP-HPLC analysis; 30 mg of crude peptide were dissolved in 30 ml of eluent A.

The solution was filtered using a PVDF filter with 0.45 μm pore diameter.

The analysis was performed under the following conditions:

- Column: Delta-Pak C18 (15 μm, 100 Å, 7.8 x 300 mm)
- Injected volume: 30 ml
- Flow rate: 2 mL/min
- Detector wavelength: 214 nm
- Full-scale: 4.0 Abs
- Eluent A: 0.05% TFA in MilliQ water
- Eluent B: 0.05% TFA in 40% isopropanol and 60% MilliQ water
- Gradient: from 10% to 60% of B in 50 minutes
- Paper velocity: 0.5 cm/min

In figure 3.3 it is possible to identify one large peak, corresponding to pure peptide. The eluate was fractioned in different vials.

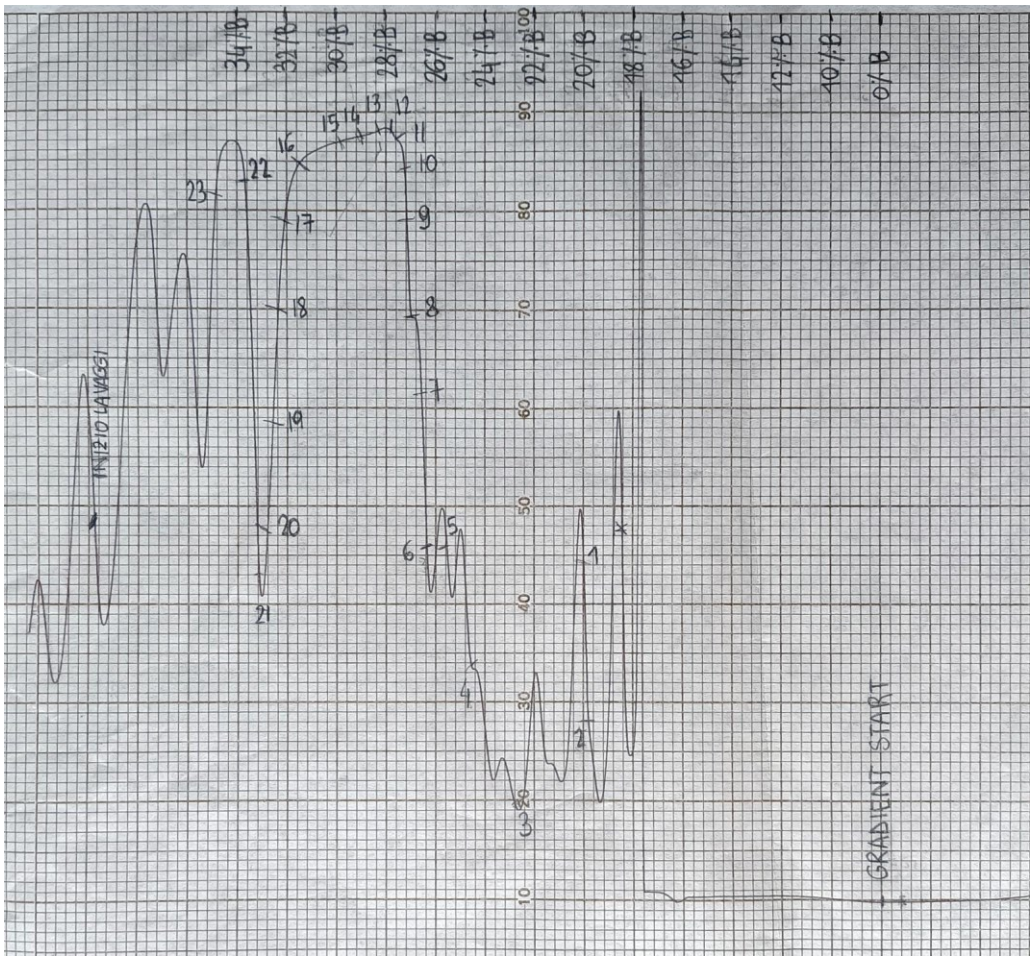


*Figure 3.3 – Crude Aoa-x- EAK semipreparative RP-HPLC chromatogram. Column: Delta-Pak C18, flow: 2 ml/min, eluent A: 0.05% TFA in MilliQ water, eluent B: 0.05% TFA in 40% isopropanol and 60% MilliQ water solution, gradient: from 10% to 60% of B in 50 minutes, injected volume: 30 ml, detector wavelength: 214 nm, full-scale: 4.0, paper velocity: 0.5 cm/min.*

Fractions from 13 to 17 were supposed pure, so they were collected together and instantly freezed in liquid nitrogen and then lyophilized, to avoid reaction of pure peptide with ketones.

An RP-HPLC analysis was carried to evaluate the purity of the collected pool.

This analysis was carried out at the following conditions:

- Column: Vydac 218TP C18 (4 µm, 60 Å, 3.9 x 300 mm)
- Injected volume: 150 µl
- Flow rate: 0.5 mL/min
- Detector wavelength: 214 nm
- Eluent A: 0.05% TFA in MilliQ water

- Eluent B: 0.05% TFA in 40% isopropanol and 60% MilliQ water
- Gradient: from 25% to 35% of B in 15 minutes

Figure 3.4 is the analytical of pool 13÷17. The total weight of pure peptide obtained was 20 mg.

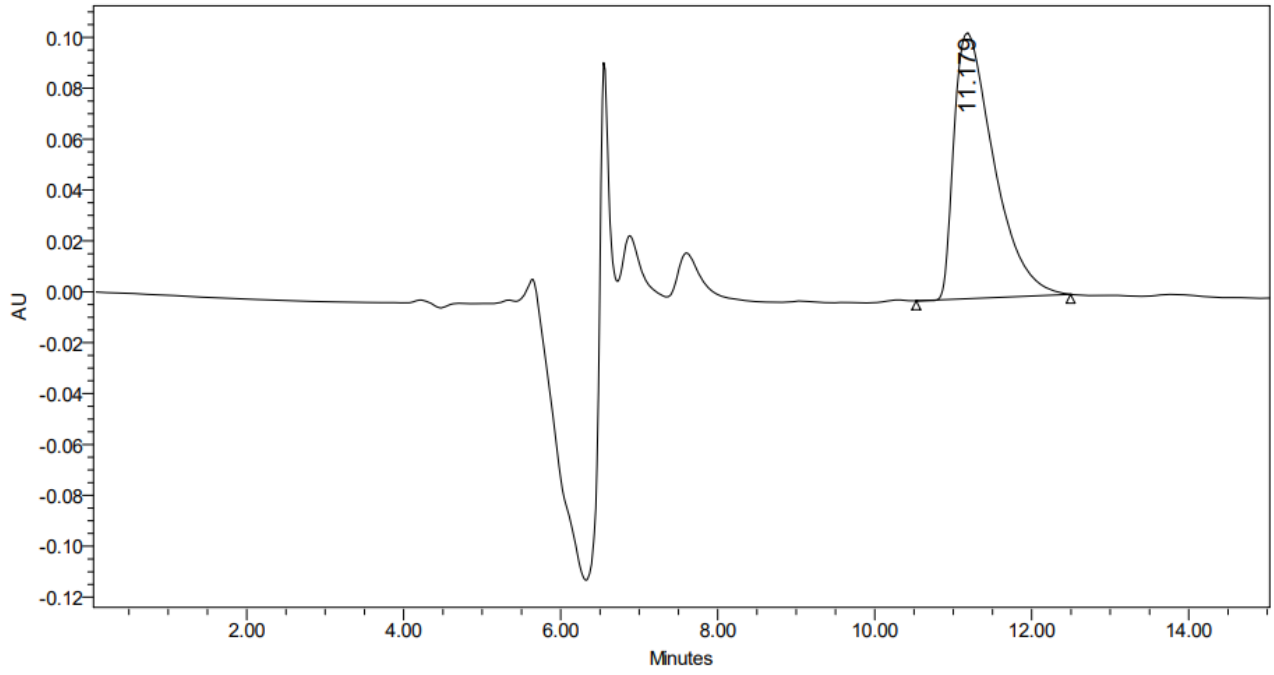


*Figure 3.4 - Aoa-x-EAK RP-HPLC analytical chromatogram. Column: Vydac 218TP C18, flow: 0.5 ml/min, eluent A: 0.05% TFA in MilliQ water, eluent B: 0.05% TFA in 40% isopropanol and 60% MilliQ water solution, gradient: from 25% to 35% of B in 15 minutes, injected volume: 150 µl, detector wavelength: 214 nm. Purity: 100%, Retention Time: 11.179 minutes.*

The collected pools were analyzed by MALDI-TOF to identify the pure peptide (Figure 3.5).

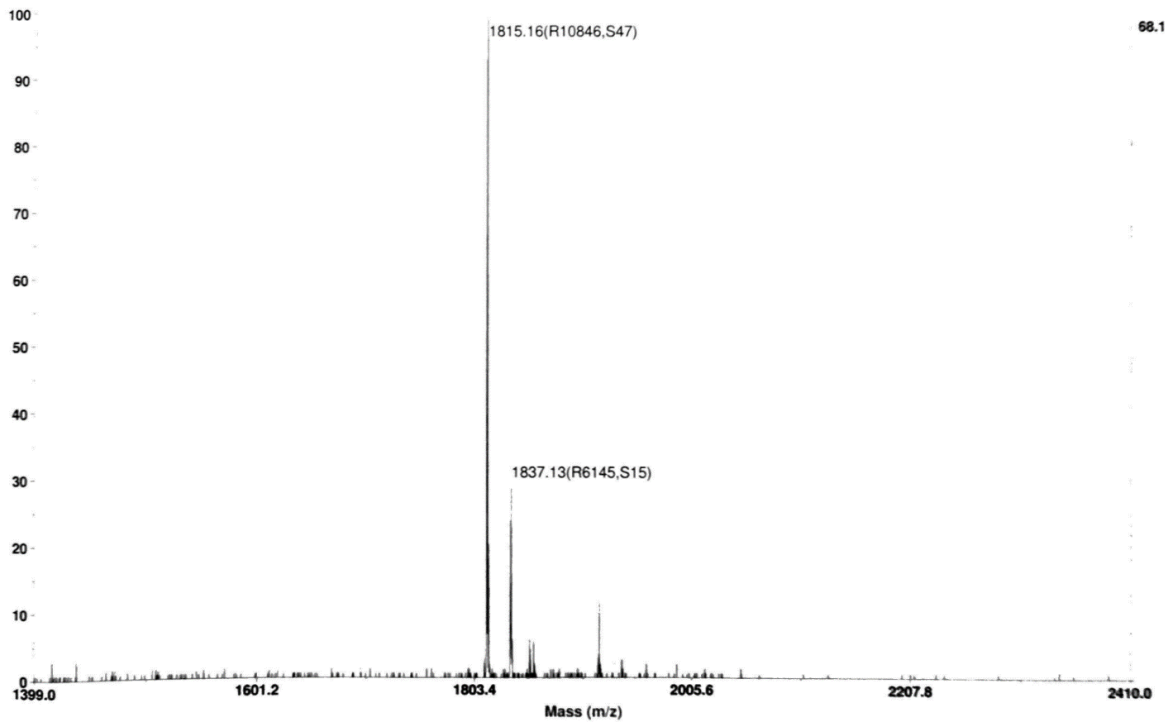


*Figure 3.5 – Mass analysis of purified Aoa-x-EAK peptide (theoretic weight: 1813.99 Da, experimental weight 1815.16 Da).*

## 3.1.2 Aoa-x-GBMP1α

Aoa-x-GBMP1α was obtained through solid phase peptide synthesis using a Syro I automatic synthesizer and Fmoc chemistry. The resin Rink Amide MBHA (substitution 0.62 mmol/g) was used as a solid support. 202 mg of resin were used, which is equal to 0.125 mmol (scale of synthesis).

The peptide sequence is:

H-Aoa-(7-aminoheptanoicacid)-Pro-Phe-Pro-Leu-Ala-Asp-His-Leu-Asn-Ser-Thr-Asn-His-Ala-Ile-Val-Gln-Thr-Leu-Val-Asn-Ser-NH2

The theoretical weight is 2587.86 Da.

Aoa group was attached separately as different conditions are needed. In fact, the aminooxy group tends to react with ketones.

### *3.1.2.1 Peptide synthesis*

A DMF solution 0.62 M was prepared for amino acids:

- Fmoc-Ala-OH
- Fmoc-Asp(OBut)-OH
- Fmoc-His(Trt)-OH
- Fmoc-Ile-OH
- Fmoc-Leu-OH
- Fmoc-Asn(Trt)-OH
- Fmoc-Pro-OH
- Fmoc-Gln(Trt)-OH
- Fmoc-Ser(But)-OH
- Fmoc-Thr(But)-OH
- Fmoc-Val-OH
- Fmoc-7-aminoheptanoic acid
- BisBoc-Aoa

A 0.62 M NMP solution was prepared for the following amino acids:

- Fmoc-Phe-OH

To increase the efficiency of the coupling, 5 equivalents of each amino acid were used with respect to resin reactive groups.

The three solutions needed for the reaction were prepared:

- 0.5 M solution of HBTU/Oxyma Pure in DMF
- 40% piperidine solution in DMF
- 1.8 N solution of DIPEA in NMP

The synthesis reaction is composed of 23 cycles, all set to double coupling, each one with a 45-minute span time.

Fmoc group removal was obtained by treating the growing peptide with 1 ml of 40% piperidine solution in DMF for 3 minutes, then again with 0.9 ml of 40% piperidine solution in DMF for 12 minutes.

The activation of the carboxyl group, during the condensation reaction, was obtained by dissolving 1 ml of amino-acid solution in 1.4 ml of HBTU/Oxyma Pure in DMF and 0.695 ml of DIPEA solution in NMP.

After the first cycle a piperidine test was performed, giving yield 98.5%.

Before the coupling with Aoa and at the end of the synthesis, ninhydrin tests were performed, giving yield, respectively, 99.3% and 99%.

For the last cycle, the coupling of Aoa group, the 1.8 N solution for DIPEA in NMP was replaced with a 2 N solution of collidine in NMP, in order to maximize the yield.

At the end of the synthesis, some washings with DCM were performed, then the resin was dried under vacuum for about 1 hour.

### *3.1.2.2 Peptide cleavage from the resin*

Peptide cleavage from resin was carried out on 840 mg of resin weighted.

The cleavage solution was prepared with:

- 0.125 ml of MilliQ water
- 0.125 ml of TES
- 4.75 ml of TFA

The solution obtained was reacted for 1 hour and 30 minutes at room temperature, rotating the reactor occasionally. The solution was then filtered, washed with TFA and dried out with rotary evaporator. The peptide synthetized was precipitated adding cold ethyl ether (4°C) under magnetic stirring, then it was filtered in a Gooch 4 and dried under vacuum for 1 hour.

Dried crude peptide obtained was 211 mg.

### *3.1.2.3 Crude peptide characterization*

To characterize Aoa-x- GBMP1α peptide, 1 mg of crude peptide was dissolved in 1 ml of eluent A, and then the solution was filtered using a PVDF filter. (Figure 3.6)

The analysis was performed under the following conditions:

- Column: Vydac 218TP C18
- Injected volume: 70 µl
- Flow rate: 0.5 mL/min
- Detector wavelength: 214 nm
- Eluent A: 0.05% TFA in MilliQ water
- Eluent B: 0.05% TFA in 40% isopropanol and 60% MilliQ water
- Gradient: from 55% to 70% of B in 30 minutes

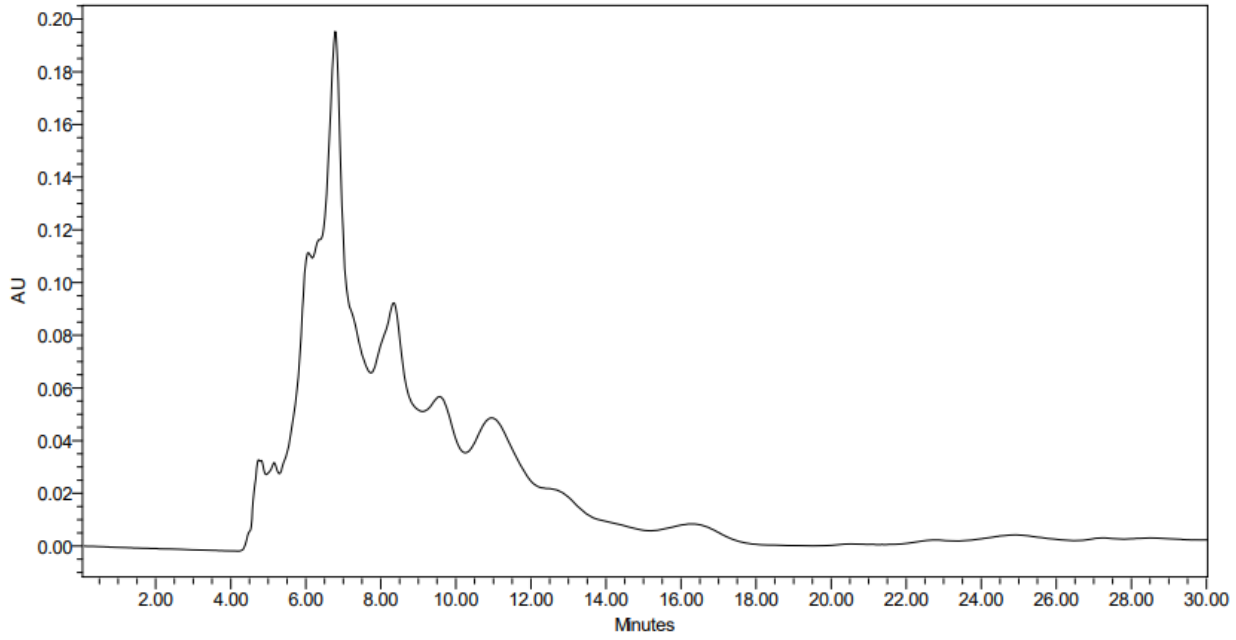


*Figure 3.6 - Crude Aoa-x-GBMP1α RP-HPLC analytical chromatogram. Column: Vydac C18, flow: 0.5 ml/min, eluent A: 0.05% TFA in MilliQ water, eluent B: 0.05% TFA in 40% isopropanol and 60% MilliQ water solution, gradient: from 55% to 70% of B in 30 minutes, injected volume: 70 µl, detector wavelength: 214 nm.*

A mass spectroscopy analysis was performed to ensure the correct molecular weight. Maldi-TOF result is reported in Figure 3.7. We can see that the theoretical weight is found.

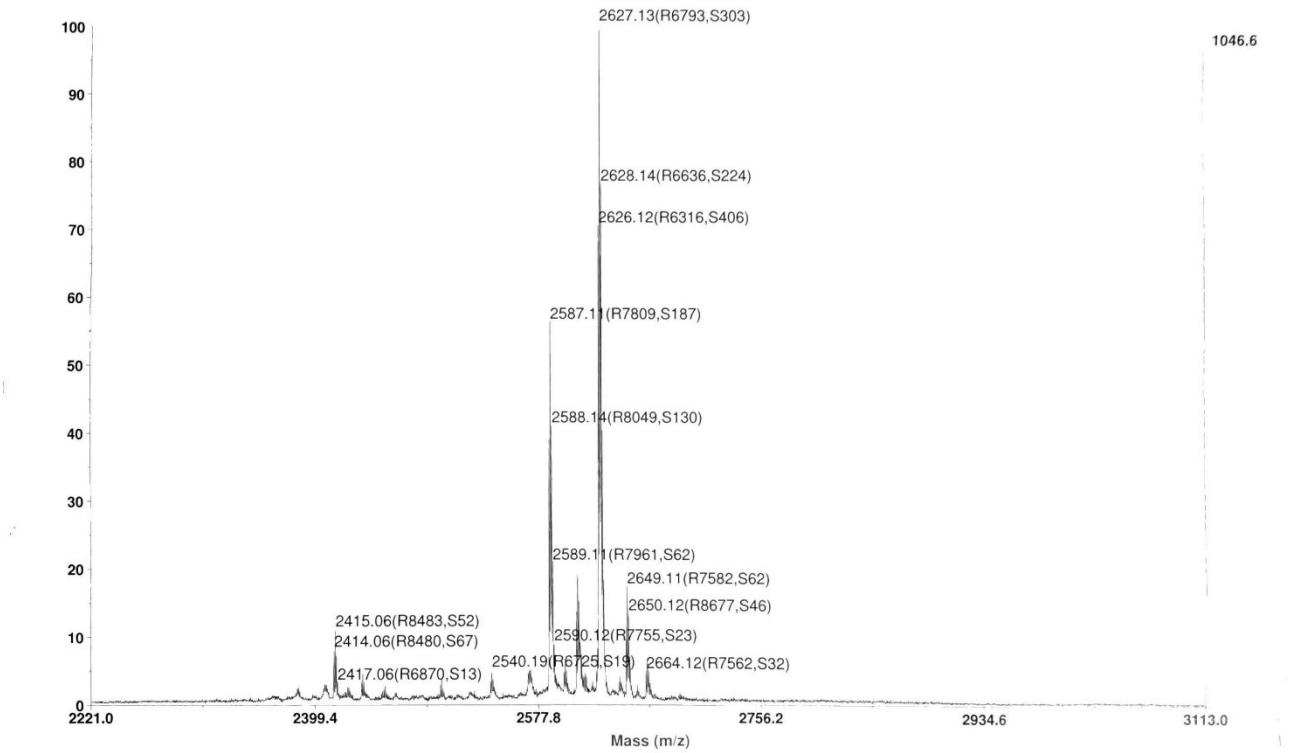


*Figure 3.7 – Mass analysis of crude Aoa-x-GBMP1α peptide (theoretic weight: 2587.86 Da, experimental weight: 2587.11 Da).*

### *3.1.2.4 Peptide purification*

The crude Aoa-x-GBMP1α peptide was purified through a RP-HPLC SP analysis. Aoa-x-GBMP1α is highly insoluble, so 20 mg of crude peptide were dissolved first with 1 ml of DMF, then with 29 ml of MilliQ water. The solution was filtered using a PVDF filter with 0.45 µm pore diameter.

The analysis was performed under the following conditions:

- Column: Zorbax 300SB C18 (5 µm, 300 Å, 9.4 × 250 mm)
- Injected volume: 20 ml
- Flow rate: 2 mL/min
- Detector wavelength: 214 nm
- Full-scale: 4.0
- Eluent A: 0.05% TFA in MilliQ water
- Eluent B: 0.05% TFA in 40% isopropanol and 60% MilliQ water
- Gradient: from 60% to 80% of B in 80 minutes
- Paper velocity: 0.5 cm/min

In figure 3.8 it is possible to identify one large peak, corresponding to pure peptide.

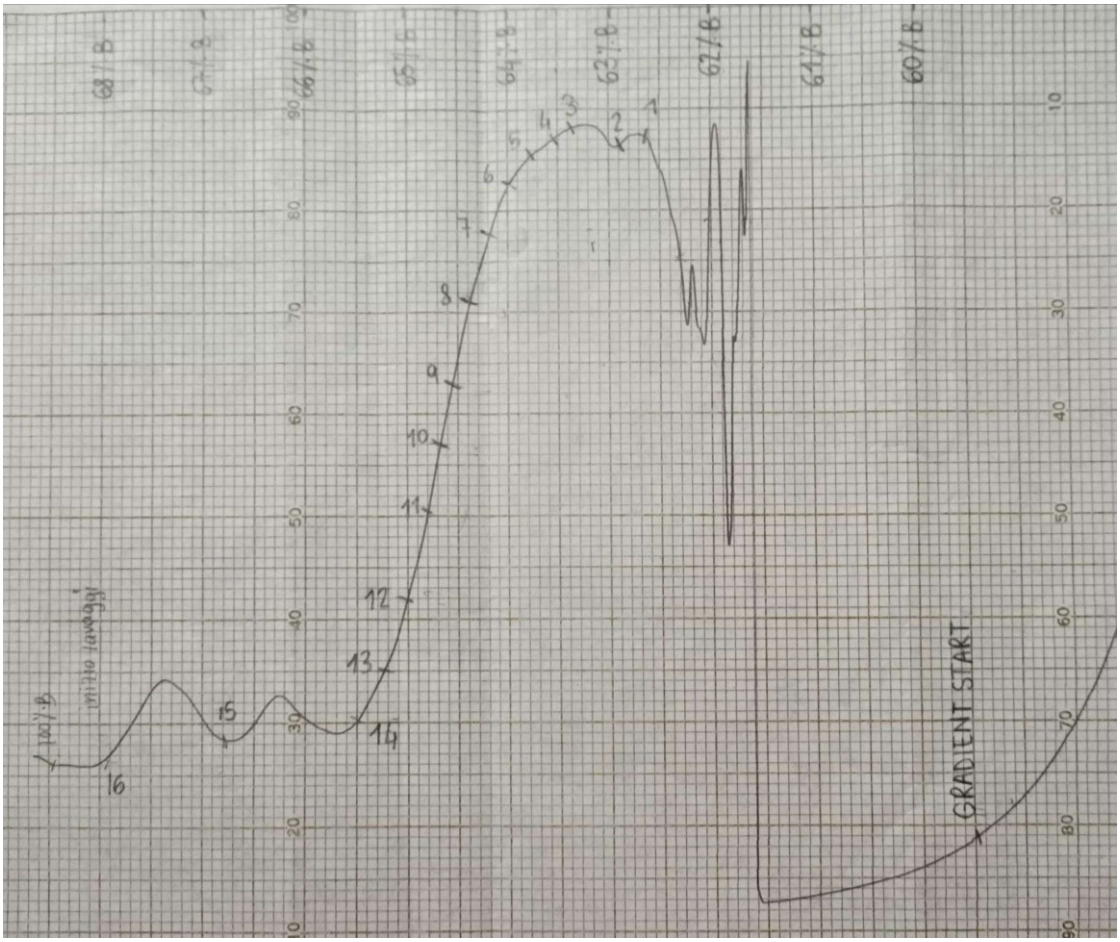


*Figure 3.8 – Crude Aoa-x-GBMP1α semipreparative RP-HPLC chromatogram. Column: Zorbax C18, flow: 2 ml/min, eluent A: 0.05% TFA in MilliQ water, eluent B: 0.05% TFA in 40% isopropanol and 60% MilliQ water solution, gradient: from 60% to 80% of B in 80 minutes, injected volume: 20 ml, detector wavelength: 214 nm, full-scale: 4.0, paper velocity: 0.5 cm/min*

The eluate was fractioned in different vials.

Fractions from 7 to 11 were supposed pure, so they were collected together and instantly freezed in liquid nitrogen and then lyophilized, to avoid reaction of pure peptide with ketones.

An RP-HPLC analysis was carried to evaluate the purity of the collected pool.

This analysis was carried out at the following conditions:

- Column: Vydac 218TP C18

- Injected volume: 70 µl
- Flow rate: 0.5 mL/min
- Detector wavelength: 214 nm
- Eluent A: 0.05% TFA in MilliQ water
- Eluent B: 0.05% TFA in 40% isopropanol and 60% MilliQ water
- Gradient: from 55% to 70% of B in 30 minutes

Figure 3.9 is the analytical of pool 7÷11.

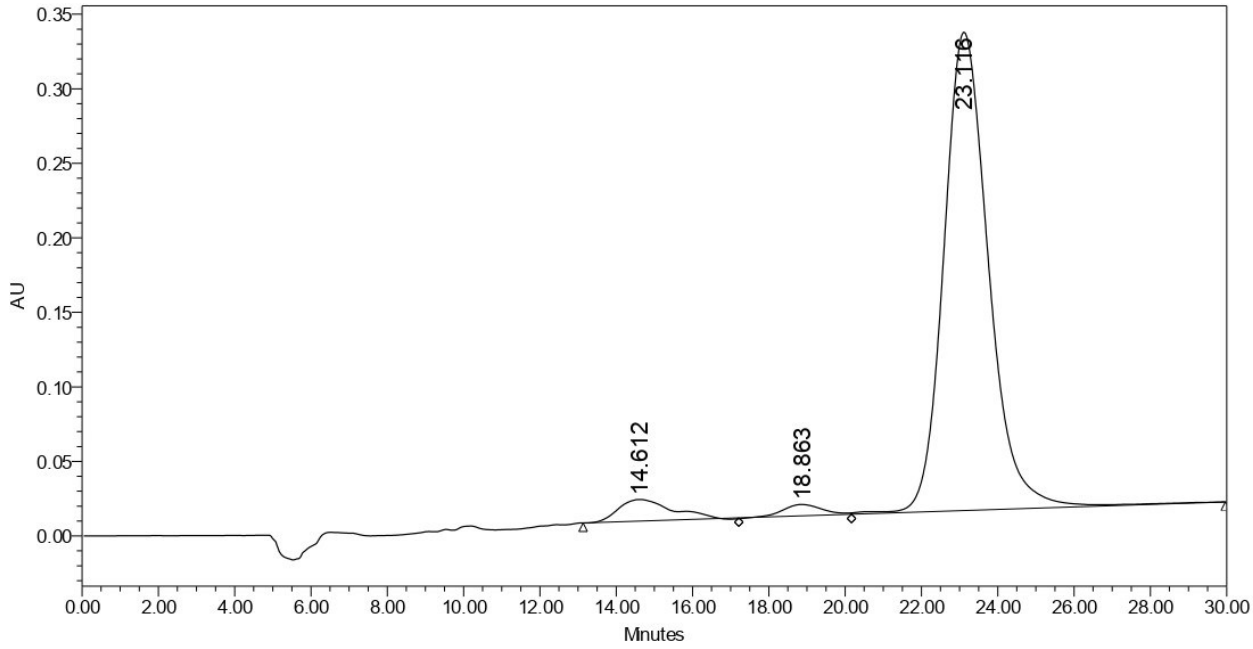


*Figure 3.9 - Purified Aoa-x-GBMP1α RP-HPLC analytical chromatogram. Column: Vydac C18, flow: 0.5 ml/min, eluent A: 0.05% TFA in MilliQ water, eluent B: 0.05% TFA in 40% isopropanol and 60% MilliQ water solution, gradient: from 55% to 70% of B in 30 minutes, injected volume: 70 µl, detector wavelength: 214 nm. Purity: 92.27%, Retention Time: 23.116 minutes.*

The total weight of pure peptide obtained was 8 mg.

The collected pool was analysed by MALDI-TOF to identify the pure peptide (Figure 3.10).

The analysis shows a mass peak of 2587.83 Da, which is equal to the theoretical weight of the pure peptide.

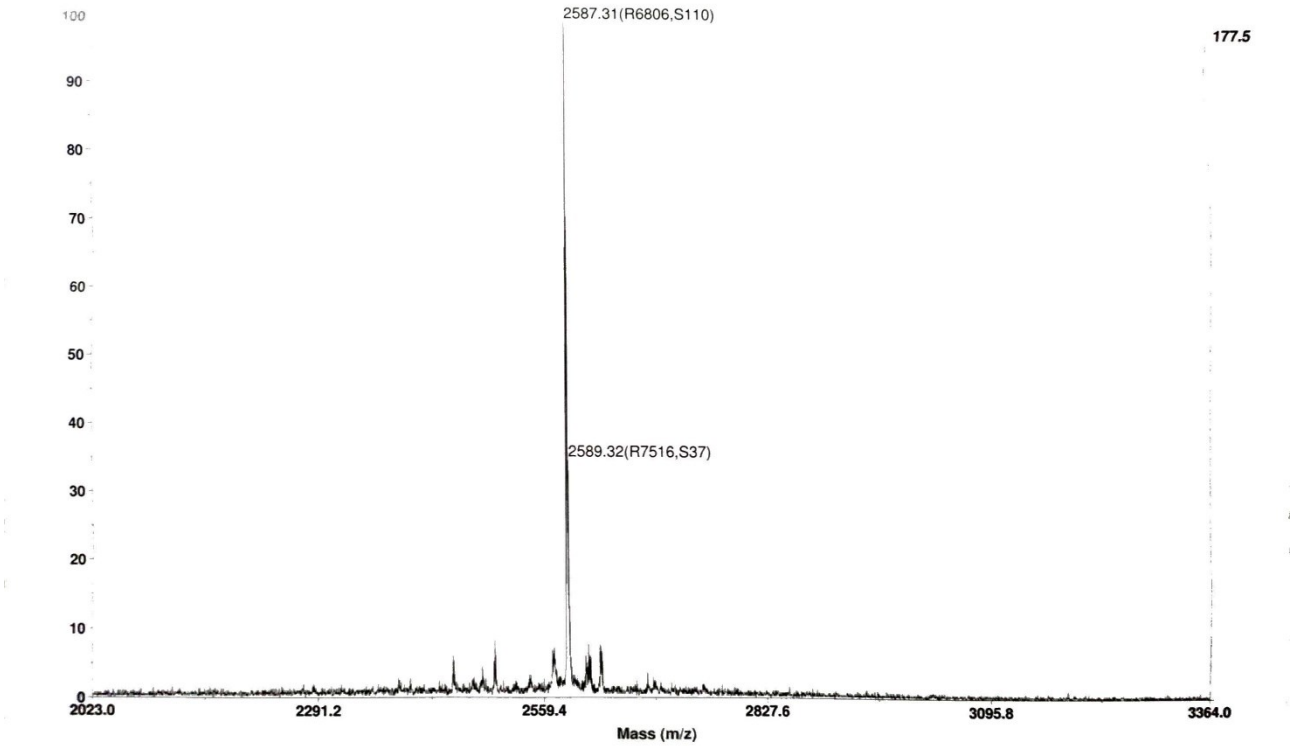


*Figure 3.10 – Mass analysis of purified Aoa-x-GBMP1α peptide (theoretic weight: 2587.86 Da, experimental weight: 2587.31 Da).*

### 3.1.3 SxGBMP1α

This peptide was already synthesized and purified, and it was available in the laboratory.

The peptide sequence is:

H-Ser-x-Pro-Phe-Pro-Leu-Ala-Asp-His-Leu-Asn-Ser-Thr-Asn-His-Ala-Ile-Val-Gln-Thr-Leu-Val-Asn-Ser-NH2

The theoretical weight is 2601.943 Da.

A mass spectroscopy analysis was performed to ensure the correct molecular weight. Maldi-TOF result is reported in Figure 3.11. In order to obtain the aldehyde-terminal peptide, the N-terminal serine had been oxidised prior to purification. The aldehyde-GBMP1α obtained is expected to have a lower molecular weight than the crude peptide by approximately 31 Da.

We can see that the theoretical weight is found.

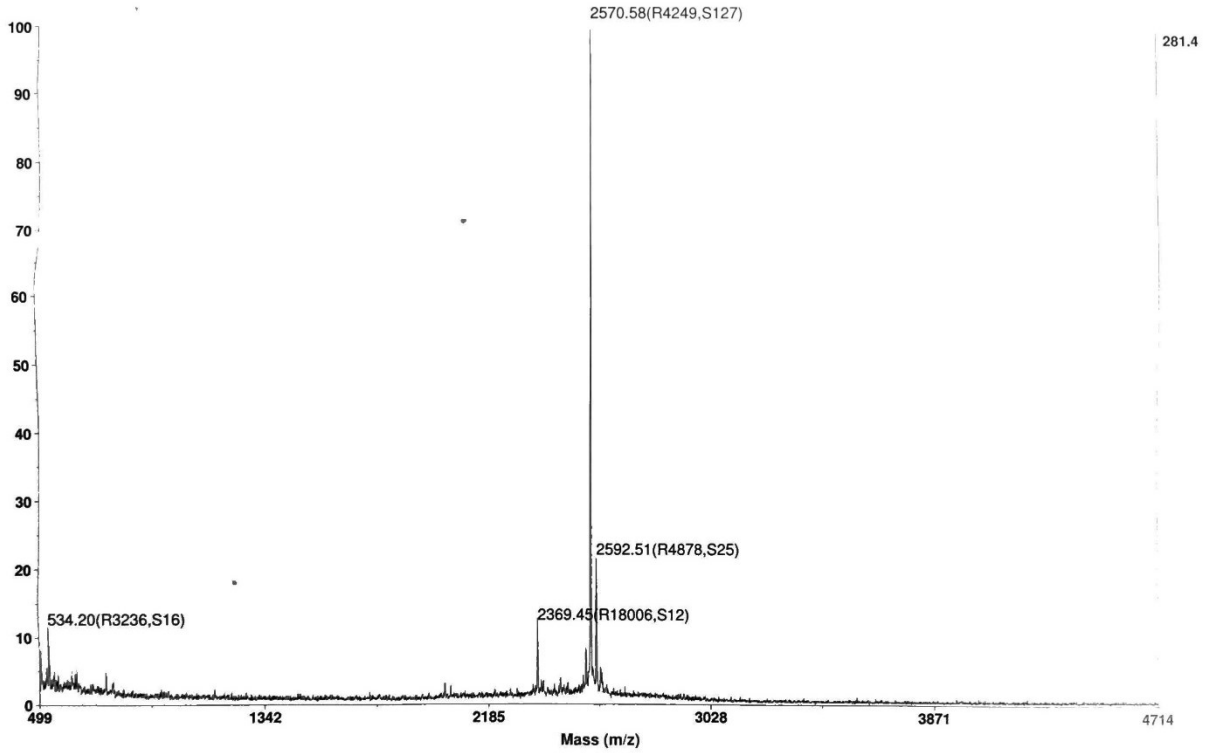


*Figure 3.11 – Mass analysis of purified GBMP1α aldehyde (expected weight: 2570.943 Da, experimental weight: 2570.58 Da).*

## 3.1.4 EAK

This peptide was already synthesized and purified, and it was present in the laboratory.

The peptide sequence is:

H-Ala-Glu-Ala-Glu-Ala-Lys-Ala-Lys-Ala-Glu-Ala-Glu-Ala-Lys-Ala-Lys-$NH_2$

The theoretical weight is 1614.79 Da.

A mass spectroscopy analysis was performed to ensure the correct molecular weight. Maldi-TOF result is reported in Figure 3.12.

We can see that the theoretical weight is found.

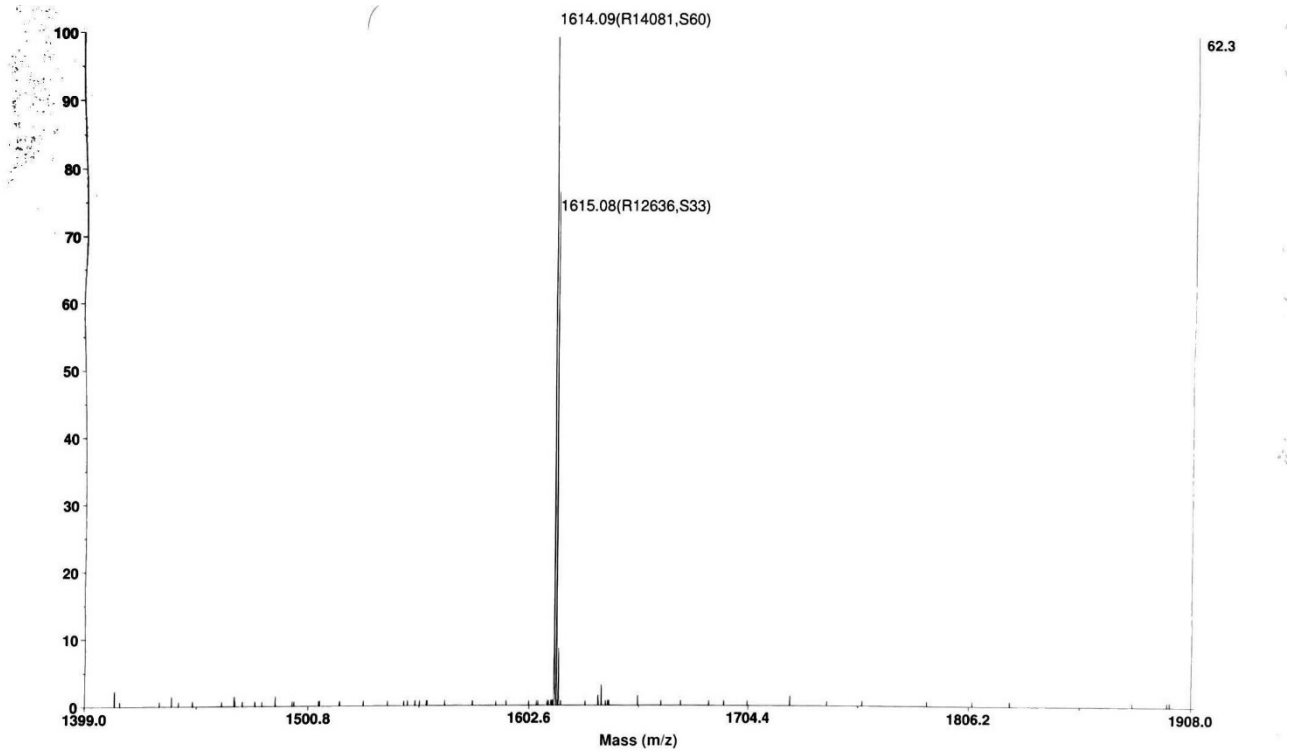


*Figure 3.12 - Mass analysis of purified EAK peptide (theoretic weight: 1614.79 Da, experimental weight: 1614.09 Da).*

## 3.2 PEEK SURFACE ROUGHNESS

In this thesis project, three different groups of PEEK disks were obtained, which differed in surface roughness. The first group, which served as a control (PEEK), was characterised by a smooth surface, while the second and third groups (R-PEEK) were obtained by sandblasting with grains of two different sizes.

### 3.2.1 PEEK lapping

All PEEK disks were initially characterized by a 3D-printed surface pattern, which was used for tests in previous thesis works.

All PEEK disks surfaces were modified using the same lapping technique as for R-PEEK and PEEK samples by a series of SiC abrasive papers, that are P800, P1200, P1500 and P2000 grit.

In table 3.13 grain size of abrasive paper are reported).

| *SANDPAPER TYPE* | *RADIUM GRAIN DIMENSION (μm)* |
|---|---|
| *P800* | 21.8±1 |
| *P1200* | 15.3±1 |
| *P1500* | 12.6±1 |
| *P2000* | 10.3±0.8 |

*Table 3.13 – Grain size of different sandpaper used in the lapping machine.*

An optical microscope was used to verify that the treated disks had a smooth and homogenous surface.

In figure 3.14 a PEEK disk after lapping process in shown.

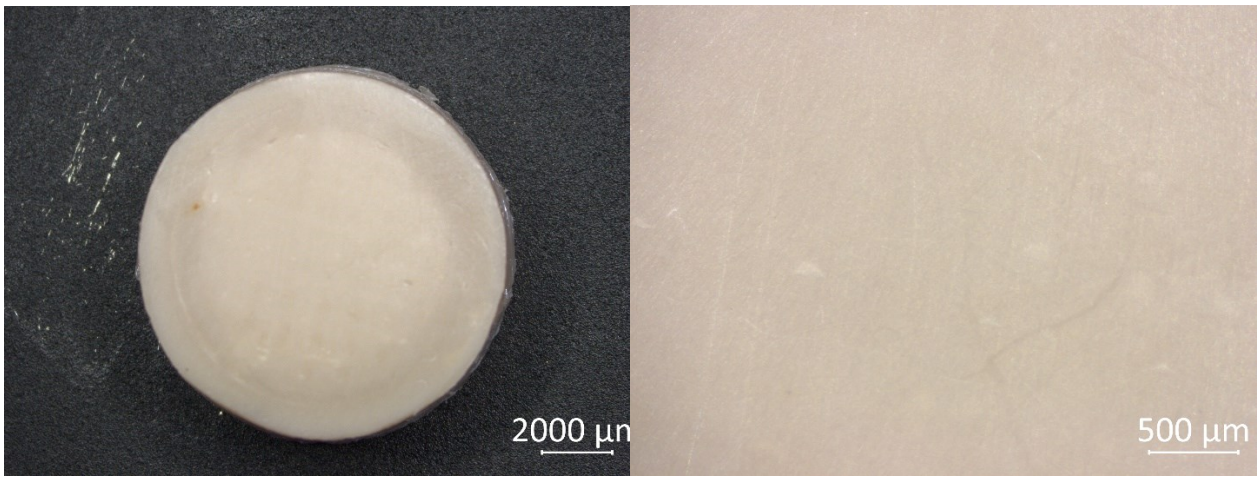


*Figure 3.14 PEEK disk lapped with sandpaper from P800 to P2000*

### 3.2.2 PEEK sandblasting

Two different groups of sandblasted disks were created based on the parameters used by Deng et al. [31]; in fact, they showed that disks treated with 110 μm grid alumina particles improved osteoblast adhesion and proliferation compared to those sandblasted with 60 μm particles.

Roughened PEEK (R-PEEK) implants were prepared by sandblasting previous-smoothed disks using respectively 60 (R60-PEEK) and 110 μm grid alumina particles (R110-PEEK) for 10 seconds in a sandblaster. The distance between the PEEK disk and the sandblast nozzle was approximately 2-3 cm.

In figure 3.15 the two types of sandblasted disks are shown.

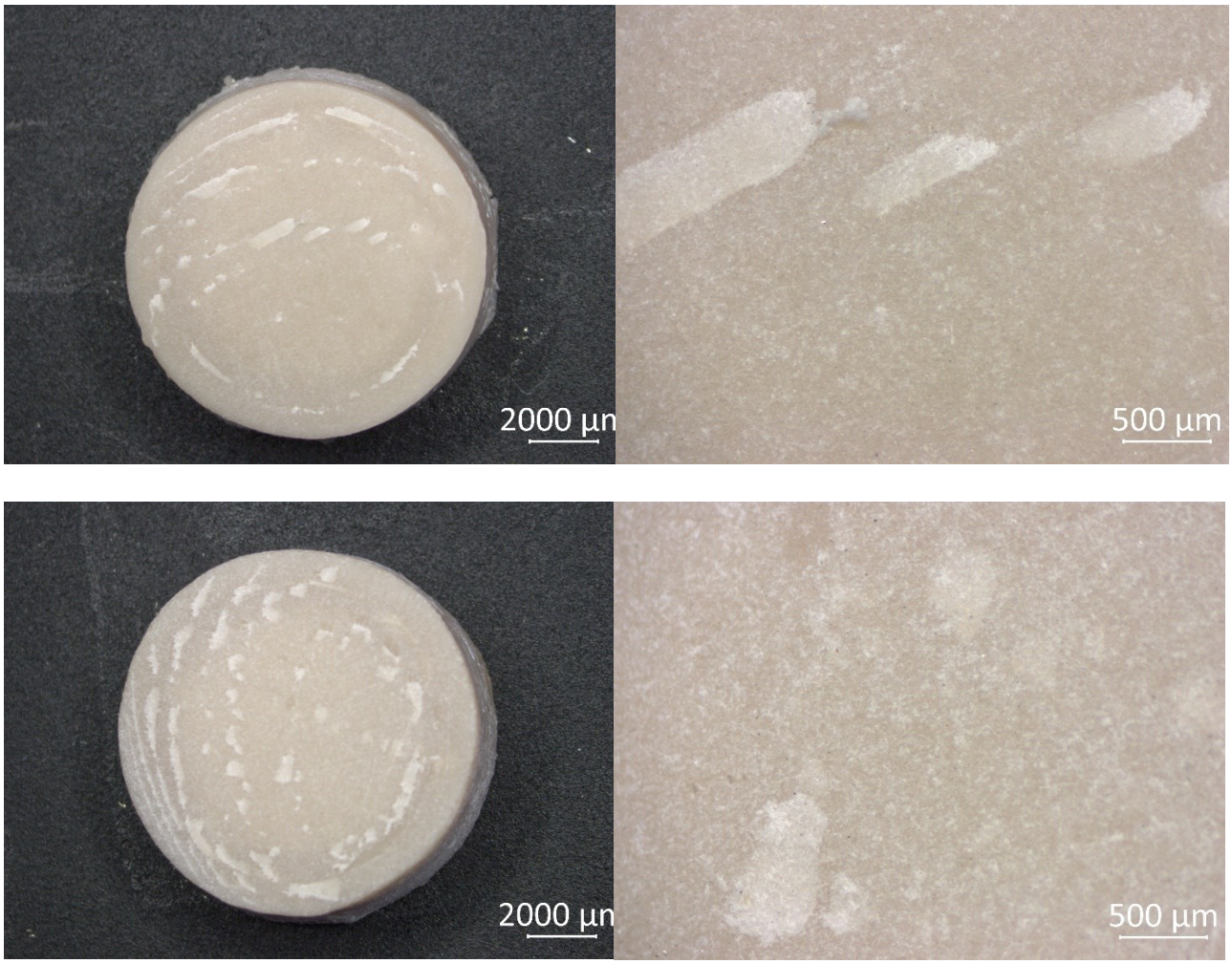


*Figure 3.15 – upper: disks sandblasted with 60 µm grid alumina particle; lower: disks sandblasted with 110 µm grid alumina particle.*

After sandblasting, the specimens were washed ultrasonically with distilled water and DMSO to prepare them for functionalization. Specimens were then dried at room temperature for overnight. PEEK disks were then subjected to profilometric analysis.

## 3.3 PEEK FUNCTIONALIZATION

### 3.3.1 Solvent selection for PEEK functionalization

Since the PEEK polymer exhibits pronounced hydrophobic characteristics, in order to maximise the interaction in the interface where functionalization occurred, several possibilities were examined in the choice of solvent. The choice of solvent was made by qualitatively assessing the best dispersion of a 2 µl drop placed on the smooth surface of a PEEK disk.

In figure 3.16, images of the dispersion of the solvents considered are shown:

- Water
- 50% DMF, 50% Water
- 50% Acetonitrile, 50% Water
- 90% Acetonitrile, 10% Water
- 50% Di-Methyl-Sulfoxide (DMSO), 50% Water
- Di-Methyl-Sulfoxide (DMSO)

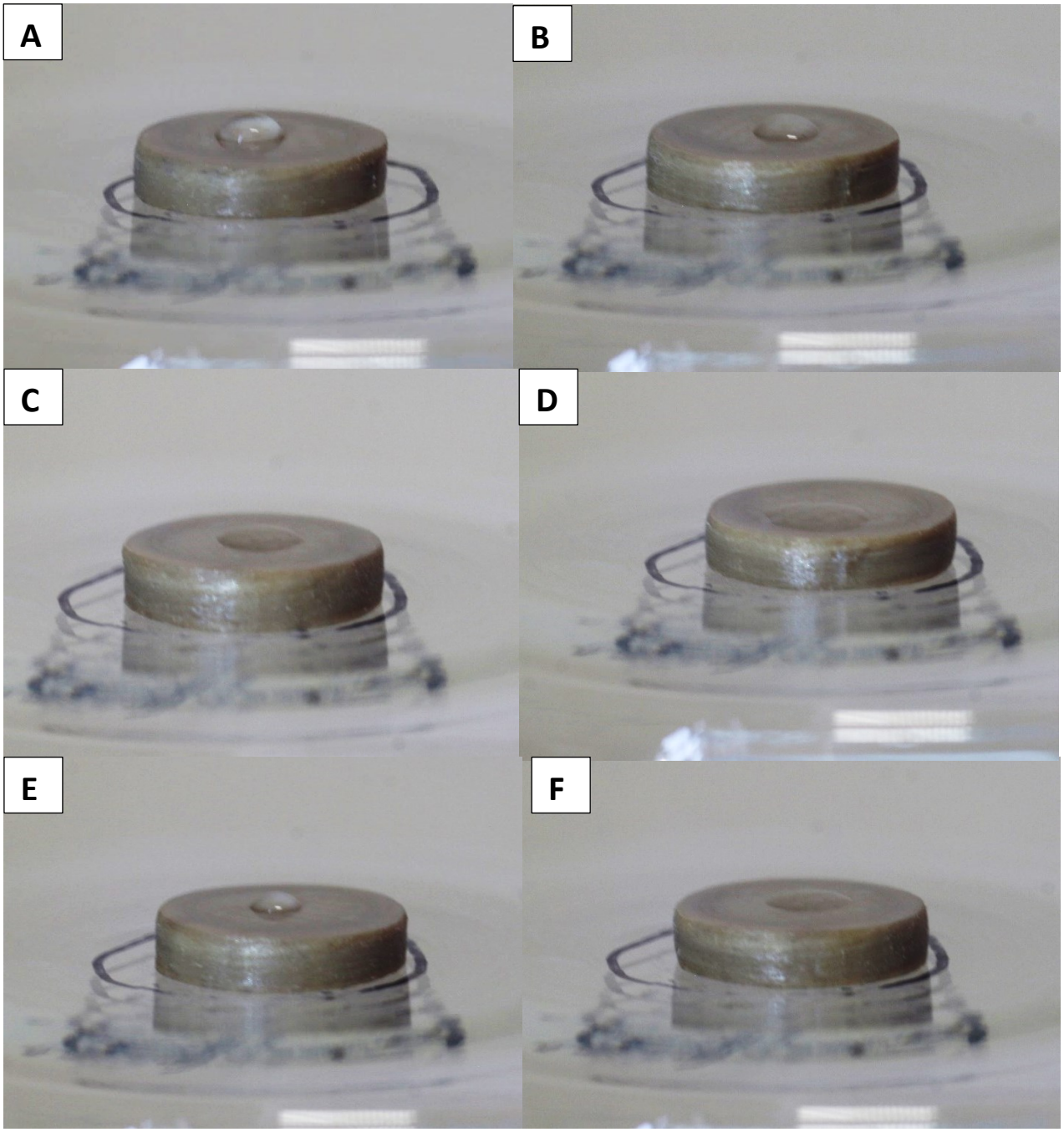


*Figure 3.16 – Qualitative evaluation of drop dispersion on PEEK disks of A: Water, B: 50% DMF, C: 50% ACN, D: 90% ACN, E: 50% DMSO, F: pure DMSO.*

As shown in figure 3.16, better dispersion is reached from 90% Acetonitrile/Water and pure DMSO. Given the difficulties and high costs of finding acetonitrile uncontaminated by ketone groups, DMSO was chosen as solvent for functionalization.

A literature search revealed a method involving DMSO used to achieve covalent functionalization through the formation of oxime. The solution for functionalization employed by Liu et al. [49] was peptide diluted in DMSO with one equivalent of AcOH.

### 3.3.2 PEEK functionalization for biological assays (proliferation and gene expression)

R110-PEEK surface was functionalized with $10^{-4}$ M concentration of Aoa-x-EAK and Aoa-x-GBMP1α peptides in DMSO with one equivalent of AcOH.

9 PEEK disks were needed:

- 3 disks for proliferation assays
- 3 disks for gene expression assays
- 3 disks for Alizarin staining

0.72 mg of pure peptide Aoa-x-EAK and 1.03 mg of pure peptide Aoa-x-GBMP1α were dissolved in 2 ml of DMSO with one equivalent of AcOH each. They were then mixed together.

A functionalization drop of 100 µl was picked up and put on each surface of PEEK disks.

The reaction took place at room temperature for 24 hours, then the disks were washed as follows:

- 3 wash cycles with DMSO
- 3 wash cycles with MilliQ water

### 3.3.3 PEEK functionalization for XPS analysis

The smooth surface of PEEK disks was functionalized:

With a $10^{-4}$ M concentration of different peptides in DMSO solution with one equivalent of AcOH.

- 1 disk was covalently functionalized with $10^{-4}$ M concentration of Aoa-x-EAK peptide. 0.27 mg of pure peptide were dissolved in 1.49 ml of DMSO with one equivalent of AcOH.

- 1 disk was covalently functionalized with $10^{-4}$ M concentration of Aoa-x-GBMP1α peptide. 0.4 mg of pure peptide were dissolved in 1.5 ml of DMSO with one equivalent of AcOH.
- 1 disk was covalently functionalized with $10^{-4}$ M concentration of Aoa-x-EAK and Aoa-x-GBMP1α peptides. 0.72 mg of pure peptide Aoa-x-EAK and 1.03 mg of pure peptide Aoa-x-GBMP1α were dissolved in 2 ml of DMSO with one equivalent of AcOH each. They were then mixed together.
- 1 disk was functionalized through adsorption with $10^{-4}$ M concentration of EAK peptide. 0.29 mg of pure peptide were dissolved in 1.79 ml of DMSO with one equivalent of AcOH.
- 1 disk was functionalized through adsorption with $10^{-4}$ M concentration of aldehyde-GBMP1α peptide. 0.1 mg of pure peptide were dissolved in 0.38 ml of DMSO with one equivalent of AcOH.

With a $10^{-4}$ M concentration of different peptides in 40 mM sodium phosphate buffer solution:

- 1 disk was functionalized through adsorption with $10^{-4}$ M concentration of EAK peptide. 0.19 mg of pure peptide were dissolved in 1.17 ml of sodium phosphate buffer solution.
- 1 disk was functionalized through adsorption with $10^{-4}$ M concentration of aldehyde-GBMP1α peptide. 0.6 mg of pure peptide were dissolved in 2.33 ml of sodium phosphate buffer solution.

Sodium phosphate buffer was prepared as follows: 1.10 g of monobasic sodium phosphate were dissolved in 208.12 ml of MilliQ water, then the solution was stirred with electromagnetic stirring to facilitate the dissolution. The solution pH was checked, and some drops of sodium hydroxide were added to stabilize the pH at 6.

A functionalization drop of 100 µl was picked up and put on each surface of PEEK disks.

The reaction took place at room temperature for 24 hours, then the disks were washed as follows:

- 3 wash cycles with DMSO and 3 wash cycles with MilliQ water for the functionalization employing DMSO.
- 3 wash cycles with 40 mM, 6 pH sodium phosphate buffer solution and 3 wash cycles with MilliQ water for the functionalization employing buffer solution.

Due to the breakage of the XPS equipment, not all samples were analysed. Results are reported for PEEK functionalized with Ald-GBMP1α in buffer and with Aoa-x-EAK in DMSO.

### 3.3.4 PEEK functionalization for WCA and FS measurements

For WCA and AFM measurements, the smooth surface of 4 PEEK disks was covalently functionalized with a $10^{-4}$ M concentration of Aoa-x-EAK and Aoa-x-GBMP1α peptides in DMSO solution with one equivalent of AcOH. 0.72 mg of pure peptide Aoa-x-EAK and 1.03 mg of pure peptide Aoa-x-GBMP1α were dissolved in 2 ml of DMSO with one equivalent of AcOH each. They were then mixed together.

A functionalization drop of 100 µl was picked up and put on each surface of PEEK disks.

The reaction took place at room temperature for 24 hours, then the disks were washed as follows:

- 3 wash cycles with DMSO
- 3 wash cycles with MilliQ water

WCA measurements were made also on non-functionalized disks:

- 3 disks smooth.
- 3 disks R60-PEEK.
- 3 disks R110-PEEK.

# CHAPTER 4
# RESULTS

## 4.1 SANDBLASTED PEEK CHARACTERIZATION

### 4.1.1 WCA measurements

WCA measurements were carried out in order to investigate the role of surface roughness in changes of wettability of the surface.

Figure 4.1 shows that sandblasting particle size influences wettability. In particular, water contact angle values increase at the increasing surface roughness. The increase in contact angle probably results from the peaks and valleys created on the surface, which constitute “geometrical barriers” to the spreading of the droplet [58].

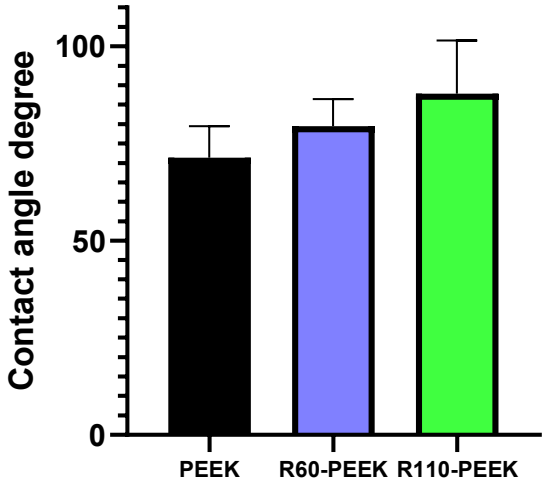


*Figure 4.1 – WCA measurements of PEEK surfaces with different roughness*

### 4.1.2 Proliferation test

H-osteoblasts proliferation test was performed in triplicate after 7 days of cells seeding PEEK, R60-PEEK and 3 R110-PEEK.

Results are shown in figure 4.2.

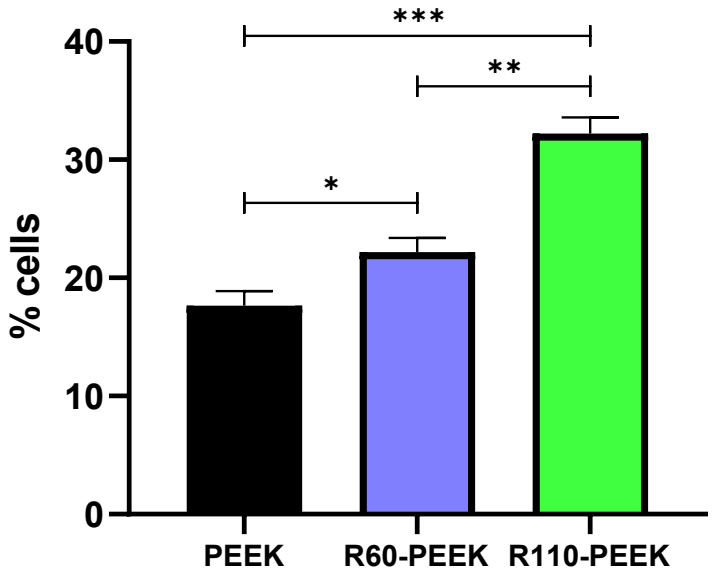


*Figure 4.2 – H-Osteoblast proliferation test at 7 days after cells seeding.*
*Significance levels: * <0.05, ** < 0.01, *** < 0.0001.*

Significant improvements in osteoblasts proliferation were detected in:

- R60-PEEK over PEEK with p value < 0.05
- R110-PEEK over PEEK with p value < 0.0001
- R110-PEEK over R60-PEEK with p value < 0.01

The results showed that the surface roughness of R110-PEEK provided significant improvements in osteoblast proliferation compared to both the smooth surface PEEK and the surface roughness of R60-PEEK, although the latter still provided a significant improvement over the smooth surface.

## 4.2 STUDIES ON FUNCTIONALIZED PEEK

### 4.2.1 Surface characterization

#### *4.2.1.1 XPS analysis*

For all samples, XPS measurements were carried out at the C1s, N1s, and O1s core levels.

XPS analysis were carried out on PEEK functionalized with:

- PEEK-Ald-BMP: PEEK functionalized with $10^{-4}$ M concentration of aldehyde-GBMP1α peptide in sodium phosphate buffer.
- PEEK-Aoa-x-EAK (DMSO): PEEK functionalized with $10^{-4}$ M concentration of Aoa-x-EAK peptide in DMSO.

Additional data in the tables below come from XPS analyses carried out in other thesis works and are given here for comparison purposes. Data considered are:

- PEEK control: untreated and non-functionalized PEEK
- PEEK-Aoa-x-BMP: PEEK functionalized with $10^{-4}$ M concentration of Aoa-x-GBMP1α peptide in sodium phosphate buffer.
- PEEK-Aoa-x-EAK (BUFFER): $10^{-4}$ M concentration of Aoa-x-EAK peptide in buffer solution.

XPS data (BE, FWHM, atomic ratios) are reported in table 4.3 and 4.5.

| Sample | Signal | Assignment | BE (eV) | FWHM | Internal Atomic ratios (%) | Atomic ratios |
|---|---|---|---|---|---|---|
| **PEEK-Control** | C1s | $C_{ar}$,C-C | 284.7 | 1.52 | 73 | 0.61 |
| | | C-N,C-O | 286.3 | | 23 | 0.19 |
| | | C=O | 287.7 | | 4 | 0.03 |
| | O1s | C=O | 531.4 | 1.79 | 51 | 0.08 |
| | | C-O | 533.4 | | 49 | 0.08 |
| **PEEK-Aoa-x-BMP** | C1s | $C_{ar}$,C-C | 284.7 | 1.67 | 56 | 0.38 |
| | | C-N | 286.1 | | 26 | 0.18 |
| | | C-O | 287.7 | | 14 | 0.09 |

| | | | | | | |
|---|---|---|---|---|---|---|
| | | C=O | 288.9 | | 4 | 0.03 |
| | N1s | C=N | 398.0 | 1.92 | 4 | 0.005 |
| | | C-N | 399.8 | | 87 | 0.09 |
| | | $-N^+$ | 401.6 | | 9 | 0.009 |
| | O1s | C=O | 531.5 | 2.16 | 72 | 0.16 |
| | | C-O | 533.1 | | 28 | 0.06 |
| **PEEK-ald-BMP** | C1s | C-C | 285.0 | 1.5 | 67 | 0.591 |
| | | CN, CO | 286.5 | | 27 | 0.24 |
| | | N-C=O | 287.7 | | 6 | 0.054 |
| | N1s | C-N | 400.1 | 1.8 | 91 | 0.021 |
| | | $-N^+$ | 402.2 | | 9 | 0.002 |
| | O1s | C=O | 531.6 | 1.9 | 42 | 0.092 |
| | | C-O | 533.4 | | 58 | 0.127 |

*Table 4.3 – XPS results for PEEK-control, PEEK functionalized with Aldeyde-GBMP1α (buffer) and Aoa-x-GBMP1α (buffer).*

The increase of the N/C ratios between peptide functionalized and peptide physio adsorbed PEEK demonstrates the success in the anchoring of the peptides (Table 4.4).

| Sample | N/C |
|---|---|
| **PEEK-Controllo** | / |
| **PEEK-AoA-x-BMP** | 0.14 |
| **PEEK-ald-BMP** | 0.03 |

*Table 4.4 – N/C ratios of functionalized and non-functionalized PEEK.*

Comparing the values of the nitrogen/carbon ratios of the samples functionalized with aldehyde-GBMP1α and Aoa-x-GBMP1α, it can be seen that the value of the latter is higher (0.03 vs. 0.14). This can be attributed to the fact that the aldehyde-GBMP1α peptide does not possess the oxyamine group, so it physio-adsorbs to the surface, which means binds reversibly, giving a lower nitrogen/carbon ratio. On the other hand, the peptide Aoa-x-GBMP1α, possessing the oxyamine group, is able to bind the ketones of PEEK, resulting in a more stable covalent bond, which gives a higher nitrogen/carbon ratio.

| Sample | Signal | Assignment | BE (eV) | FWHM | Internal Atomic ratios (%) | Atomic ratios |
|---|---|---|---|---|---|---|
| **PEEK-Controllo** | C1s | $C_{ar}$,C-C | 284.7 | 1.52 | 73 | 0.61 |
| | | C-N,C-O | 286.3 | | 23 | 0.19 |
| | | C=O | 287.7 | | 4 | 0.03 |
| | O1s | C=O | 531.4 | 1.79 | 51 | 0.08 |
| | | C-O | 533.4 | | 49 | 0.08 |
| **PEEK-AoA-x-EAK (BUFFER)** | C1s | $C_{ar}$,C-C | 284.7 | 1.59 | 67 | 0.50 |
| | | C-N | 286.2 | | 23 | 0.17 |
| | | C-O | 287.3 | | 5 | 0.04 |
| | | C=O | 288.3 | | 5 | 0.04 |
| | N1s | C=N | 398.5 | 1.57 | 7 | 0.003 |
| | | C-N | 399.9 | | 77 | 0.03 |
| | | $-N^+$ | 401.0 | | 16 | 0.006 |
| | O1s | C=O | 531.7 | 2.04 | 65 | 0.14 |
| | | C-O | 533.3 | | 35 | 0.08 |
| **PEEK-AoA-x-EAK (DMSO)** | C1s | C-C | 285.0 | 1.7 | 66 | 0.48 |

| | | | | | | |
|---|---|---|---|---|---|---|
| | | C-N,C-O | 286.6 | | 27 | 0.197 |
| | | N-C=O | 288.4 | | 6 | 0.047 |
| | N1s | CN | 400.1 | 1.9 | 91 | 0.049 |
| | | $-N^+$ | 402.2 | | 9 | 0.005 |
| | O1s | C=O | 531.5 | 1.9 | 49 | 0.109 |
| | | C-O | 533.2 | | 51 | 0.113 |

*Table 4.5 – XPS results of PEEK functionalized with Aoa-x-EAK in buffer and DMSO.*

In both table 4.2 and 4.4, C1s spectra are made of three components. The first component, fixed at 285.0 eV, is assigned to aromatic and aliphatic carbons; the second at around 286.5 eV to C-N and C-O; the third at about 288.3 eV is due to N-C=O carbons.
N1s spectra are made of two components. The first at around 400 eV is due to CN nitrogens of the peptide backbone and the second at about 402 eV to protonated nitrogens.
O1s spectra are made of two components. The first component, at nearly 531.5 eV, is associated with C=O oxygens; the second, at nearly 533.2-533.6 eV, with C-O oxygens.

Peptide immobilization on the PEEK surface is evidenced by the appearance of the N1s signals typical of the peptide.

N/C ratios are reported in Table 4.6.

| Sample | N/C |
|---|---|
| **PEEK-Controllo** | / |
| **PEEK-AoA-x-EAK (BUFFER)** | 0.056 |
| **PEEK-Aoa-x-EAK (DMSO)** | 0.07 |

*Table 4.6 – N/C ratios of functionalized and non-functionalized PEEK.*

To give an evaluation of the functionalization method used in this thesis, the nitrogen/carbon ratios of PEEK functionalized with Aoa-x-EAK in aqueous solvent and in organic solvent can be compared. In the first case, functionalization was done by means of a $10^{-4}$ M solution of peptide in sodium phosphate buffer (pH 6), whereas in the second case, functionalization was done by means of a $10^{-4}$ M solution of peptide with an equivalent of AcOH in DMSO. With the same reaction time (24 hours), the nitrogen/carbon ratio is higher in the case where the functionalization was done with DMSO (0.07), compared to the functionalization done in buffer (0.056). It can therefore be concluded that functionalization with DMSO can be a viable alternative to functionalization in aqueous solvent.

Further XPS analysis should be done by comparing the nitrogen/carbon ratios of PEEK functionalized with Aoa-x-EAK and EAK and PEEK functionalized with Aoa-x-GBMP1α dissolved in organic and aqueous solvent.

### *4.2.1.2 WCA measurements*

WCA was measured to determine functionalized PEEK's wettability at a concentration of $10^{-4}$ M (working solution). Non functionalized surface (PEEK-control) and Aoa-x-EAK+Aoa-x-GBMP1α functionalized surface (PEEK-EAK-BMP) were considered.

The results are shown in Figure 4.7.

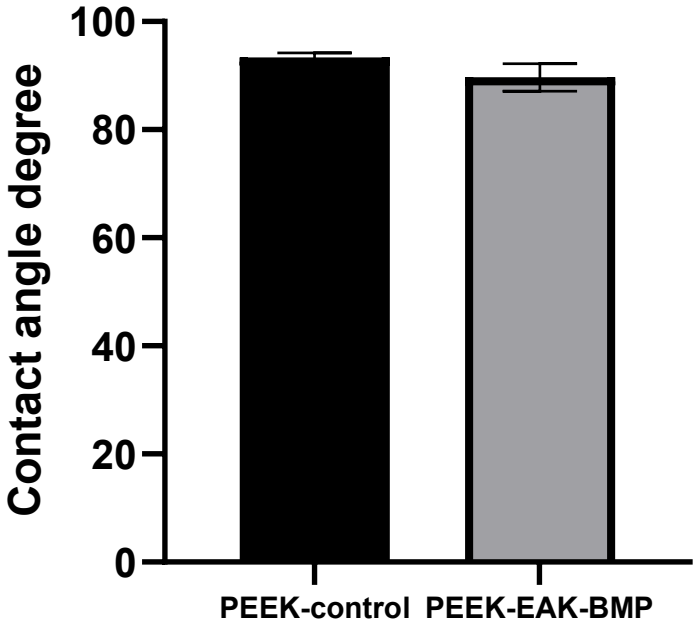


*Figure 4.7 - WCA measurements of functionalized PEEK scaffolds.*

It is evident that PEEK-EAK-BMP surface is more wettable than unfunctionalized PEEK, as their WCA is lower than the control. However, the difference between the two surfaces is not statistically relevant. Furthermore, the WCA value of the surfaces functionalized with both Aoa-x-EAK and Aoa-x-GBMP1α was lower than the value of functionalization with Aoa-x-GBMP1α alone, but higher than the value of functionalization with Aoa-x-EAK alone.

### *4.2.1.3 Force Spectroscopy measurements*

Atomic Force Microscopy was performed on the scaffolds to determine differences in Young modulus and adhesion forces. PEEK-EAK-BMP and untreated PEEK-control surfaces were considered.

In Figure 4.8, graphs of Young modulus distribution are reported.

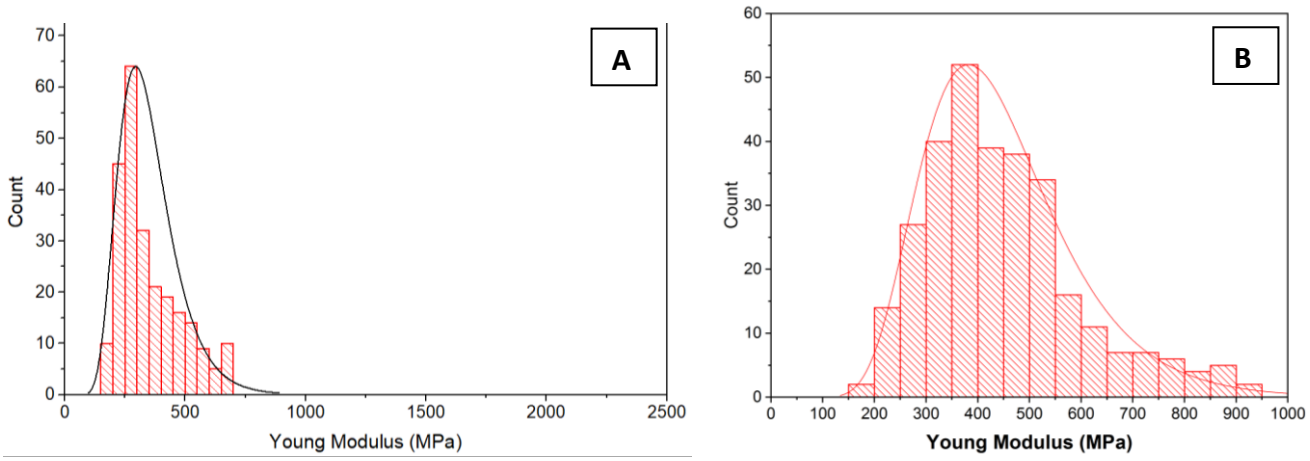


*Figure 4.8 - Young modulus curves obtained by AFM measurements. A: unfunctionalized PEEK-control, B: PEEK-EAK-BMP.*

In figure 4.9 it can be noted that untreated PEEK has the lowest Young modulus, thus its surface is more deformable. Surface functionalization has the effect of increasing stiffness at the interface. Furthermore, mixed functionalization allows intermediate Young's modulus values to be obtained, which are higher than those obtained with functionalization with Aoa-x-EAK alone but lower than those obtained with functionalization with Aoa-x-GBMP1α alone.

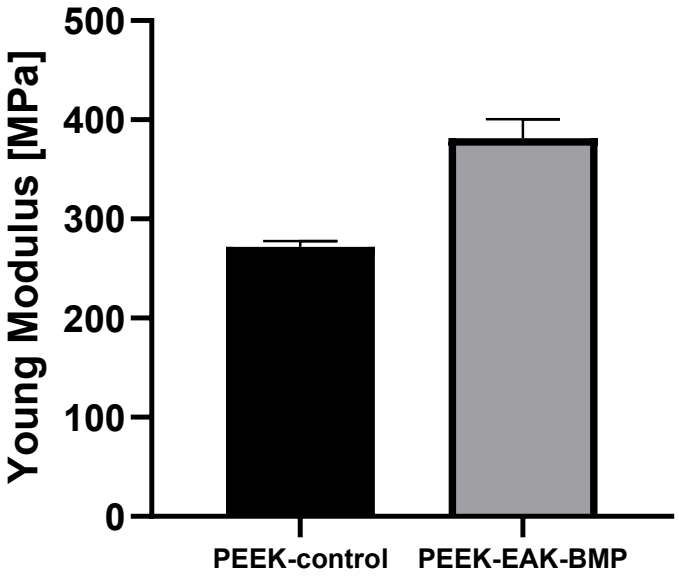


*Figure 4.9 – Difference in superficial Young modulus between unfunctionalized and functionalized PEEK.*

Figure 4.10 shows values of adhesion forces between the tip and the sample.

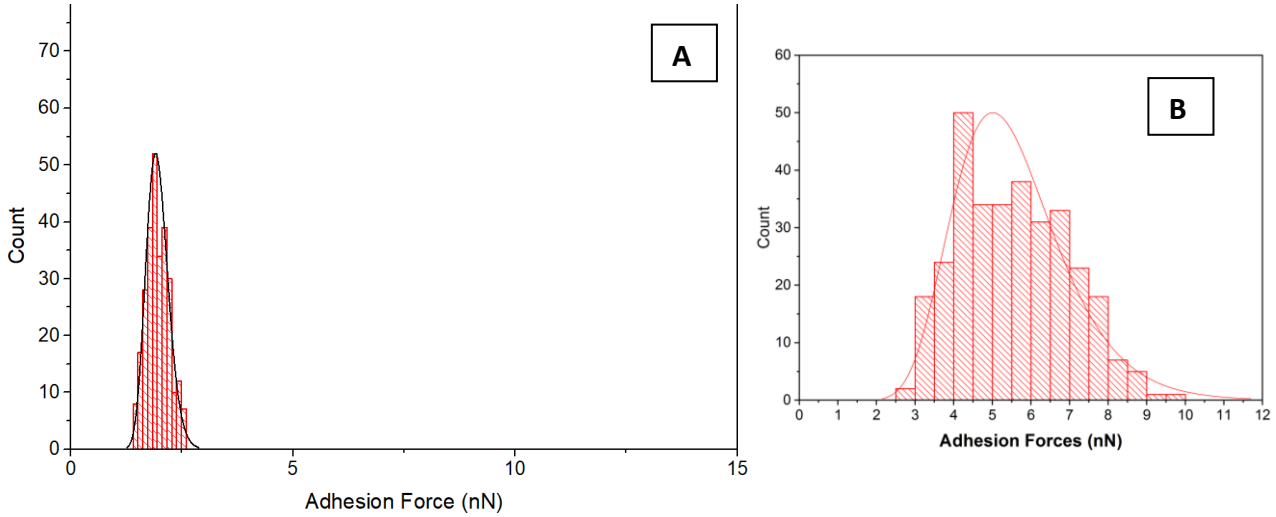


*Figure 4.10 - Adhesion curves obtained by AFM measurements. A: unfunctionalized PEEK-control, B: PEEK-EAK-BMP*

In this case, it should be noted that untreated PEEK has very low adhesion forces, while the values increase in functionalized PEEK (figure 4.11)

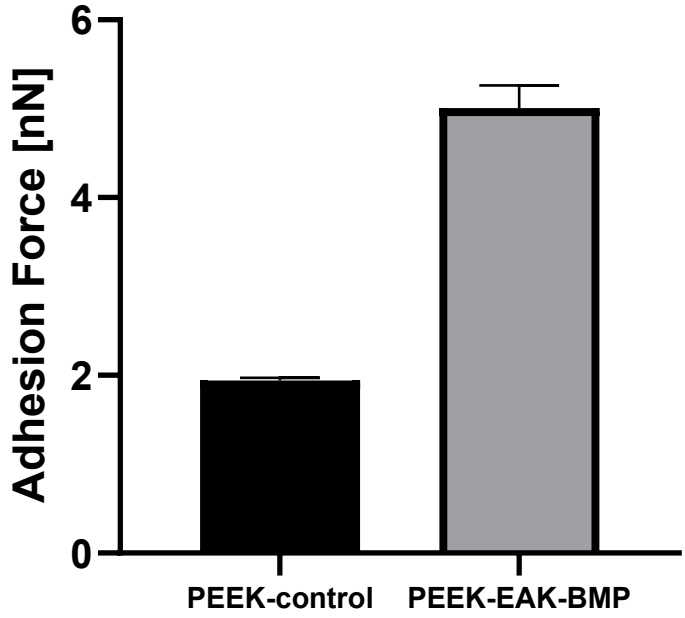


*Figure 4.11 - Difference in adhesion forces between unfunctionalized and functionalized PEEK.*

## 4.2.2 BIOLOGICAL ASSAYS

### *4.2.2.1 Quantitative Real-Time Polymerase Chain Reaction*

qRT-PCR was performed in triplicate after 3 days of cells seeding on non-functionalized and functionalized-sandblasted PEEK. Samples were tested for the expression of VTN, RUNX2 and SPP1, as described in paragraph 2.3.14.3.

The gene of which expression has been analysed are genes coding for proteins fundamental for osteoblasts. In particular, protein encoded by gene VTN is involved in adhesion of osteoblasts, the protein encoded by gene RUNX2 is essential for osteoblastic differentiation and SPP1 is the gene coding for Osteopontin, a bone matrix protein.

After qPCR, data obtained was elaborated: for every sample, the number of cycles needed by a specific gene to get past the threshold (set when the curve becomes exponential), Ct, was normalized to the Ct value of the housekeeping gene GAPDH:

$$\Delta Ct_{sample} = Ct_{gene} - Ct_{GAPDH}$$

Then, this value was normalized to the control (untreated PEEK):

$$(\Delta\Delta Ct)_{sample} = \Delta Ct_{sample} - \Delta Ct_{control}$$

Thanks to this normalization, gene expression for every gene is equal to 1 for the control. In this way, it can be determined whether a gene is over or under-expressed respect to the control.

Results are shown in figure 4.12.

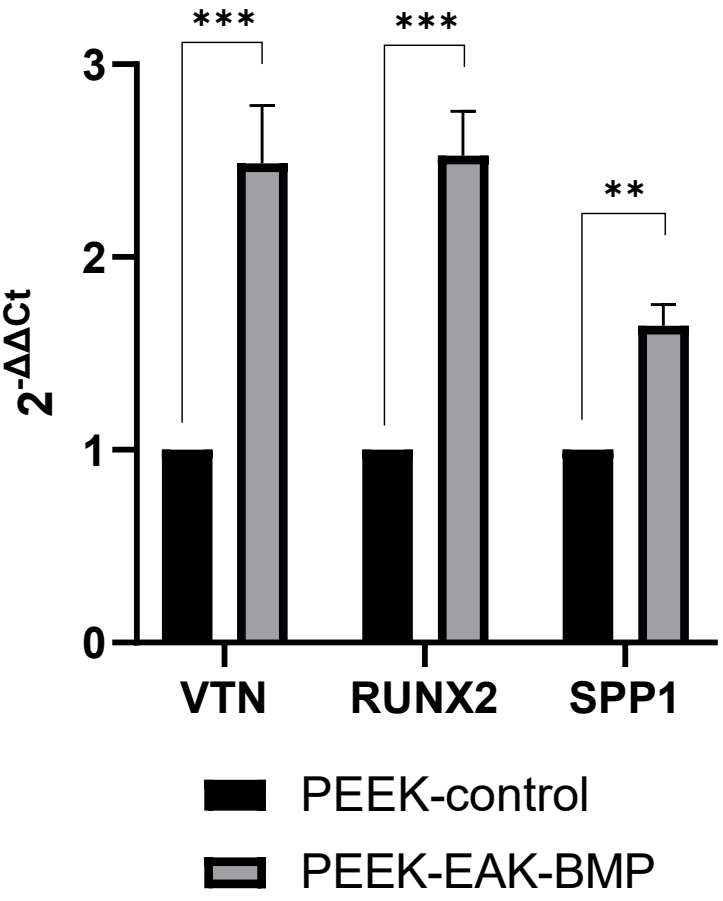


*Figure 4.12 – Gene expression at day 3 after HOB cells seeding on functionalized and non-functionalized PEEK. Significance levels: ** < 0.005, *** < 0.0001.*

Results show that both VTN, RUNX2 and SPP1 genes are overexpressed in functionalized scaffold with respect to the control. In particular, functionalized surface express VTN and RUNX2 genes with an increase of about 150% with respect to de control; furthermore, functionalized samples express SPP1 gene with an increase of about 60%.

# CHAPTER 5

# CONCLUSIONS

Cassari et al. [44, 45], showed that the peptide Aoa-x-EAK increased osteoblastic proliferation one day after seeding and that the peptide Aoa-x-GBMP1α was able to increase calcium deposition at 21 days after seeding. Therefore, it was decided to functionalize PEEK with both EAK and GBMP1α peptides in order to demonstrate the synergistic activity of the two bioactive sequences. Aoa-x-EAK and Aoa-x-GBMP1α peptides were synthetized, purified, and characterized in the Chemical Bioengineering Laboratory of the Department of Industrial Engineering of Padova. PEEK polymer disks used in previous thesis work were first lapped to obtain a smooth surface and then sandblasted, with particle sizes of 60 and 110 μm, to obtain two different types of surface roughness and to investigate which of them was preferable to osteoblasts. The PEEK discs were then functionalized with Aoa-x-EAK and Aoa-x-GBMP1α to increase the bioactivity of the PEEK surface. Functionalized PEEK disks were analyzed through surface, mechanical, and biological tests. The main findings are reported below.

WCA measurements showed that the value of the contact angle increases as the surface roughness of the sample increases. This seems not to confirm what stated in the paper of Deng et al. [31], where an increase in roughness was shown to lead to an increase in surface wettability. According to what sustained by Ourahmoune et al. [58], this result is probably due to the peaks and valleys formed on the surface that act as a "geometric barrier" to the spreading of the droplet.

An osteoblast proliferation test was performed on the non-functionalized PEEK disks and revealed, confirming what was stated by Deng et al. [31], significantly better cell adhesion on the R110-PEEK surface, compared to both the smooth counterpart (control) and the R60-PEEK surface. However, also R60-PEEK surface has been shown to significantly increase osteoblast proliferation. This is probably due to the fact that the rougher is the surface, the larger is the surface area, offering more binding sites for adhesive protein that is an essential prerequisite for cell adhesion and proliferation.

XPS results on samples confirmed the peptides presence by the appearance of the N1s signals typical of the peptides themselves. In particular, a comparison of N/C ratio of functionalization with either ald-GBMP1α and Aoa-x-GBMP1α suggests that the latter is covalently bound to the surface. Furthermore, XPS data show that employing DMSO instead of an aqueous medium as solvent used for functionalization results in a higher N/C ratio; this is probably because PEEK is hydrophobic and the interactions with the solvent where the peptide is dissolved increase when the solvent is organic (e.g., DMSO), allowing wider contact between surface and solution. It can therefore be concluded that functionalization with DMSO can be a viable alternative to functionalization in aqueous solvent.

WCA results established qualitatively that functionalization induces superficial modification on the samples; in fact, functionalized surface has shown to have lower contact angle value and to be more hydrophilic than control. Furthermore, mixed functionalization, and thus the influence of the Aoa-x-EAK peptide, results in a higher surface hydrophilicity than with Aoa-x-GBMP1α alone, obtained by Cassari et al. [45] However, it is not possible to achieve the same hydrophilicity of the surface functionalized with only Aoa-x-EAK peptide, as there is the balance of the hydrophobic peptide Aoa-x-GBMP1α.

Force spectroscopy measurements showed that the functionalization causes increasing stiffness at the interface, because peptides organize themselves to build a composite system with strong inter-chain interactions, thus raising the Young modulus value for the functionalized surface. Furthermore, mixed functionalization allows intermediate Young modulus values to be obtained, which are higher than those obtained with functionalization with Aoa-x-EAK alone but lower than those obtained with functionalization with Aoa-x-GBMP1α alone by Cassari et al. [45]. Force spectroscopy analyses showed that untreated PEEK surface has low adhesion force because there is low interaction between the cantilever tip and the sample. In fact, peptide presence on the surface allows the formation of weak bonds, mostly intermolecular forces, and this translates into higher adhesion force values.

Considering biological characterization, qPCR test at 3 days from h-osteoblasts seeding, revealed that functionalized scaffolds are able to significantly overexpress genes VTN, RUNX2 and SPP1. The major increases are noticed for VTN and RUNX2. Furthermore, mixed functionalization with Aoa-x-EAK and Aoa-x-GBMP1α allows a gene expression of RUNX2 at 3 days higher than that measured at 7 days with Aoa-x-EAK or Aoa-x-GBMP1α alone. However, further analyses with more time points are needed to evaluate the late markers' expression.

In the future, further XPS analysis should be done by comparing the nitrogen/carbon ratios of PEEK functionalized with Aoa-x-EAK and EAK and PEEK functionalized with Aoa-x-GBMP1α employing organic and aqueous solvent. Moreover, biological tests, including Scanning Electron

Microscopy, Live and Dead assays, Alizarin staining, proliferation tests and gene expression assays are in progress to compare biological properties and characteristics of functionalized and non-functionalized PEEK.

In the next future, the samples could be analysed with different peptide combinations, and *in vivo* tests should be performed.

# Ringraziamenti

Vorrei innanzitutto ringraziare la professoressa Monica Dettin per avermi dato l'opportunità di lavorare a questo progetto, la disponibilità, i suggerimenti e le preziose indicazioni che mi ha fornito in questi mesi.

Un sentito ringraziamento a Leonardo per la fiducia, il supporto e per essere stato in questi mesi una guida attenta e disponibile.

Vorrei ringraziare i miei genitori Simonetta e Giuseppe, che da sempre mi sostengono nella realizzazione dei miei progetti. Non smetterò mai di esservi riconoscente per avermi permesso di arrivare fino a qui.

Ringrazio il mio fidanzato Angelo, per avermi ascoltato e supportato fino allo sfinimento in ogni momento di questo percorso. Grazie per il tempo che mi hai dedicato e perché ci sei sempre stato.

Infine, un sentito grazie a parenti, amici e compagni di università. Grazie per essere stati miei complici, ognuno a suo modo, in questo percorso intenso ed entusiasmante, nel bene e nel male.

# Bibliography

[1] Donald W.Buck II, Gregory A. Dumanian, “Bone Biology and Physiology: Part I. The fundamentals”, Plast Reconstr Surg, 2012 June, 129(6): 1314-1320

[2] Buckwalter JA, Glimcher MJ, Cooper RR, Recker R., “Bone biology”, J Bone Joint Surg Am, 1995; 77:1256–1275.

[3] Clarke B, “Normal bone anatomy and physiology”, Clin J Am Soc Nephrol, 2008, Suppl.3: S131–S139.

[4] C. Di Bello, A.Bagno, “Biomateriali: dalla scienza dei materiali alle applicazioni cliniche”, Pàtron Editore, Bologna, 2016

[5] Wang W, Yeung KWK. “Bone grafts and biomaterials substitutes for bone defect repair: A review”. Bioact Mater. 2017 Jun 7;2(4):224-247. doi: 10.1016/j.bioactmat.2017.05.007.

[6] Roberts TT, Rosenbaum AJ. “Bone grafts, bone substitutes and orthobiologics: the bridge between basic science and clinical advancements in fracture healing. Organogenesis”. 2012 Oct-Dec;8(4):114-24. doi: 10.4161/org.23306.

[7] Annj Zamuner, Paola Brun, Roberta Ciccimarra, Francesca Ravanetti, Lorenzo Veschini, Hamada Elsayed, Stefano Sivolella, Giovanna Iucci, Andrea Porzionato, Lucy Di Silvio, “Biofunctionalization of bioactive ceramic scaffolds to increase the cell response for bone regeneration”, Biomed. Mater. 16 055007

[8] Shibuya N, Jupiter DC. “Bone graft substitute: allograft and xenograft”. Clin Podiatr Med Surg. 2015 Jan;32(1):21-34. doi: 10.1016/j.cpm.2014.09.011.

[9] Mayer Tenenhaus, Hans-Oliver Rennekampff, “Current Concepts in Tissue Engineering: Skin and Wound”, Plast Reconstr Surg. 2016 Sep;138(3 Suppl):42S-50

[10] Langer R, Vacanti J. “Advances in tissue engineering”. J Pediatr Surg. 2016 Jan;51(1):8-12. doi: 10.1016/j.jpedsurg.2015.10.022.

[11] Fergal J. O'Brien, “Biomaterials & scaffolds for tissue engineering”, Materials Today, Volume 14, Issue 3, 2011, Pages 88-95, ISSN 1369-7021, https://doi.org/10.1016/S1369-7021(11)70058-X.

[12] Ye G, Bao F, Zhang X, Song Z, Liao Y, Fei Y, Bunpetch V, Heng BC, Shen W, Liu H, Zhou J, Ouyang H. “Nanomaterial-based scaffolds for bone tissue engineering and regeneration”. Nanomedicine (Lond). 2020 Aug;15(20):1995-2017. doi: 10.2217/nnm-2020-0112.

[13] Park JY, Park SH, Kim MG, Park SH, Yoo TH, Kim MS. “Biomimetic Scaffolds for Bone Tissue Engineering”. Adv Exp Med Biol. 2018;1064:109-121. doi: 10.1007/978-981-13-0445-3_7.

[14] Kelly Alvarez and Hideo Nakajima, “Metallic Scaffolds for Bone Regeneration”, Materials 2009, 2, 790-832; doi:10.3390/ma2030790

[15] Sumner DR, Turner TM, Igloria R, Urban RM, Galante JO.” Functional adaptation and ingrowth of bone vary as a function of hip implant stiffness”. J Biomech. 1998 Oct;31(10):909-17. doi: 10.1016/s0021-9290(98)00096-7.

[16] Duan, K.; Wang, R., “Surface modifications of bone implants through wet chemistry”, J. Mater.Chem. 2006, 16, 2309-2321.

[17] Polak JM, Bishop AE. “Stem cells and tissue engineering: past, present, and future”. Ann N Y Acad Sci. 2006 Apr; 1068:352-66. doi: 10.1196/annals.1346.001.

[18] Roberts SJ, Howard D, Buttery LD, Shakesheff KM. “Clinical applications of musculoskeletal tissue engineering”. Br Med Bull. 2008; 86:7-22. doi: 10.1093/bmb/ldn016.

[19] Seong JM, Kim BC, Park JH, Kwon IK, Mantalaris A, Hwang YS. “Stem cells in bone tissue engineering”. Biomed Mater. 2010 Dec;5(6):062001. doi: 10.1088/1748-6041/5/6/062001.

[20] Perić Kačarević Ž, Rider P, Alkildani S, Retnasingh S, Pejakić M, Schnettler R, Gosau M, Smeets R, Jung O, Barbeck M. “An introduction to bone tissue engineering”. Int J Artif Organs. 2020 Feb;43(2):69-86. doi: 10.1177/0391398819876286.

[21] J.B., P. & R.S., L, “Biomaterials: An Introduction” (Plenum, 2002).

[22] Bharadwaz A, Jayasuriya AC. “Recent trends in the application of widely used natural and synthetic polymer nanocomposites in bone tissue regeneration”. Mater Sci Eng C Mater Biol Appl. 2020 May; 110:110698. doi: 10.1016/j.msec.2020.110698.

[23] Xiaoyan Tang, Shalumon Kottappally Thankappan, Paul Lee, Sahar E. Fard, Matthew D. Harmon, Katelyn Tran, Xiaojun Yu, “Polymeric Biomaterials in Tissue Engineering and Regenerative Medicine”, Natural and Synthetic Biomedical Polymers, 2014, Pages 351-371

[24] Najeeb S, Zafar MS, Khurshid Z, Siddiqui F. “Applications of polyetheretherketone (PEEK) in oral implantology and prosthodontics”. J Prosthodont Res. 2016 Jan;60(1):12-9. doi: 10.1016/j.jpor.2015.10.001.

[25] Panayotov IV, Orti V, Cuisinier F, Yachouh J. “Polyetheretherketone (PEEK) for medical applications”. J Mater Sci Mater Med. 2016 Jul;27(7):118. doi: 10.1007/s10856-016-5731-4.

[26] Kurtz SM, Devine JN. “PEEK biomaterials in trauma, orthopedic, and spinal implants”. Biomaterials. 2007 Nov;28(32):4845-69. doi: 10.1016/j.biomaterials.2007.07.013.

[27] S. Kurtz, “Synthesis and Processing of PEEK for Surgical Implants”.

[28] Gu X, Sun X, Sun Y, Wang J, Liu Y, Yu K, Wang Y, Zhou Y. “Bioinspired Modifications of PEEK Implants for Bone Tissue Engineering”. Front Bioeng Biotechnol. 2021 Jan 12;8:631616. doi: 10.3389/fbioe.2020.631616.

[29] Dettin M, Conconi MT, Gambaretto R, Bagno A, Di Bello C, Menti AM, Grandi C, Parnigotto PP. “Effect of synthetic peptides on osteoblast adhesion”. Biomaterials. 2005 Aug;26(22):4507-15. doi: 10.1016/j.biomaterials.2004.11.023.

[30] Ma R, Tang T. “Current strategies to improve the bioactivity of PEEK”. Int J Mol Sci. 2014 Mar 28;15(4):5426-45. doi: 10.3390/ijms15045426.

[31] Deng Y, Liu X, Xu A, Wang L, Luo Z, Zheng Y, Deng F, Wei J, Tang Z, Wei S. “Effect of surface roughness on osteogenesis in vitro and osseointegration in vivo of carbon fiber-reinforced polyetheretherketone-nanohydroxyapatite composite”. Int J Nanomedicine. 2015 Feb 17;10:1425-47. doi: 10.2147/IJN.S75557.

[32] Han X, Sharma N, Xu Z, Scheideler L, Geis-Gerstorfer J, Rupp F, Thieringer FM, Spintzyk S. “An In Vitro Study of Osteoblast Response on Fused-Filament Fabrication 3D Printed PEEK for Dental and Cranio-Maxillofacial Implants”. J Clin Med. 2019 May 31;8(6):771. doi: 10.3390/jcm8060771.

[33] Groß A, Hashimoto C, Sticht H, Eichler J. “Synthetic Peptides as Protein Mimics”. Front Bioeng Biotechnol. 2016 Jan 19;3:211. doi: 10.3389/fbioe.2015.00211.

[34] Edwards-Gayle CJC, Hamley IW. “Self-assembly of bioactive peptides, peptide conjugates, and peptide mimetic materials”. Org Biomol Chem. 2017 Jul 19;15(28):5867-5876. doi: 10.1039/c7ob01092c.

[35] Lee S, Trinh THT, Yoo M, Shin J, Lee H, Kim J, Hwang E, Lim YB, Ryou C. “Self-Assembling Peptides and Their Application in the Treatment of Diseases”. Int J Mol Sci. 2019 Nov 21;20(23):5850. doi: 10.3390/ijms20235850.

[36] Brun P, Zamuner A, Cassari L, D'Auria G, Falcigno L, Franchi S, Contini G, Marsotto M, Battocchio C, Iucci G, Dettin M. “Chitosan Covalently Functionalized with Peptides Mapped on Vitronectin and BMP-2 for Bone Tissue Engineering”. Nanomaterials (Basel). 2021 Oct 21;11(11):2784. doi: 10.3390/nano11112784.

[37] Chen Y, Ma B, Wang X, Zha X, Sheng C, Yang P, Qu S. “Potential Functions of the BMP Family in Bone, Obesity, and Glucose Metabolism”. J Diabetes Res. 2021 Jun 23;2021:6707464. doi: 10.1155/2021/6707464.

[38] S. Petersen, “Biofunctionalization”, BioNanoMaterials, vol. 18, no. 1-2, 2017

[39] Kieltyka RE, Bastings MM, van Almen GC, Besenius P, Kemps EW, Dankers PY. “Modular synthesis of supramolecular ureidopyrimidinone-peptide conjugates using an oxime ligation strategy”. Chem Commun (Camb). 2012 Feb 1;48(10):1452-4. doi: 10.1039/c1cc14728e.

[40] Rose. K., “Facile synthesis of homogeneous artificial protein”, (1994) J. Am. Chem. Soc., 116, 30-33

[41] H. C. Kolb, M. G. Finn and K. B. Sharpless, "Click Chemistry: Diverse Chemical Function from a Few Good Reactions". Angewandte Chemie (International ed. in English, vol. 40, no. 11, pp. 2004-2021, 2001.

[42] G. Thumshirn, U. Hersel, S. L. Goodman and H. Kessler, "Multimeric Cyclic RGD Peptides as Potential Tools for Tumor Targeting: Solid-Phase Peptide Synthesis and Chemoselective Oxime Ligation," Chemistry - A European Journal, vol. 9, no. 12, pp. 2717-2725, 2003.

[43] X. Meng and K. J. Edgar, "“Click” reactions in polysaccharide modification," Progress in Polymer Science, vol. 53, pp. 52-85, 2016.

[44] Cassari L, Zamuner A, Messina GML, Marsotto M, Chen H, Gonnella G, Coward T, Battocchio C, Huang J, Iucci G, Marletta G, Di Silvio L, Dettin M. Bioactive PEEK: “Surface Enrichment of Vitronectin-Derived Adhesive Peptides”. Biomolecules. 2023 Jan 28;13(2):246. doi: 10.3390/biom13020246.

[45] Cassari L., Zamuner A., Messina G., Marsotto M., Chang H., Coward T., Battocchio C., Iucci G., Marletta G., Di Silvio L., Dettin M., “Strategie for the Covalent Anchoring of a BMP-2 Mimetic

Peptide to PEEK Surface for Bone Tissue Engineering", Materials 2023; 16(10), 3896. Doi: https://doi.org/10.3390/ma16103869

[46] R. B. Merrifield, "Solid Phase Peptide Synthesis. I. The Synthesis of a Tetrapeptide," Journal of the American Chemical Society, vol. 85, no. 14, p. 2149–2154, 1963.

[47] R. B. Merrifield, "Solid Phase Peptide Synthesis. I. The Synthesis of a Tetrapeptide," Journal of the American Chemical Society, vol. 85, no. 14, p. 2149–2154, 1963.

[48] L. A. Carpino and G. Y. Han, "9-Fluorenylmethoxycarbonyl amino-protecting group," The Journal of Organic Chemistry, vol. 37, no. 22, p. 3404–3409, 1972.

[49] G. Chen, M. Fan, Y. Liu, B. Sun, M. Liu, J. Wu, N. Li and M. Guo, "Advances in MS Based Strategies for Probing Ligand-Target Interactions: Focus on Soft Ionization Mass Spectrometric Techniques," Frontiers in chemistry, vol. 7, no. 703, 2019.

[50] G. Mezö, I. Szabó, I. Kertész, R. Hegedüs, E. Orbán, U. Leurs, S. Bösze, G. Halmos and M. Manea, "Efficient synthesis of an (aminooxy) acetylated-somatostatin derivative using (aminooxy)acetic acid as a 'carbonyl capture' reagent," Journal of Peptide Science, vol. 17, no. 1, pp. 39-46, 2010.

[51] Dettin M, Zamuner A, Naso F, Monteleone A, Spina M, Gerosa G. "Natural Scaffolds for Regenerative Medicine: Direct Determination of Detergents Entrapped in Decellularized Heart Valves". Biomed Res Int. 2017; 2017:9274135. doi: 10.1155/2017/9274135.

[52] Chelushkin PS, Leko MV, Dorosh MY, Burov SV. "Oxime ligation in acetic acid: efficient synthesis of aminooxy-peptide conjugates". J Pept Sci. 2017 Jan;23(1):13-15. doi: 10.1002/psc.2931.

[53] Liu F, Hakami RM, Dyas B, Bahta M, Lountos GT, Waugh DS, Ulrich RG, Burke TR Jr. "A rapid oxime linker-based library approach to identification of bivalent inhibitors of the Yersinia pestis protein-tyrosine phosphatase", YopH. Bioorg Med Chem Lett. 2010 May 1;20(9):2813-6. doi: 10.1016/j.bmcl.2010.03.058.

[54] J. Domke, S. Dannöhl, W. J. Parak, O. Müller, W. K. Aicher and M. Radmacher, "Substrate dependent differences in morphology and elasticity of living osteoblasts investigated by atomic force microscopy," Colloids and Surfaces B: Biointerfaces, vol. 19, no. 4, pp. 367-379, 2000.

[55] E. Takai, K. D. Costa, A. Shaheen, C. T. Hung and X. E. Guo, "Osteoblast Elastic Modulus Measured by Atomic Force Microscopy Is Substrate Dependent," Annals of Biomedical Engineering, vol. 33, no. 7, p. 963–971, 2005.

[56] Brun P, Zamuner A, Battocchio C, Cassari L, Todesco M, Graziani V, Iucci G, Marsotto M, Tortora L, Secchi V, Dettin M. “Bio-Functionalized Chitosan for Bone Tissue Engineering”. Int J Mol Sci. 2021 May 31;22(11):5916. doi: 10.3390/ijms22115916.

[57] Bernabè G, Pauletto A, Zamuner A, Cassari L, Castagliuolo I, Brun P, Dettin M. “Exploiting Conserved Quorum Sensing Signals in Streptococcus mutans and Streptococcus pneumoniae”. Microorganisms. 2022 Nov 30;10(12):2386. doi: 10.3390/microorganisms10122386.

[58] Ourahmoune R, Salvia M, Mathia TG, Mesrati N. “Surface morphology and wettability of sandblasted PEEK and its composites”. Scanning. 2014 Jan-Feb; 36(1):64-75. doi: 10.1002/sca.21089.